



UNIL | Université de Lausanne

Unicentre

CH-1015 Lausanne

<http://serval.unil.ch>

---

Year : 2021

## Oncogenic potential of CDCP1 overexpression

D'Ambrosio Mariantonietta

D'Ambrosio Mariantonietta, 2021, Oncogenic potential of CDCP1 overexpression

Originally published at : Thesis, University of Lausanne

Posted at the University of Lausanne Open Archive <http://serval.unil.ch>

Document URN : urn:nbn:ch:serval-BIB\_6FEFA9B413912

### **Droits d'auteur**

L'Université de Lausanne attire expressément l'attention des utilisateurs sur le fait que tous les documents publiés dans l'Archive SERVAL sont protégés par le droit d'auteur, conformément à la loi fédérale sur le droit d'auteur et les droits voisins (LDA). A ce titre, il est indispensable d'obtenir le consentement préalable de l'auteur et/ou de l'éditeur avant toute utilisation d'une oeuvre ou d'une partie d'une oeuvre ne relevant pas d'une utilisation à des fins personnelles au sens de la LDA (art. 19, al. 1 lettre a). A défaut, tout contrevenant s'expose aux sanctions prévues par cette loi. Nous déclinons toute responsabilité en la matière.

### **Copyright**

The University of Lausanne expressly draws the attention of users to the fact that all documents published in the SERVAL Archive are protected by copyright in accordance with federal law on copyright and similar rights (LDA). Accordingly it is indispensable to obtain prior consent from the author and/or publisher before any use of a work or part of a work for purposes other than personal use within the meaning of LDA (art. 19, para. 1 letter a). Failure to do so will expose offenders to the sanctions laid down by this law. We accept no liability in this respect.



**UNIL** | Université de Lausanne

Faculté de biologie  
et de médecine

**Institut/Section/Département de Institute of Oncology Research (IOR,  
Bellinzona)**

## **Oncogenic potential of CDCP1 overexpression**

**Thèse de doctorat ès sciences de la vie (PhD)**

présentée à la

Faculté de biologie et de médecine  
de l'Université de Lausanne

par

**D'Ambrosio Mariantonietta**

Biologiste diplômé ou Master de l'Université de Milano Bicocca

### **Jury**

Prof. Sanjiv Luther, Président  
Prof. Pedro Romero, Directeur de thèse  
Prof. Andrea Alimonti, Co-directeur de thèse (Institute of Oncology Research, IOR, Bellinzona)  
Prof. Marco Demaria, Expert  
Prof. Roger Geiger, Expert

Lausanne  
(2021)



UNIL | Université de Lausanne  
Faculté de biologie  
et de médecine

**Ecole Doctorale**  
Doctorat ès sciences de la vie

## Imprimatur

Vu le rapport présenté par le jury d'examen, composé de

<b>Président·e</b>	Monsieur	Prof.	Sanjiv	<b>Luther</b>
<b>Directeur·trice de thèse</b>	Monsieur	Prof.	Pedro	<b>Romero</b>
<b>Co-directeur·trice</b>	Monsieur	Prof.	Andrea	<b>Alimonti</b>
<b>Expert·e·s</b>	Monsieur	Prof.	Marco	<b>Demaria</b>
	Monsieur	Prof.	Roger	<b>Geiger</b>

le Conseil de Faculté autorise l'impression de la thèse de

**Madame Mariantonietta D'Ambrosio**

Master, Université de Milan Bicocca, Italie

intitulée

**Oncogenic potential of CDCP1 overexpression**

Date de l'examen : 30 septembre 2021

Date d'émission de l'imprimatur : Lausanne, le 15 novembre 2021

pour le Doyen  
de la Faculté de biologie et de médecine

Prof. Niko GELDNER  
Directeur de l'Ecole Doctorale

## **Acknowledgement**

First, I want to thank my family for always supporting me and give me the motivation to continue this work, also if distance and COVID did not make it easy.

Then I want to thank all my colleagues that I had the luck to meet during these five years. They were for me a family.

I want to thank Emiliano Pasquini and Manuel Colucci

I want to thank my PI, Andrea Alimonti for giving me the opportunity to be part of his group. Our relation was not always easy, but he helped me to become stronger.

Finally, but not less important, I want to say thanks to all my old friends for having always ears to listen to me even from a distance.

## Summary

CUB domain-containing protein 1 (CDCP1), also known as SIMA135, gp140, CD318, or Trask, is a transmembrane protein frequently overexpressed in several human cancers such as colon, renal, lung, and breast cancers. Several papers have demonstrated that CDCP1 is a potent oncogene that drives cancer development, invasion, and metastasis. However, the role of CDCP1 in prostate cancer and its contribution to tumor progression in the presence of additional genetic events, such as PTEN loss, has not been yet investigated.

To this purpose, in the present work, we generated four new transgenic mouse models of CDCP1:

1. A prostate conditional mouse model in which CDCP1 is overexpressed only in the mouse prostate epithelium, either a) alone or b) in cooperation with loss of *Pten*;
2. A full body transgenic mouse model where CDCP1 is ubiquitously overexpressed upon tamoxifen activation, either a) alone or b) in cooperation with loss of *Pten*.

Thanks to these models, we showed that CDCP1 overexpression in prostatic epithelium led to metastatic castration-resistant prostate cancer (mCRPC) by increasing the activation of the SRC/MAPK pathway. By staining different human prostate cancer tissue macro arrays (TMA), we found that CDCP1 is overexpressed in a subset of advanced human CRPCs, and cooperates with PTEN loss to promote the emergence of this disease. Notably, treatment with anti-CDCP1 immunoliposomes (ILs) loaded with a chemotherapeutic drug, in combination with enzalutamide, significantly inhibits prostate tumor progression. Further, exploiting the full-body CDCP1 overexpressing mouse models, we showed that CDCP1 promotes lymphomagenesis, both alone and in cooperation with the loss of one allele of *Pten*. In conclusion, we demonstrated that CDCP1 is a potent oncogene that drives both mCRPC and lymphoma development. Since CDCP1 is a transmembrane protein, it can be targeted by either monoclonal antibodies, small molecules or immune-liposomes.

## Résumé

Le domaine CUB contenant la protéine 1 (CDCP1), également connue sous le nom de SIMA135, gp140, CD318 ou Trask, est une protéine transmembranaire qui est fréquemment surexprimée dans plusieurs types de tumeurs humaines, tels que le cancer du côlon, du rein, du poumon et du sein.

Plusieurs articles ont démontré que CDCP1 est un puissant oncogène entraînant le développement, l'invasion et les métastases du cancer. Cependant, le rôle de CDCP1 dans le cancer de la prostate et sa contribution à la progression tumorale en présence d'un autre événement oncogénique, tel que la perte d'expression de PTEN, n'a pas encore été étudié.

À cette fin, dans le présent travail, nous avons généré quatre nouveaux modèles de souris transgéniques :

1. Un modèle murin conditionnel de la prostate dans lequel CDCP1 est surexprimé uniquement dans l'épithélium de la prostate, soit a) seul, soit b) en coopération avec la perte d'expression de *Pten* ;
2. Un modèle de souris transgénique où CDCP1 est surexprimée de manière ubiquitaire lors de son activation induite par le tamoxifène, soit a) seul, soit b) en coopération avec la perte d'expression de *Pten*.

Grâce aux premiers modèles, nous avons montré que la surexpression de CDCP1 dans l'épithélium prostatique conduit au développement du cancer de la prostate métastatique résistant à la castration (mCRPC), en augmentant l'activation de la cascade de signalisation SRC/MAPK. De plus, lors de la coloration de microréseaux tissulaire (TMA) provenant d'échantillons humains du cancer de la prostate, nous avons constaté que CDCP1 est surexprimée dans un sous-ensemble de CRPC humains avancés et coopère avec la perte d'expression de PTEN pour favoriser l'émergence de la maladie. Notamment, le traitement avec des immunoliposomes (ILs) anti-CDCP1 dans lesquels sont encapsulés des agents chimiothérapeutiques, en association avec l'enzalutamide, inhibe significativement la progression tumorale prostatique. De plus, en exploitant les modèles de

surexpression de CDCP1 de manière ubiquitaire, nous avons montré que CDCP1 initie la tumorigenèse dans les ganglions lymphatiques, à la fois seul et en coopération avec la perte d'un allèle de *Pten*, et conduit au développement d'un lymphome à cellules B, favorisant l'expansion du centre germinatif.

En conclusion, nous avons démontré que CDCP1 est un puissant oncogène capable d'induire à la fois le mCRPC et le développement du lymphome. De plus, puisqu'il s'agit d'une protéine transmembranaire, des anticorps monoclonaux, des petites molécules ou des immunoliposomes pourraient être utilisés efficacement afin de cibler pharmacologiquement et spécifiquement, CDCP1, limitant ainsi la toxicité systémique.

## List of abbreviation

CDCP1	CUB domain containing protein 1
SFKs	Src-family kinases members
PKC $\delta$	Protein kinase C delta
mCRPC	Metastatic castration resistant prostate cancer
CRPC	Castration resistant prostate cancer
SIMA135	Subtractive immunization associated 135 kDa
Trask	Transmembrane and associated with Src kinases
CD	Cluster differentiation
ECD	Extracellular domain
ICD	Intracellular domain
HMW	High molecular weight
LMW	Low molecular weight
Y	Tyrosine
TGF- $\beta$	Transforming growth factor beta
TGFR1	Transforming growth factor beta receptor
EGFR	Epidermal growth factor receptor
DDAs	Disulfide bond disrupting agents
HER2/ERBB2	Epidermal growth factor receptor 2
PCa	Prostate cancer
PTEN	Phosphatase and tensin homolog
NHL	Non-Hodgkin Lymphoma
HL	Hodgkin Lymphoma

DLBCL	Diffuse large B-cell lymphoma
FL	Follicular lymphoma
GCB	Germinal center B-cell lymphoma
ABC	Activated B-cell lymphoma
GC	Germinal center
PB-CRE	Probasin-Cre recombinase
PDXs	Patients derived xenografts
PIN	Prostatic intraepithelial neoplasia
HGPIN	High grade prostatic intraepithelial neoplasia
LGPIN	Low grade prostatic intraepithelial neoplasia
PI3K	Phosphoinositide 3-kinase
PIP3	Phosphatidylinositol-triphosphate
PIP2	Phosphatidylinositol-diphosphate
CHIP	Cromatin immunoprecipitation
TMAAs	Tumor microarrays
IHC	Immunohistochemistry
AR	Androgen receptor
FAD	Full androgen deprivation
ADI	Androgen deprivation insensitive
ADS	Androgen deprivation sensitive
DHT	Dihydrotestosterone
ILs	Immuno-liposomes
FAB	Antigen-binding fragment
EPR	Enhanced permeability and retention
WT	Wild-type

MEFs	Mouse embryonic fibroblast
ADT	Androgen deprivation therapy
PNA	Peanut agglutinin
CD95	Fas or apoptosis antigen 1
mAb	Monoclonal antibody
Ig	Immunoglobulin
PBS	Phosphate-buffered saline
Sa- $\beta$ -gal	Senescence associated $\beta$ -galactosidase
AP	Anterior Prostate
VP	Ventral Prostate
DLP	Dorsal-lateral Prostate
qRT-PCR	Quantitative real time PCR

# Table of Contents

<b>Title page</b>	<b>1</b>
<b>Imprimatur</b>	<b>2</b>
<b>Acknowledgements</b>	<b>3</b>
<b>Summary</b>	<b>4</b>
<b>Summary in French</b>	<b>5</b>
<b>List of abbreviation</b>	<b>7</b>
<b>Table of content</b>	<b>10</b>
<b>List of Figures and Tables</b>	<b>12</b>
<b>1. Introduction</b>	<b>14</b>
1.1. CDCP1	14
1.2. CDCP1 structural features	14
1.3. CDCP1 interaction	16
1.4. CDCP1 expression in tumors	18
1.5. CDCP1 supports tumor cells proliferation	19
1.6. CDCP1 as a therapeutic target	20
1.7. Generation of two different CDCP1 transgenic mouse models	20
1.8. PTEN	22
1.9. Prostate cancer	24
1.10. Lymphoma	26
<b>2. Aims</b>	<b>29</b>
<b>3. Results: CDCP1 overexpression drives prostate cancer progression and can be targeted in vivo</b>	<b>30</b>
3.1. Generation of the prostate conditional CDCP1 overexpressing mouse model	31
3.2. CDCP1 overexpression in <i>Pten</i> -loss genetic background drives to metastasis	34
3.3. CDCP1 overexpression in <i>Pten</i> -loss context drives to CRPC	36
3.4. CDCP1 overexpression leads to senescence evasion	38
	<b>10</b>

3.5. CDCP1 overexpression in human prostate cancer TMA	43
3.6. Androgen deprivation induces CDCP1 expression in PTEN deficient cells	45
3.7. CDCP1 as a therapeutic target for prostate cancer	48
<b>4. Results: CDCP1 full-body overexpression leads to Germinal center B cell lymphoma</b>	<b>51</b>
4.1. CDCP1 full-body overexpression	51
4.2. CDCP1 overexpression drives B cell lymphoma development	53
4.3. CDCP1 overexpression leads to GCB development	55
4.4. CDCP1 overexpression in cervical lymph nodes triggers several oncogenic pathways	58
4.5. CDCP1 overexpression and targeting in different human lymphoma cell lines	60
<b>5. Discussion</b>	<b>62</b>
<b>6. Materials and methods</b>	<b>66</b>
6.1. Acquisition of MEFs	66
6.2. Cell culture and reagents	66
6.3. CDCP1 protein expression in human prostate cancer TMAs	67
6.4. Bioinformatic analysis	68
6.5. Immunoblotting	69
6.6. Autopsy and Histopathology	70
6.7. RNA extraction for RNA-sequencing	71
6.8. RNA-sequencing analysis	71
6.9. Quantitative real-time PCR	72
6.10. FACS staining	73
6.11. ChIP assay	74
6.12. Proliferation and senescence assays	75
6.13. Liposome formulation	75
6.14. Statistics	76
6.15. Study approval	77
<b>References</b>	<b>79</b>
<b>Annex 1</b>	<b>88</b>
<b>Annex 2</b>	<b>89</b>
	11

## List of figures and Tables

**Figure 1:** CDCP1 structure.

**Figure 2:** CDCP1-SFKs-PKC $\delta$  multiprotein complex.

**Figure 3:** CDCP1 interaction with EGFR.

**Figure 4:** CDCP1 interaction with HER2.

**Figure 5:** CDCP1 interaction with TGF $\beta$ .

**Figure 6:** Generation of new transgenic mouse models overexpressing CDCP1.

**Figure 7:** Schematic representation of the most important factors involved in PTEN pathway.

**Figure 8:** Prostate cancer progression and development.

**Figure 9:** Schematic representation of GC-derived lymphoma and cell maturation in GC.

**Figure 10:** Graphical abstract “CDCP1 overexpression drives prostate cancer progression and can be targeted in vivo”.

**Figure 11:** Prostate conditional overexpression of CDCP1.

**Figure 12:** CDCP1 overexpression in prostate induce PIN and HGPIN.

**Figure 13:** CDCP1 overexpression in *Pten*-loss context drive to metastasis.

**Figure 14:** CDCP1 overexpression in *Pten*-loss context drive to CRPC.

**Figure 15:** CDCP1 overexpression lead to senescence evasion.

**Figure 16:** Src inhibition or c-Myc downregulation restores senescence response.

**Figure 17:** CDCP1 overexpression leads to senescence evasion in human prostate cancer cell lines.

**Figure 18:** CDCP1 overexpression in human prostate cancer TMAs.

**Figure 19:** Negative correlation between CDCP1 and PTEN in human datasets.

**Figure 20:** Androgen receptor inhibits CDCP1 transcription.

**Figure 21:** Androgen deprivation induces CDCP1 overexpression in PTEN deficient cells.

**Figure 22:** CDCP1 as a therapeutic target for prostate cancer.

**Figure 23:** Graphical abstract “CDCP1 full-body overexpression leads to Germinal Center B cell lymphoma”.

**Figure 24:** CDCP1 full-body overexpression.

**Figure 25:** CDCP1 overexpression leads to B cell lymphoma development.

**Figure 26:** CDCP1 overexpression leads to GCB development.

**Figure 27:** Clonality of B cell lymphoma.

**Figure 28:** Pathways activated by CDCP1 overexpression in Cervical Lymphnodes.

**Figure 29:** CDCP1 overexpression and targeting in different human lymphoma cell lines.

**Figure 30:** Schematic representation of the role of CDCP1 in mCRPC.

**Table 1:** Primers for RT-PCR (Mouse).

**Table 2:** Primers for RT-PCR (Human).

# 1. Introduction

## 1.1 CDCP1

CUB domain containing-protein 1 (CDCP1) is a cell surface glycoprotein also known as subtractive immunization associated 135 kDa (SIMA135)<sup>1</sup>, gp140<sup>2</sup> and transmembrane and associated with Src kinases (Trask)<sup>3</sup> and has been assigned the cluster of differentiation (CD) designation CD318<sup>4</sup>.

A processed form of CDCP1 was identified for the first time in 1996. It can be phosphorylated in response to  $\alpha_6\beta_4$  integrin-mediated keratin adhesion to laminin. A few years later, Scherl-Mostageer et al. identified for the first time the complete DNA sequence of CDCP1 and showed that it was highly transcribed in lung and colon cancer cell lines<sup>5,6</sup>.

More recently, in 2003, the protein sequence of CDCP1 was isolated entirely by using a clever *in vivo* immunological approach to identify proteins functionally involved in metastasis.

Then, in two studies, CDCP1 was identified as a protein kinase C $\delta$  (PKC $\delta$ ) and a tetraspanin CD9-interacting protein<sup>5,6</sup>.

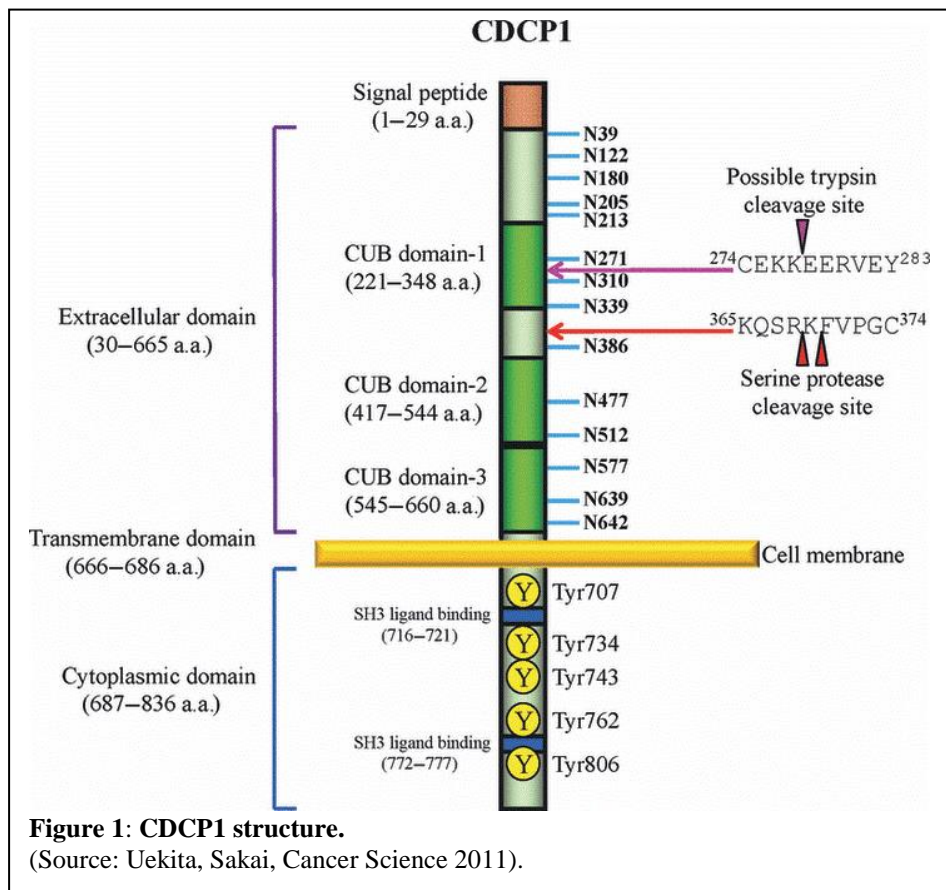
Several studies have already shown that CDCP1 has a role in cancer progression in different cancer types such as kidney, breast, lung, and colon, and its overexpression correlates with poor outcome and metastasis<sup>5,6</sup>.

## 1.2 CDCP1 structural features

CDCP1 is an 836 amino-acid cell surface glycoprotein containing a 29 residue amino-terminal signal peptide, an extracellular domain (ECD) of 636 amino-acids, a transmembrane domain of 21, and a cytoplasmic/intracellular domain (ICD) of 150 amino acids.

The ECD contains three regions with low homology to complement protein subcomponents C1r/C1s, urchin embryonic growth factor, and bone morphogenetic protein 1 (CUB) domains, 14 consensus N-glycosylation sites and, 20 cysteines likely involved in disulfide bond formation (Figure 1)<sup>3,7,8</sup>.

CUB domains are almost exclusively found in secreted proteins and in a few transmembrane proteins. These domains are approximately 110 amino acids long and have four conserved cysteines that form a  $\beta$ -sandwich fold<sup>7</sup>. CUB domains proteins are involved in a wide range of biological functions. However, the importance of the CUB domains for the roles of several proteins remains unknown<sup>9</sup>.



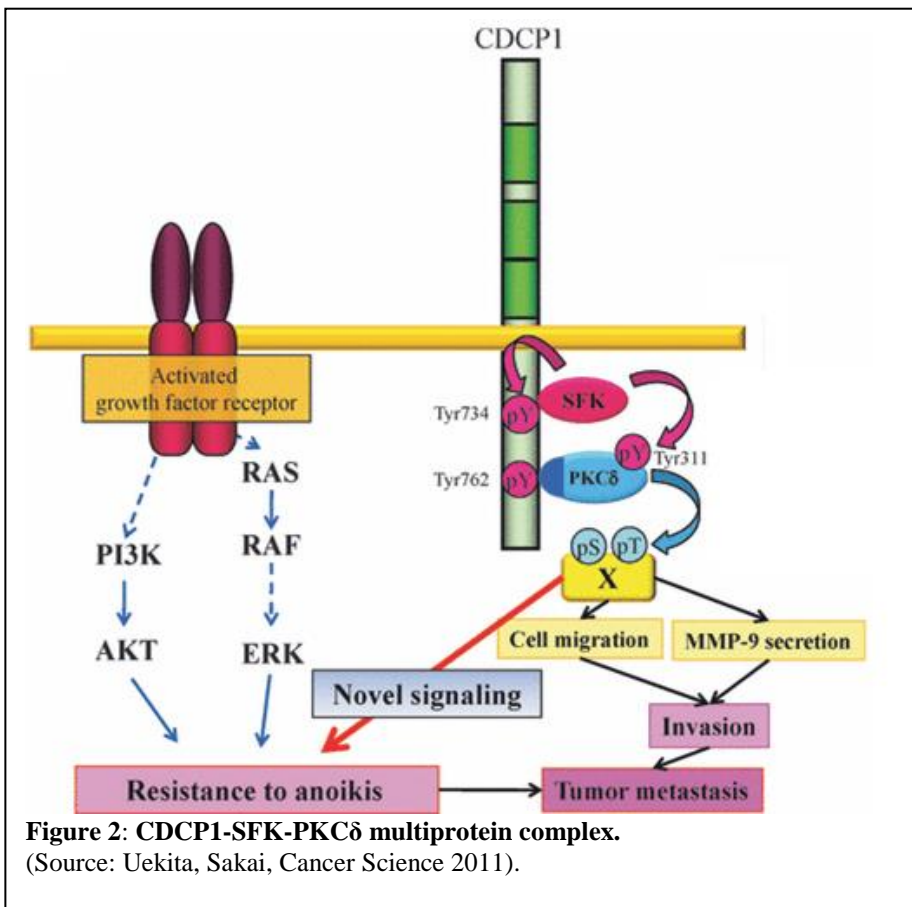
The ICD contains five tyrosine phosphorylation sites. It has been demonstrated that tyrosine phosphorylation is required for CDCP1 complete function and interaction with other proteins<sup>2</sup>. Twelve of the consensus N-glycosylation sites and 19 of the extracellular

cysteines are widely conserved in mammals (humans, chimpanzees, dogs, cows, mice, and rats). CDCP1 total molecular weight is 135-140 kDa (high molecular weight CDCP1; HMW-CDCP1), but it can also be processed, thanks to the interaction with different proteolytic enzymes such as trypsin, pepsinogen, and serine proteases, to low molecular weight (LMW) form of 70 kDa. This cleavage is related to the activation of Src kinases and tumor metastasis<sup>8,10</sup>.

### 1.3 CDCP1 interaction

CDCP1 can interact with many proteins thanks to its ICD, but its extracellular ligand is still unknown<sup>10</sup>.

It has been reported a tyrosine phosphorylation-dependent binding of SFKs and PKC $\delta$  to CDCP1, and that CDCP1 could be phosphorylated by SFKs, including Src, Yes, and Fyn<sup>2,3,5,11,12</sup>. Phosphorylation of CDCP1 starts at Y734, allowing the binding of Src binding to this site. This



binding promotes additional phosphorylation at Y743 and Y762. Phosphorylation at Y762 recruits PKC $\delta$ , which binds to phospho-Y762. This phosphorylation is required for the formation of a CDCP1-SFK-PKC $\delta$  multiprotein complex (Figure 2). Altogether, these

phosphorylation events promote cell migration and metastasis dissemination in different tumor types such as melanoma, renal, and lung carcinoma<sup>10</sup>.

It has been found that CDCP1 can also form a ternary complex with Src and EGFR and that this

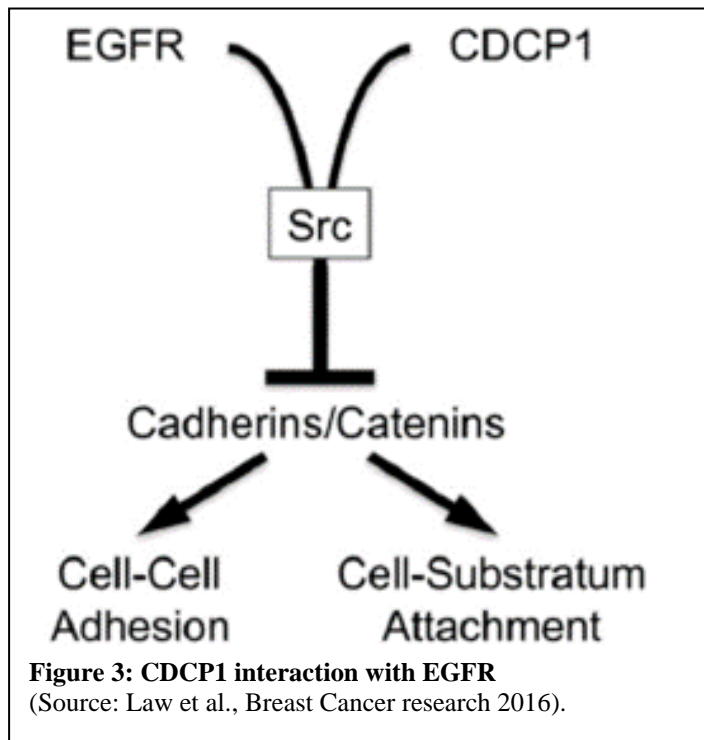


**Figure 3: CDCP1 interaction with EGFR**  
(Source: Law et al., Breast Cancer research 2016).

complex mediates Src activation and Src-dependent tyrosine phosphorylation of CDCP1 and EGFR. CDCP1/EGFR/Src ternary complex activates several signaling responses that contribute to cancer aggressiveness and metastasis spread (Figure 3)<sup>13</sup>. This ternary complex has also been used as a target for breast cancer therapy, thanks to Disulfide bond disrupting agents (DDAs). These compounds destroy this complex and,

therefore, could be used to avoid metastasis dissemination<sup>13</sup>.

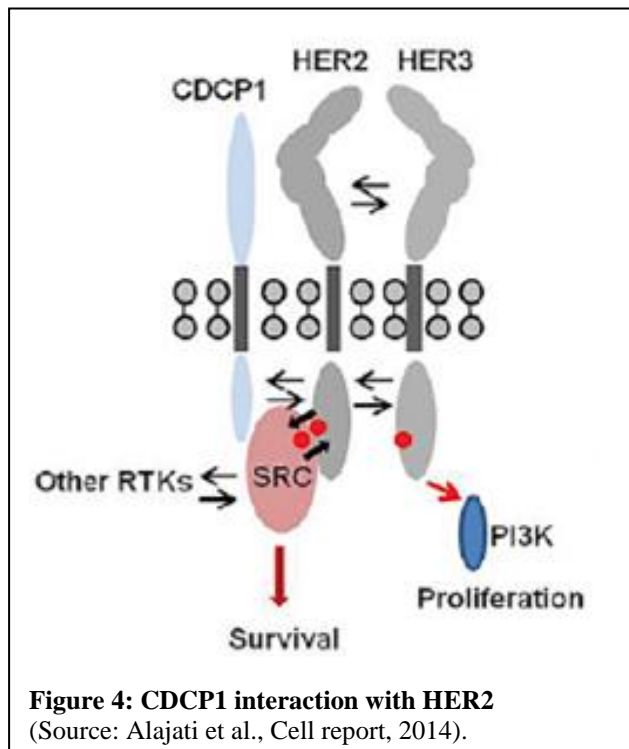


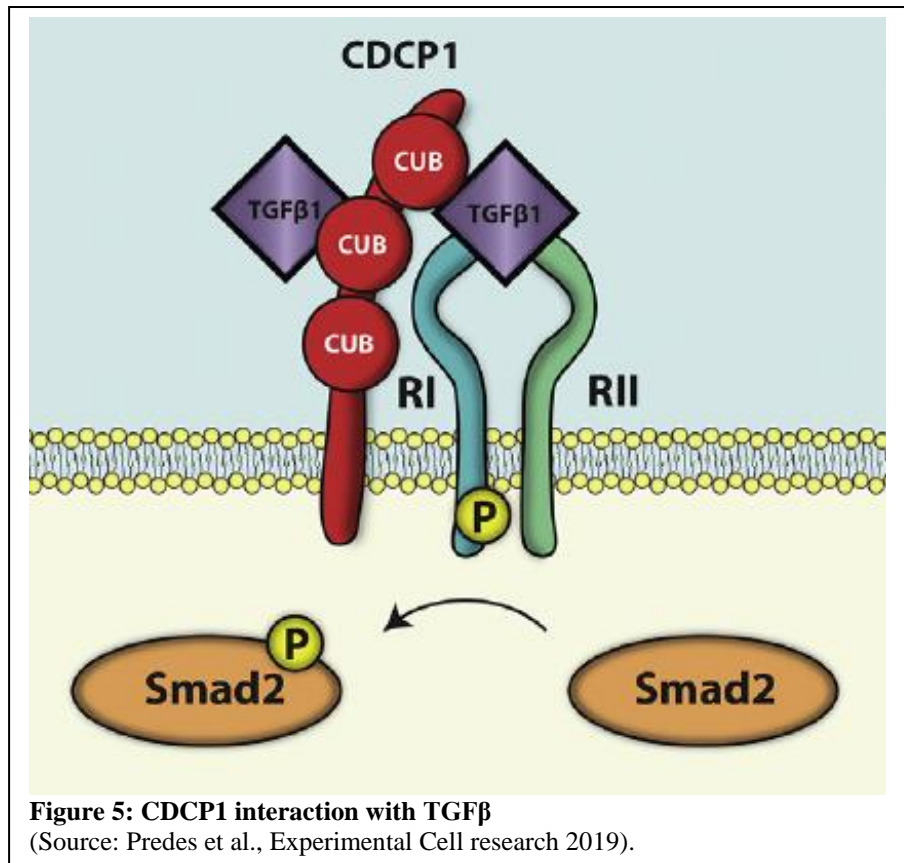
**Figure 4: CDCP1 interaction with HER2**  
(Source: Alajati et al., Cell report, 2014).

Another essential interaction of CDCP1 in breast cancer is its interaction with epidermal growth factor receptor 2 (HER2). It has been demonstrated that CDCP1 interacts with HER2, independently from Src activation, thanks to its ICD. The interaction of CDCP1 and HER2 results in SRC recruitment at the cell membrane, facilitating its interaction with HER2. Therefore, CDCP1 promotes HER2 phosphorylation, which in turn sustains the Src phosphorylation (Figure 4). This feedback loop led to Trastuzumab

resistance in breast cancer<sup>14</sup>.

It has also been demonstrated that the CUB domains of CDCP1 bind directly to TGF- $\beta$ 1 and activate its pathway in a Smad2 dependent manner, increasing Smad2 phosphorylation. This binding requires the activation of TGF $\beta$ RI but does not involve Src kinase activity. This binding also occurs with CDCP1 mutated form, Y734F and Y762F that are unable to bind Src<sup>10</sup>. ECD domain of CDCP1 interacts with TGF- $\beta$ 1, which could be responsible for tumor progression and metastasis in several organs (Figure 5).

It has been shown that CDCP1 associates with proteins involved in cell-cell adhesion and cell



adhesion to the extracellular matrix, including N- and P-cadherin and syndecans<sup>3</sup>, E-cadherin,<sup>15</sup> and  $\beta$ 1-integrin<sup>16</sup>.

#### 1.4 CDCP1 expression in tumors

Dysregulated expression of CDCP1 has been associated with several cancers. Compared with the relative normal tissue, elevated CDCP1 mRNA levels were also detected in several solid tumors, including colon, lung, and breast cancers. Awakura et al.<sup>17</sup> and Ikeda et al.<sup>18</sup> analyzed CDCP1 expression in 230 renal carcinoma and 200 lung adenocarcinoma patient samples, respectively. The former showed that CDCP1 is expressed in the normal kidney and in more of the 30% of tumor

samples. They also showed that CDCP1 overexpression in renal carcinoma correlates with advanced tumors and bad prognosis<sup>18</sup>.

Further, in lung adenocarcinoma, CDCP1 expression correlates with increased occurrence of lymph nodes metastasis and tumor relapse with five years disease-free and overall survival rates significantly lower for patients with high CDCP1 expression<sup>17</sup>.

A small study of breast cancers biopsies showed that CDCP1 expression correlates with Ki67 positivity, while in colon cancer, CDCP1 positivity correlates with a more aggressive colon cancer<sup>18</sup>. CDCP1 may also be an independent marker of leukemia, bone marrow, mesenchymal stem/progenitor cells, and neural cells.

Since normal B and T lymphocytes and granulocytes, monocytes, erythrocytes, and thrombocytes completely lack CDCP1 expression, its presence could be a good diagnostic marker for blood cancers<sup>19-21</sup>.

Notably, analysis of CDCP1 expression at protein levels in renal, lung, breast, and colon cancer shows that it is mainly present in epithelial tumors, and its overexpression is frequently associated with poor prognosis and tumor cells migration, as it allows cancer cells to survive and metastasize in the absence of cell adhesion<sup>10,13</sup>.

For all these reasons, CDCP1 represents a potential marker to target tumor cells. However, since tumors do not selectively express it, but also healthy tissues and stem/progenitor cells, treatments locally targeting CDCP1 are preferable to reduce undesired organ toxicity.

### **1.5 CDCP1 supports tumor cells proliferation**

Several studies exploiting cell lines both *in vitro* and *in vivo* demonstrated that CDCP1 expression stimulates cells proliferation. Uekita et al. showed that CDCP1 is bound to SFK in human lung cancer cell lines, where its phosphorylation is required to overcome anoikis and permit *in vitro* anchorage-independent growth<sup>11</sup>. Notably, although CDCP1 downregulation in A549 lung cancer cell lines does

not affect tumor growth in mice, it has a striking effect in reducing metastasis formation after tail vein injection<sup>11</sup>.

The same group also showed that CDCP1 expression promotes invasion and peritoneal dissemination in mice of gastric cancer cell lines.

This evidence indicates that CDCP1 is involved in cell migration, proliferation, and anchorage-independent growth. For this reason, its blockade could be helpful to prevent tumor metastasization.

### **1.6 CDCP1 as a therapeutic target**

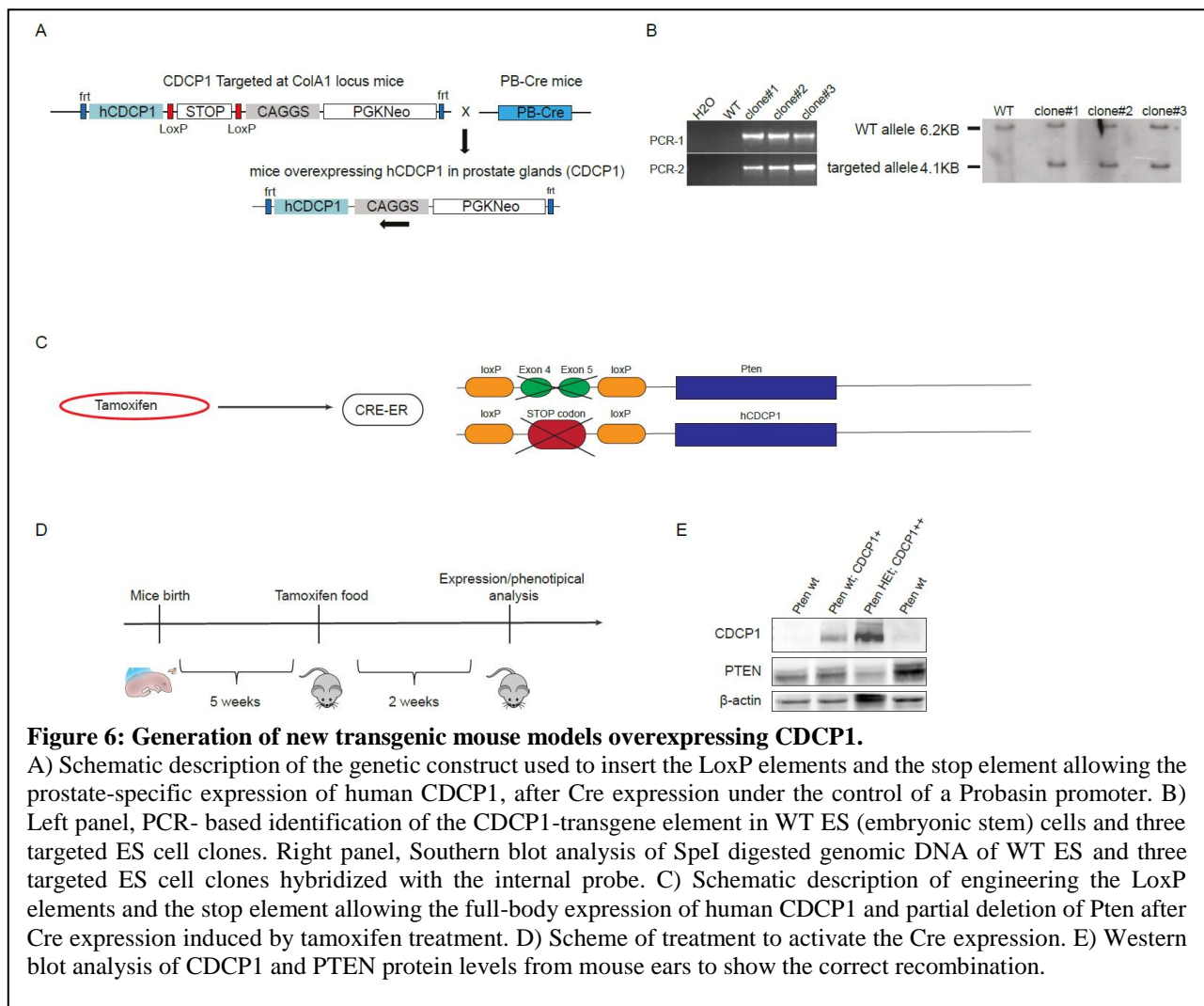
CDCP1 is expressed in several tumor types, and many studies identified it as responsible for cell proliferation, cell survival in the condition of non-attachment, cell resistance to anoikis, and metastasis dissemination<sup>10,11,13,20</sup>.

Furthermore, CDCP1 has been implicated in tumor resistance to cytotoxic chemotherapy agents, such as Gentamicin in pancreatic cancer, and allows cancer cells to resist cell death induced by targeted therapy, such as next-generation BCR-ABL inhibitors for leukemia<sup>22</sup>. CDCP1 is also frequently upregulated in breast cancer cells that acquire resistance to Trastuzumab, thus providing a new mechanism for therapy resistance<sup>14,23</sup>. CDCP1 is a transmembrane protein that can be easily targeted with monoclonal antibodies or small molecules. Indeed, monoclonal antibodies that degrade CDCP1 protein have already been developed for cancer therapy by different companies<sup>24,25</sup>. Interestingly, CDCP1 mRNA expression has been detected in a range of organs, including skeletal muscle, esophagus, and rectum, CDCP1 protein levels are much higher in tumor tissues (at least three times higher). Moreover, CDCP1 KO mice are born healthy and do not develop any syndromes. Finally, mice treated with CDCP1 antibodies did not show any signs of toxicity. Thus, CDCP1 is an excellent target for cancer therapy.

### **1.7 Generation of two different CDCP1 transgenic mouse models**

Since CDCP1 could have oncogenic potential in different tissue, we decided to focus our study on understanding and characterizing the tumorigenic impact of CDCP1 in different cancer models. To achieve this aim, we took advantage of new transgenic mouse models.

We generated four different transgenic mouse models overexpressing CDCP1. In these models, CDCP1 was overexpressed either alone or with the partial or complete loss of the tumor suppressor gene PTEN.



The mouse models we generated are described as follows:

1. The Probasin-CRE *Pten* CDCP1: we constructed a pCAGGS vector with a transcriptional STOP sequence flanked by loxP sites upstream of *CDCP1*-cDNA. The resulting pCAGGS-loxP-STOP-loxP-*CDCP1*-vector and PGK-FlpO plasmid were co-electroporated into the

ColA locus of modified embryonic stem cells KH2<sup>26</sup> (Figure 6A). PCR and Southern blot analysis confirmed gene integration and recombination events (Figure 6B). Next, we crossed CDCP1 mice with *PB-Cre4* mice for prostate-specific expression of CDCP1<sup>27</sup> (Figure 6A) in prostate epithelial cells.

2. The CRE-ER *Pten* CDCP1: CRE-ER mice are characterized by a total body inducible CRE, whose expression is induced upon tamoxifen treatment. We crossed these *CDCP1* mice and *Pten*<sup>loxP/loxP</sup> mice (Figure 6C). The result of this crossing is the full-body overexpression of CDCP1 and/or loss of one allele of *Pten* only after tamoxifen treatment<sup>28,29</sup>. To establish this model, we administered Tamoxifen to the mice at five weeks of age by food for two weeks (Figure 6D, E).

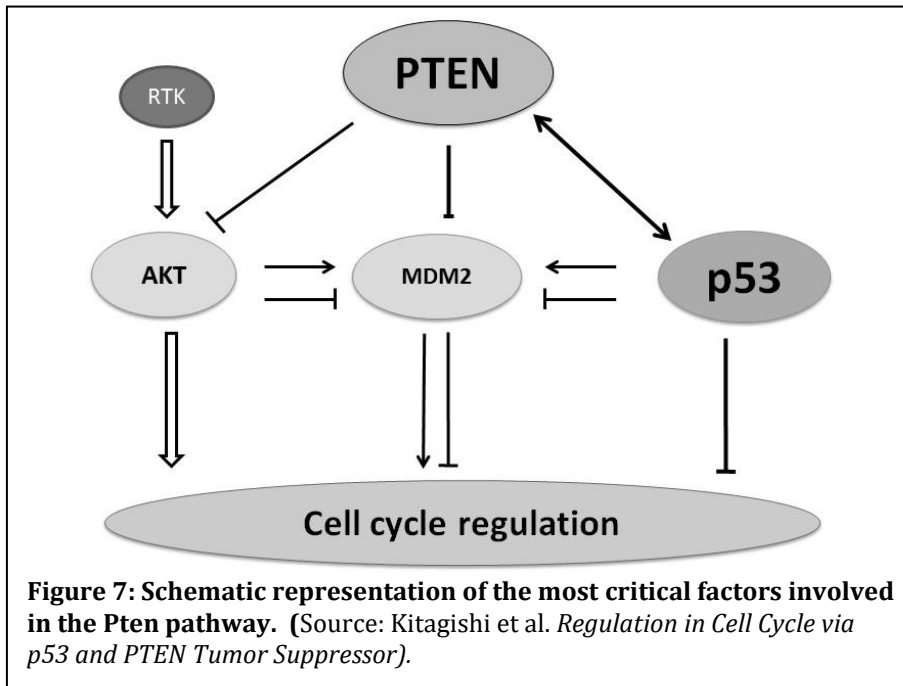
## 1.8 PTEN

Phosphatase and Tensin-Homolog-Gene (PTEN) is a tumor suppressor gene, and its inactivation, deletion, or somatic mutations can be associated with different types of cancer, like glioma, melanoma, carcinoma of the endometrium, kidney, breast, lung, and prostate<sup>30</sup>. It is one of the most mutated and deleted tumor suppressor genes in human cancer, and it is often found downregulated in the absence of genetic loss or mutation.

PTEN is a dual-specificity phosphatase located on chromosome 10q23: through its catalytic domain, it can dephosphorylate serine, threonine, and tyrosine residues. Two  $\alpha$ -helix motifs flank this catalytic core. The most diffused mutation in PTEN happens within exon 5, which encodes the catalytic domain, resulting in PTEN loss-of-function<sup>31</sup>.

PTEN achieves its tumor suppressor activity in two ways: (i) dephosphorylating phospho-proteins and phospho-lipids and (ii) negatively regulating the survival phosphoinositide 3-kinase (PI3K)/AKT pathway.

PTEN acts as a tumor suppressor gene converting the phosphatidylinositol-triphosphate (PIP3) in phosphatidylinositol-diphosphate (PIP2), preventing AKT activation. When PTEN is lost in tumor contest, AKT can be activated: this event correlates with uncontrolled cell proliferation, decreased apoptosis, and enhanced tumor angiogenesis (Figure 7)<sup>32</sup>.



PTEN chromosomal region shows high rates of loss of heterozygosity (LOH) in many human malignancies, but PTEN can also show point mutations or epigenetic mutations<sup>33</sup>. Approximately 70% of prostate cancer (PCa) patients exhibit mutation or

loss of PTEN; furthermore, PTEN is lost in 40% of metastatic PCa.

In PCa, the most frequent mutations in PTEN are large deletions and genomic rearrangements. PTEN deletion is not found in the benign glandular epithelium or low-grade prostatic intraepithelial neoplasia (PIN), but it is found in 23% of high-grade prostatic intraepithelial neoplasia (HGPIN) and in 68% of PCa. Thus, PTEN alterations give malignant potential to prostate cancer<sup>33</sup>.

When PTEN is deleted in prostate cancer, the expression of AR is also reduced, meaning that castration cannot be effective. The patients with PTEN deletion show castration resistance: they show after castration the re-growth of the tumor called hormone-refractory or prostate cancer castration-resistant (CRPC)<sup>34</sup>. PTEN deletion, predominantly heterozygous, was also found in lymphoma patients, particularly in Germinal center B cell (GCB) lymphoma, both in homozygosis and

heterozygosis. It can also be mutated in this disease, and the most common mutation is the loss-of-function alteration caused by reduced instability<sup>35</sup>.

## **1.9 Prostate cancer**

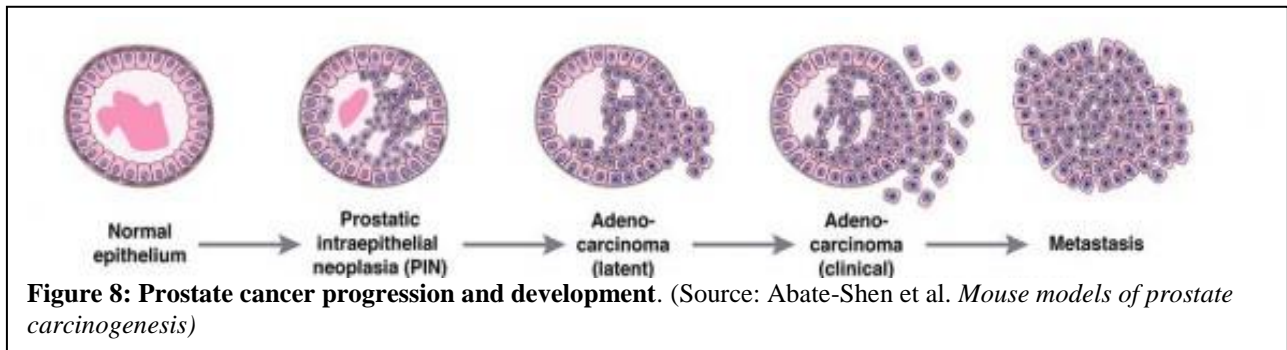
Prostate cancer (PCa) is the second leading cause of cancer-related deaths in males after lung cancer<sup>36</sup>. Despite recent progress, prostate cancer represents a major cause of cancer-related mortality and disease in men. The prostate cancer outcome is influenced by different risk factors, like age, race, nationality, diet, and family history. The only possible risk factor that can be controlled is diet. A diet low in fat is associated with a reduced risk of prostate cancer. The risk of developing this disease increases with age; indeed, more than 70% of all prostate cancers are diagnosed in men over age 65. Race is also considered a major risk factor. African Americans have the highest prostate cancer incidence rates in the world. Interestingly, the disease is common in North America and North-western Europe and rare in Asia, Africa, and South America<sup>37</sup>.

Another important risk factor for the onset of this pathology is the familiar background. For example, subjects primarily related to prostate cancer patients exhibit a higher risk of developing prostate cancer than men in the general population. Indeed, several evidence correlates prostate cancer with X-linked factors<sup>37</sup>.

While prostate cancer is an age-related disorder, various processes are also known to initiate prostate tumorigenesis, such as oxidative stress and DNA damage, genetic and epigenetic alterations, inflammation, genetic factors, and telomere-shortening. Although many of the risk factors for prostate cancer such as age, race, and family history cannot be controlled, early detection and screening methods have improved the outcome of PCa patients<sup>38</sup>.

The development of PCa is a multistep process: it begins with prostate hyperplasia characterized by cell proliferation, but the architecture of the glands remains unaffected; subsequently, when the proliferating cells start to invade the stroma surrounding the glands, PCa is called low-grade

intraepithelial neoplasia (LGPIN). During the progression of this disease, when the invasion of the stroma becomes massive, the phenotype of the tumor is classified as high-grade PIN (HGPIN). When the cells acquire migratory and invasive capacity, the local invasive PCa can reach distant tissues and



form new colonies that respect the original epithelium forming metastasis<sup>39</sup> (Figure 8). Prostate cancer cells are reported to metastasize to the lung, liver, and pleura, the most frequent site of metastasis remains to be in bone, referred to as osteoblastic lesions<sup>40,41</sup>. The transformation of a normal prostate epithelium can start with different events like the loss-of-function mutation of a tumor suppressor gene and the gain-of-function of an oncogene. When prostate cancer is diagnosed, conventional treatment regimens include surgical excision (radical prostatectomy), irradiation through external beam therapy, or implantation of radioactive “seeds” (brachytherapy). In advanced PCa, these therapies are followed or substituted by androgen deprivation therapy, which initially reduces the levels of Prostate-specific-antigen (PSA) in the blood due to tumor reduction. However, in most cases, the tumor relapses. For these reasons, the current research is trying to find new therapeutic strategies that can cooperate with androgen deprivation to eradicate prostate cancer<sup>38</sup>.

The use of genetically engineered mouse models has significantly enhanced our understanding of different stages of the disease, including the molecular mechanisms of metastasis<sup>42,43</sup>. One of the most frequently lost genes in advanced and metastatic prostate cancer is PTEN<sup>44</sup>. Loss of Pten alone gives rise to invasive adenocarcinoma. However, its combination with other genetic alterations, such as mutations in KRas<sup>45</sup> and loss of Smad4<sup>46</sup>, triggers the metastatic potential of these tumors. Interestingly, constitutive activation of MAPK pathway through KRas mutation or loss of Smad4

alone does not lead to prostate carcinoma, suggesting a potential role of Pten-loss in initiating tumorigenesis.

### **1.10 Lymphoma**

Lymphomas are highly heterogeneous diseases, varying by both the type of malignant cell and the tumor location. They most frequently originate from B cells, and the two main groups of B-cell lymphomas, B-cell non-Hodgkin lymphomas (NHL) and Hodgkin lymphomas (HL), account for about 80% and 15% of all lymphomas<sup>47</sup>.

NHL is the most common in the developed world, with the highest incidence rates in the USA, Australia, New Zealand, and Europe, and the lowest in Eastern and South Central Asia. However, the rare T-cell neoplasms are more common in Asia than in other regions. The most common NHL subtypes by far in developed countries are diffuse large B-cell lymphoma (DLBCL) (about 30%) and follicular lymphoma (FL) (about 20%). All other NHL subtypes have a frequency of less than 10%. Many subtypes are characterized by a slight preponderance of males, most striking in mantle cell lymphoma (70% males), whereas females predominate in follicular lymphoma. NHL is the sixth most common cause of cancer-related death in the USA after prostate, breast, lung, colorectal, and bladder cancer<sup>48</sup>.

About 95% of the lymphomas are of B-cell origin, and the remaining are T-cell malignancies. This might be surprising at first glance, given the similar frequency of B and T cells in the human body, but it is understandable considering the specific factors that influence the pathogenesis of B-cell lymphomas. Various types of B-cell lymphoma can have very different clinical behaviors and therefore require different treatment strategies.

DLBCL is the most common and heterogeneous type of B-cell lymphoma. It can be classified into two molecularly distinctive subtypes: (i) germinal center B-cell-like (GCB) and (ii) activated B-cell-like (ABC)<sup>49</sup>.

GCB lymphoma derives from the clonal expansion of a Germinal center B cell, reflecting the highly dynamic nature of the structures that B cell forms transiently in secondary lymphoid organs upon encountering a foreign pathogen, enabling the generation and selection of clones with high-affinity antibodies<sup>50</sup>.

The fundamental immunological function of the GC comes with a dangerous downside: the exact genetic mechanisms that enable the development of high-affinity immunoglobulin receptors of different isotype classes are involved in the malignant transformation of B cells<sup>51</sup> (Figure 9).

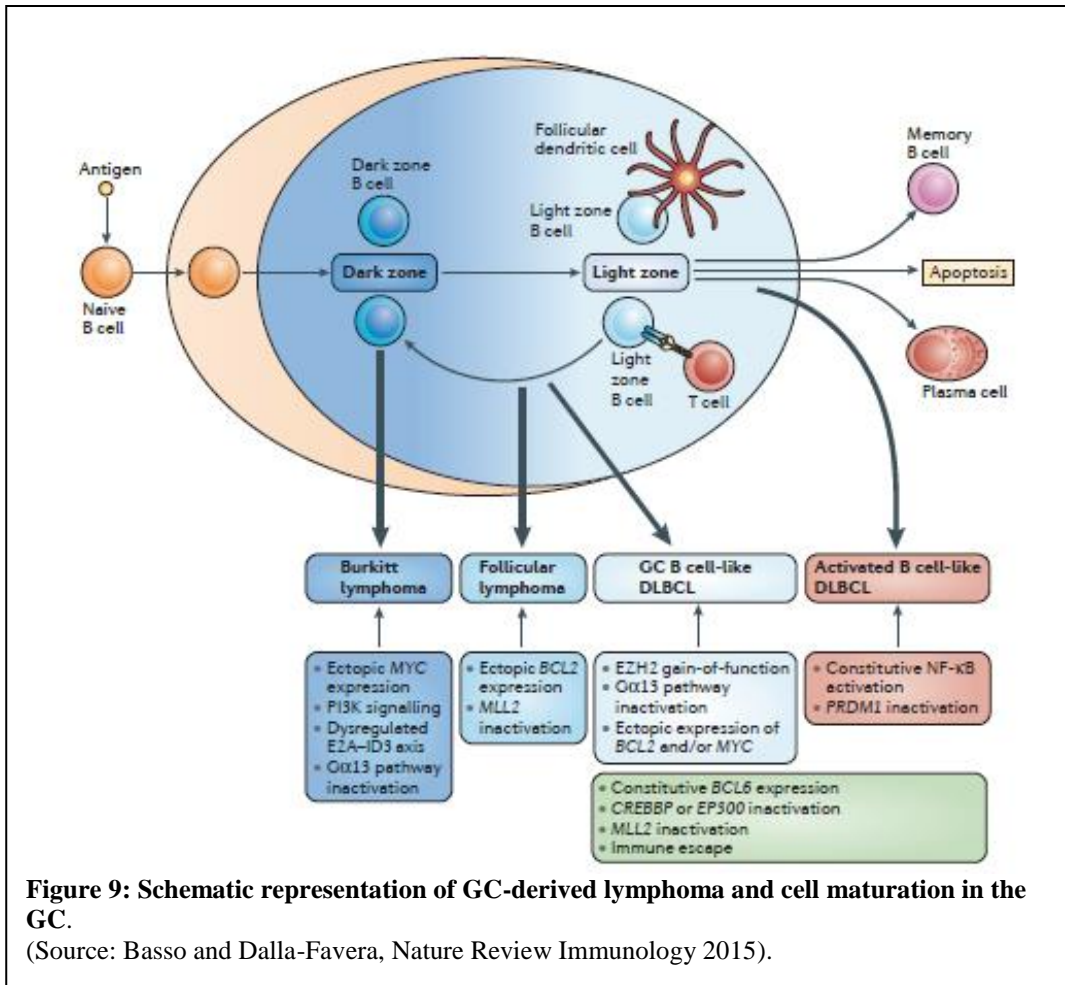
To better characterize these diseases, animal models have become very useful since they can reflect the intrinsic heterogeneity of these kinds of cancers, therefore allowing to perform experiments in a model closer to patients.

The murine models of B-cell lymphoma can be either spontaneous or induced in transgenic mice or by various types of transfer of tumor cells into wild-type mice.

The most known mouse model to study lymphoma is the one carrying c-Myc overexpression. One of the most used is the E $\mu$ -myc transgenic mouse model for the study of B-cell lymphoma; these mice develop B-cell lymphomas at 100% incidence rate<sup>47</sup>.

Another transgenic mouse in the lymphoma field is the one carrying the translocation of the N-Myc gene under the IgH enhancer and with only a subtle modification of the endogenous Myc expression level, thus resulting in an indolent disease and only 25% incidence after 9 to 12 months<sup>47</sup>.

To understand the mechanisms linked to lymphomagenesis in more detail, researchers have introduced more strategies to transfer variously modified tumor cells into immunodeficient or immune-compromised hosts. These approaches introduce the potential bias of tumor injection to specific tissue sites and cannot follow the progressive induction and development of tumors from a few malignant cells. Despite these weaknesses, tumor injection models are instrumental because they let us study the impact of different mutations on tumor aggressiveness<sup>47</sup>.



## 2. Aims

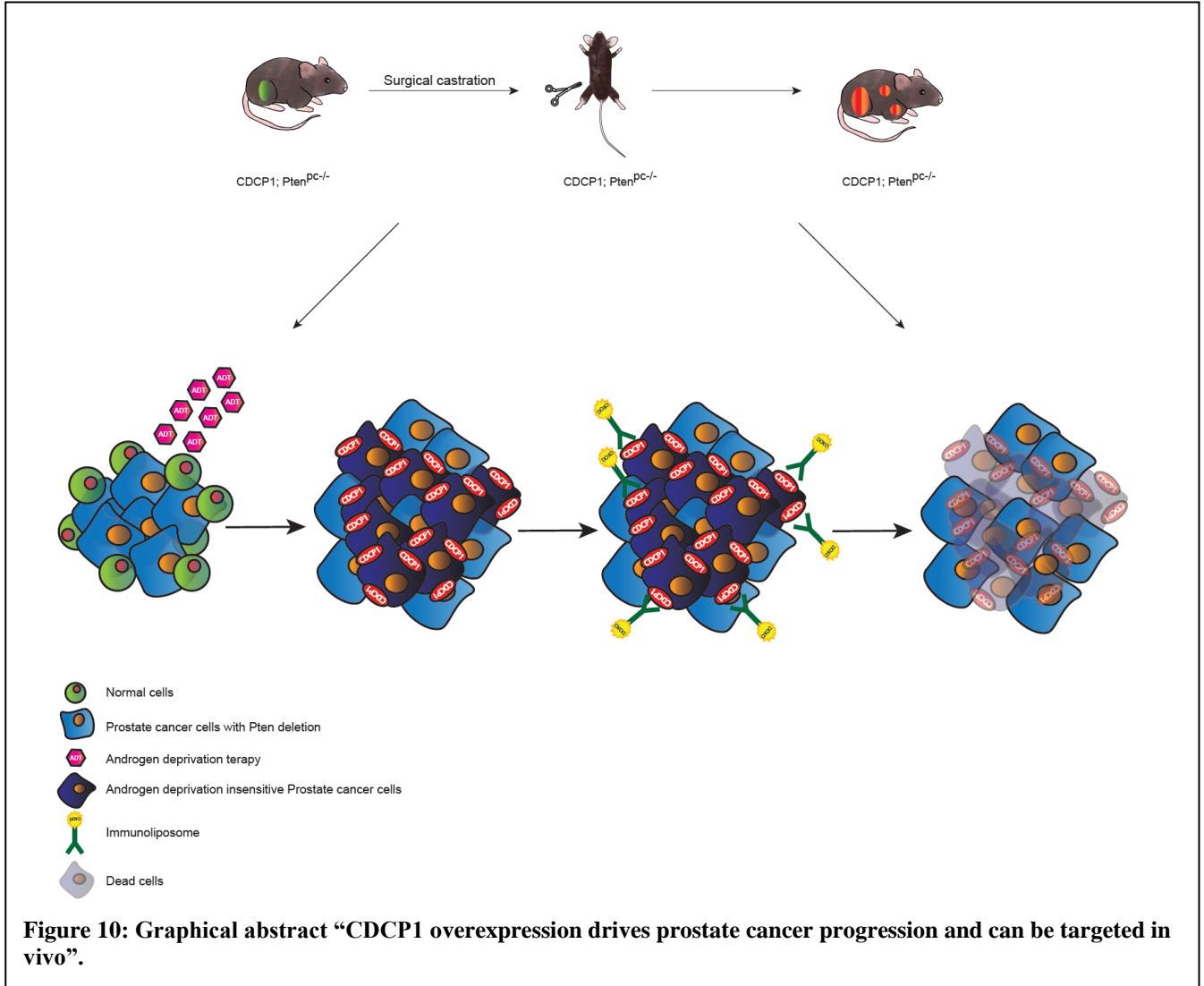
The aims of CDCP1 overexpression in prostate cancer (PCa) context:

- Characterize the role of CDCP1 overexpression in prostate cancer development.
- Assess how CDCP1 overexpression drives metastatic castration-resistant prostate cancer (mCRPC).
- Explore CDCP1 ability as a therapeutic target in androgen-independent context.
- Use CDCP1 monoclonal antibodies (mAb) or immune-liposomes (ILs) in combination with Enzalutamide in mice affected by castration-resistant PCa.

The aims of CDCP1 full-body overexpression are:

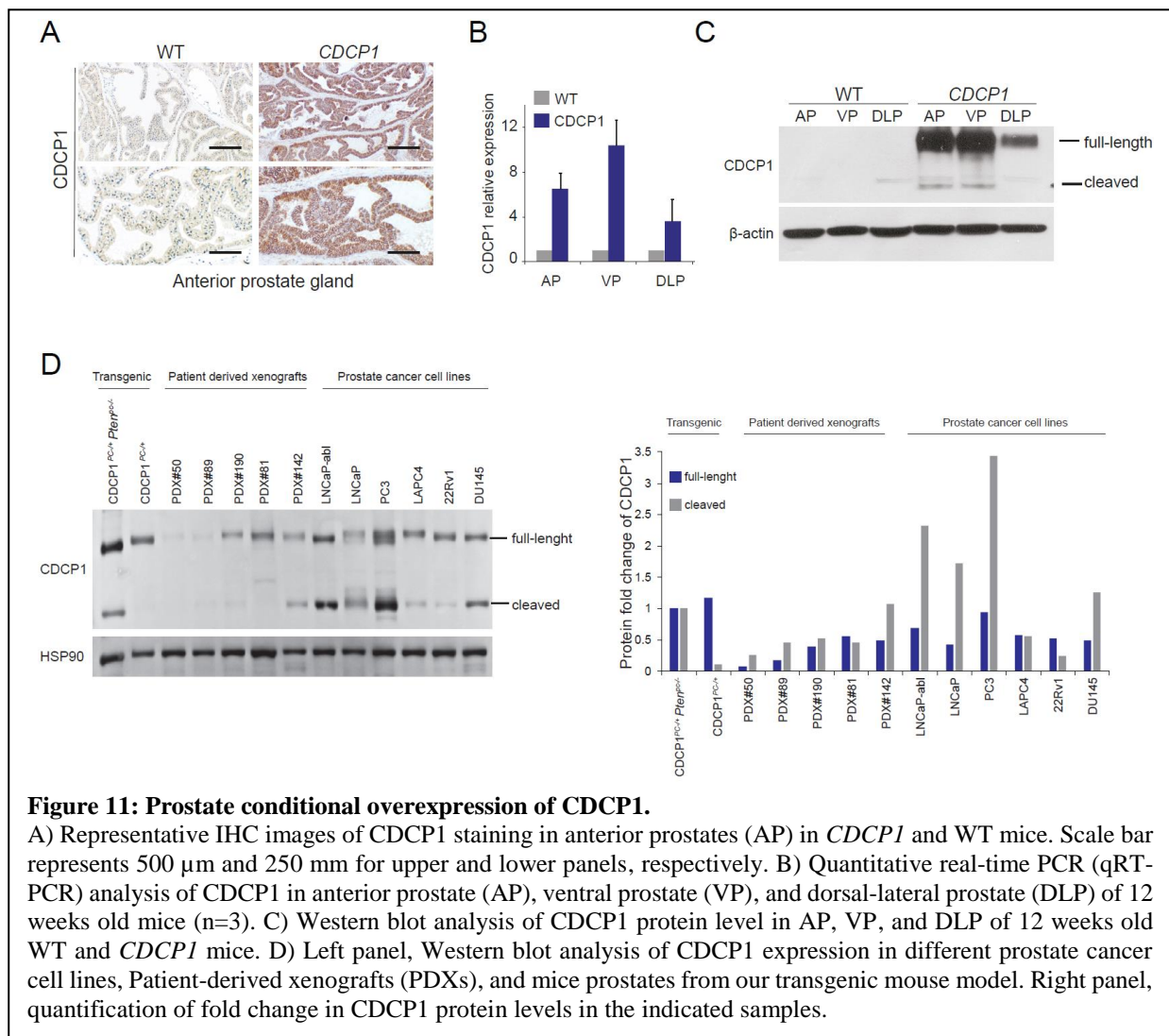
- Characterize the role of CDCP1 overexpression in other tissues.
- Investigate the potential oncogenic role of CDCP1 full-body overexpression, alone or in combination with loss of *Pten*.
- Evaluate CDCP1 as a target for therapy in different cancer types.

### 3. Results: CDCP1 overexpression drives prostate cancer progression and can be targeted in vivo



### 3.1 Generation of the prostate Conditional CDCP1 model

In order to characterize the role of CDCP1 in PCa, we crossed *CDCP1* mice with *Pb-Cre4* mice for prostate-specific expression of CDCP1<sup>27</sup>. IHC, RT-PCR, and western blot analyses were performed on prostate tissues of 10-weeks old *CDCP1*; *Pb-Cre* mice (*CDCP1*<sup>pcLSL/+</sup>, hereafter referred to as CDCP1) and confirmed the prostate-specific expression of CDCP1 (Figure 11A-C). Of note, the expression of CDCP1 in a panel of human prostate tumor cell lines, patient-derived prostate cancer xenografts (PDXs), and tumors collected from CDCP1+ mice did not show significant differences in the CDCP1 levels (Figure 11D), thereby demonstrating that overexpression of CDCP1 in our mouse model is similar to the CDCP1 levels in human tumors.



Next, we examined tumor incidence in *CDCP1* mice over 24 months. *CDCP1* mice developed prostate hyperplasia between 4-6 months of age at 50% penetrance. Following on, *CDCP1* mice between 7-9 months of age developed a high penetrance of PIN. These mice developed high-grade PIN (HGPN) lesions after 14 months of age with 100% penetrance and showed high Ki67 expression (Figures 12A-C). These data show that *CDCP1* alone can induce PCa development. In parallel, western blot analysis revealed a significant increase of Src and Erk1/2 phosphorylation in the prostatic epithelium of *CDCP1* mice and *CDCP1*+ MEFs derived from this model (Figure 12D-E).

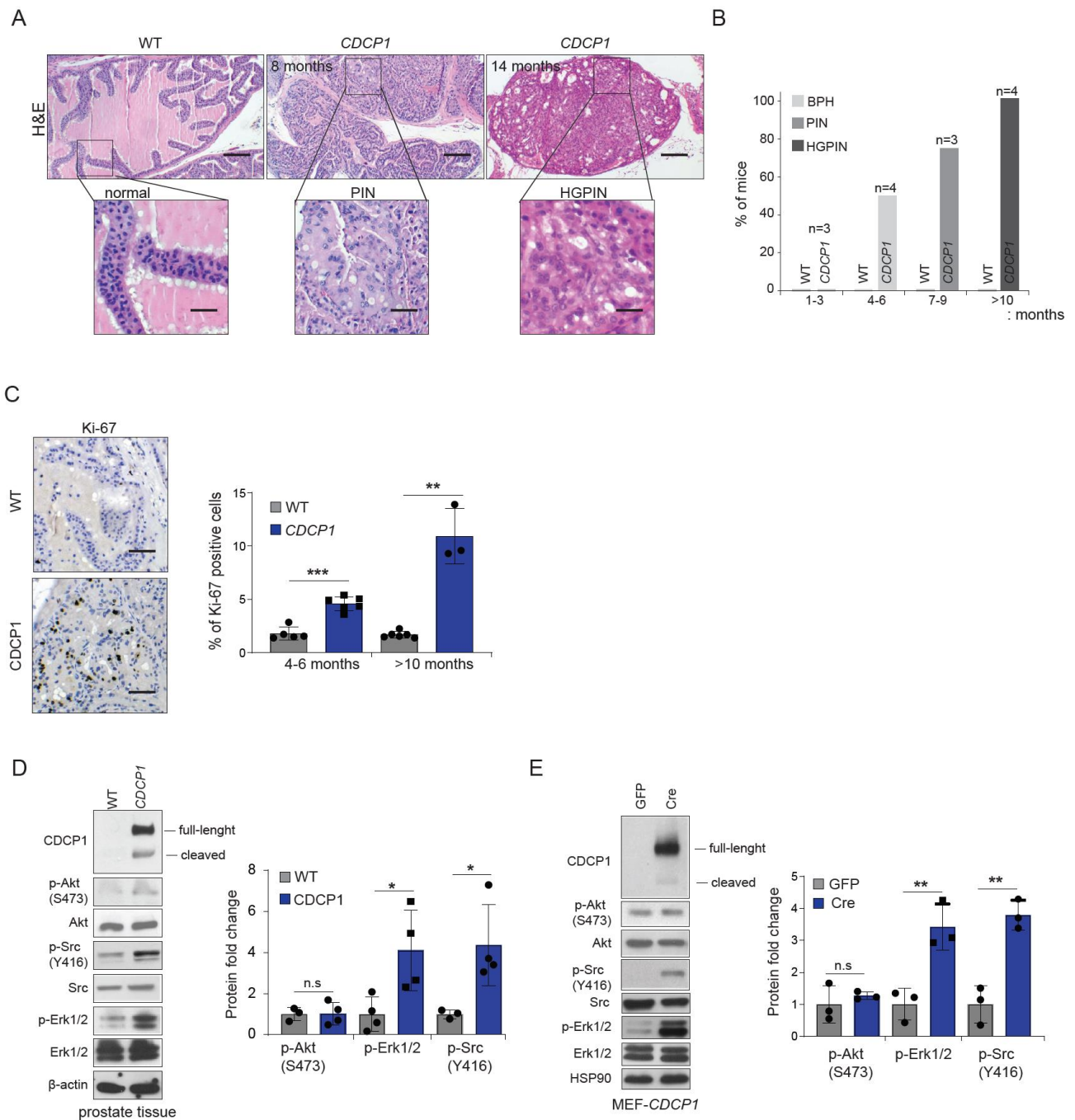


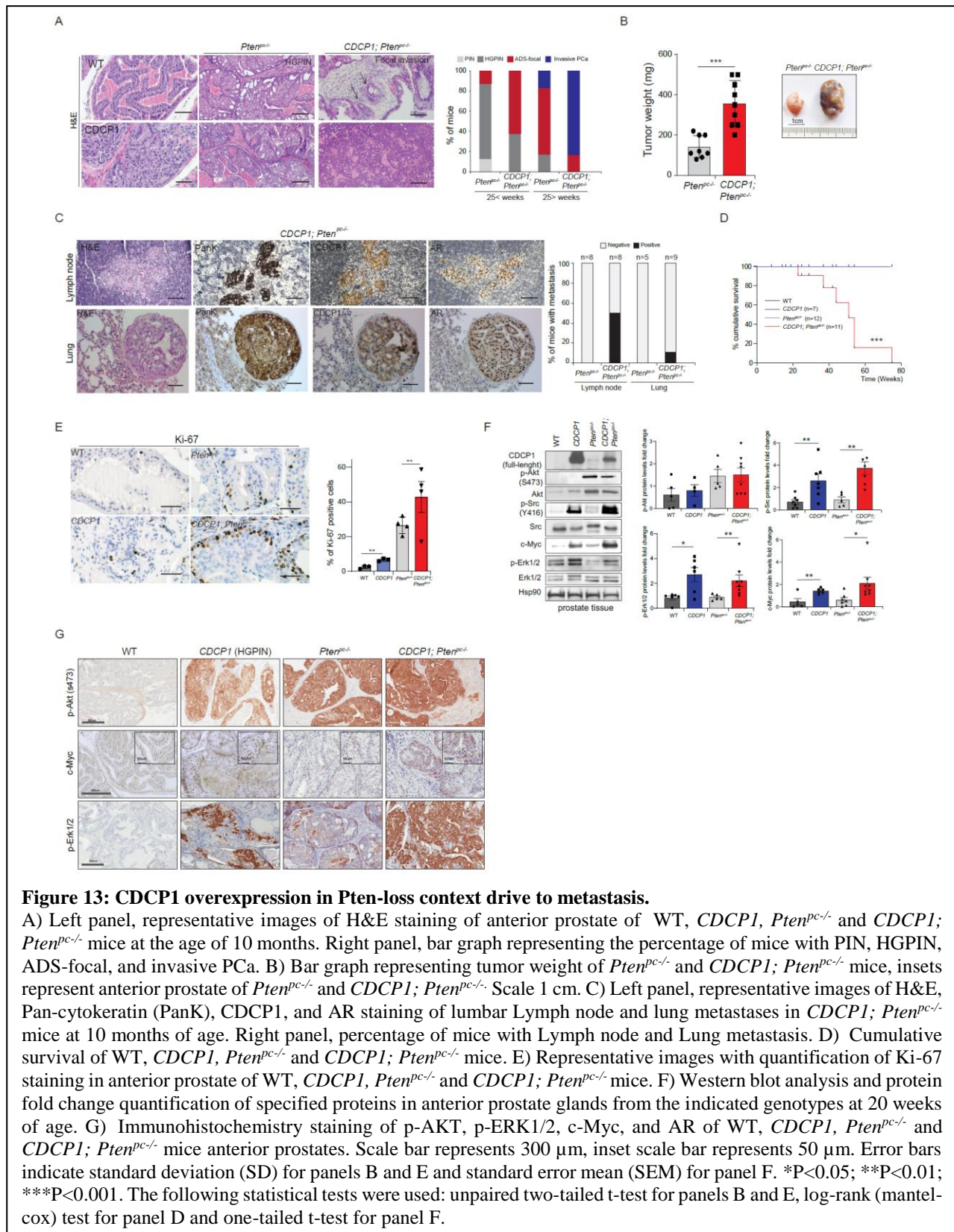
**Figure 12: CDCP1 overexpression in prostate induce PIN and HGPIN.**

A) Representative images of H&E staining of anterior prostate of WT and *CDCP1* mice. Boxes represent regions in higher magnification in WT mice, prostatic intraepithelial neoplasia (PIN), and High-grade PIN (HGPIN) in *CDCP1* mice. Scale Bar represents 5 mm. B) Histopathological characterization and quantification of the prostate in WT and *CDCP1* mice. C) IHC staining with quantification of Ki-67 in representative anterior prostate of over 10 months old WT and *CDCP1* mice. Scale Bar represents 5 mm (n=3 to n=7 for each genotype). D) Western blot analysis with quantification of major downstream targets of CDCP1 signaling in anterior prostates of 4 months old WT and *CDCP1* mice. p-Akt, p-Erk1/2, and p-Src are normalized to their total proteins in *CDCP1* prostates compared to WT prostates (n = 4). E) Western blot analysis with quantification of major downstream targets of CDCP1 signaling in mouse embryonic fibroblast (MEFs) from *CDCP1* transgenic mice infected with retroviral vector overexpressing GFP or Cre. p-Akt, p-Erk1/2, and p-Src are normalized to their total proteins in transgenic MEF-*CDCP1* infected with GFP or Cre retro-virus vectors (n = 3). Error bars indicate standard deviation (SD). \*P<0.05; \*\*P<0.01; \*\*\*P<0.001. Statistical test used: 2-tailed t-test.

### 3.2 CDCP1 overexpression in *Pten*-loss genetic background drives to metastasis

To further model the interplay between *Pten* and CDCP1 *in vivo*, we crossed *CDCP1* mice with *Pten*-null prostate conditional mice (*Pten<sup>pc-/-</sup>*) to obtain *CDCP1; Pten<sup>pc-/-</sup>* double mutant mice. While mono-allelic loss or mutations in *PTEN* is associated with benign prostate tumors<sup>27,52</sup>, complete loss of *PTEN* is frequently observed in human metastatic prostate cancers<sup>53</sup>. However, complete loss of *Pten* in the mouse is not sufficient to promote metastatic prostate cancer, and additional genetic hits are needed to promote the onset of metastases<sup>36</sup>. Strikingly, by the age of 25 weeks, *CDCP1; Pten<sup>pc-/-</sup>* mice develop focally invasive adenocarcinoma, which over time, progresses to highly aggressive carcinoma at later time points, a phenotype that has never been observed in *Pten<sup>pc-/-</sup>* mice (Figure 13A). Notably, the macroscopic analysis showed a significant increase in weight and volume of *CDCP1; Pten<sup>pc-/-</sup>* tumor compared to their counterparts (Figure 13B). Importantly, histopathological analysis of *CDCP1; Pten<sup>pc-/-</sup>* mice revealed metastatic spread of epithelial tumor nodules, positive for Pan-Cytokeratin (PanK), CDCP1 and AR, to draining lumbar lymph nodes in 50% of the cases (n=4/8) analyzed and to the lung in 11% of cases (n=1/9) (Figures 13C). The histological features of these metastases resembled those of the primary prostate tumors. By contrast, *Pten<sup>pc-/-</sup>* mice did not develop metastasis, as previously reported<sup>36,46,54</sup>. Additionally, Kaplan-Meier cumulative survival analysis showed that *CDCP1; Pten<sup>pc-/-</sup>* mice died or had to be euthanized due to extensive tumor burden at the age of 60-80 weeks (Figure 13D).

Of note, none of the age-matched *Pten*<sup>pc-/-</sup> mice died, indicating a profound effect of CDCP1 overexpression on the survival of *Pten*<sup>pc-/-</sup> mice.



Moreover, the percentage of Ki-67 positive cells was significantly higher in *CDCP1; Pten<sup>pc/-</sup>* mice when compared to their counterpart mice (Figure 13E). At the molecular level, western blot analysis revealed that *CDCP1; Pten<sup>pc/-</sup>* tumors showed elevated levels of Src and p-Erk1/2 while p-Akt was not changed compared to *Pten<sup>pc/-</sup>* tumors (Figure 13F). Since activated Src is known to regulate c-Myc levels<sup>55-57</sup>, we reasoned that CDCP1 overexpression could drive c-Myc overexpression through Src. Indeed, CDCP1 overexpressing tumors showed increased levels of c-Myc expression (Figure 13F). Furthermore, IHC analysis revealed high c-Myc and p-Erk1/2 in *CDCP1; Pten<sup>pc/-</sup>* tumors compared to *Pten<sup>pc/-</sup>* tumors (Figure 13G).

### **3.3 CDCP1 overexpression in *Pten*-loss context drives to CRPC**

We next checked whether CDCP1 could also promote resistance to androgen deprivation therapy (ADT). To this end, we performed surgical castration in both *Pten<sup>pc/-</sup>* and *CDCP1; Pten<sup>pc/-</sup>* mice. While *Pten<sup>pc/-</sup>* tumors responded to castration as previously reported<sup>58</sup>, *CDCP1; Pten<sup>pc/-</sup>* did not, as shown by tumor weight, volume, histopathological analysis, and IHC for Ki-67 (Figure 14A-D). Resistance to castration in *CDCP1; Pten<sup>pc/-</sup>* tumors were associated with higher p-Src, p-Erk1/2 and c-Myc compared to *Pten<sup>pc/-</sup>* tumors, thus explaining the emergence of CRPC in this genetic background (Figure 14F-G). These data were additionally validated *in vivo* by challenging C57BL/6 mice with prostate epithelial TRAMP-C1 cells overexpressing CDCP1 (TRAMP-C1-CDCP1). Overexpression of CDCP1 in TRAMP-C1 cells significantly increased the levels of p-Src and p-Erk1/2 (Figure 14H), accelerated the emergence of castration-resistance and shortened the survival of TRAMP-C1-CDCP1 mice when compared to the control group (Figure 14I).

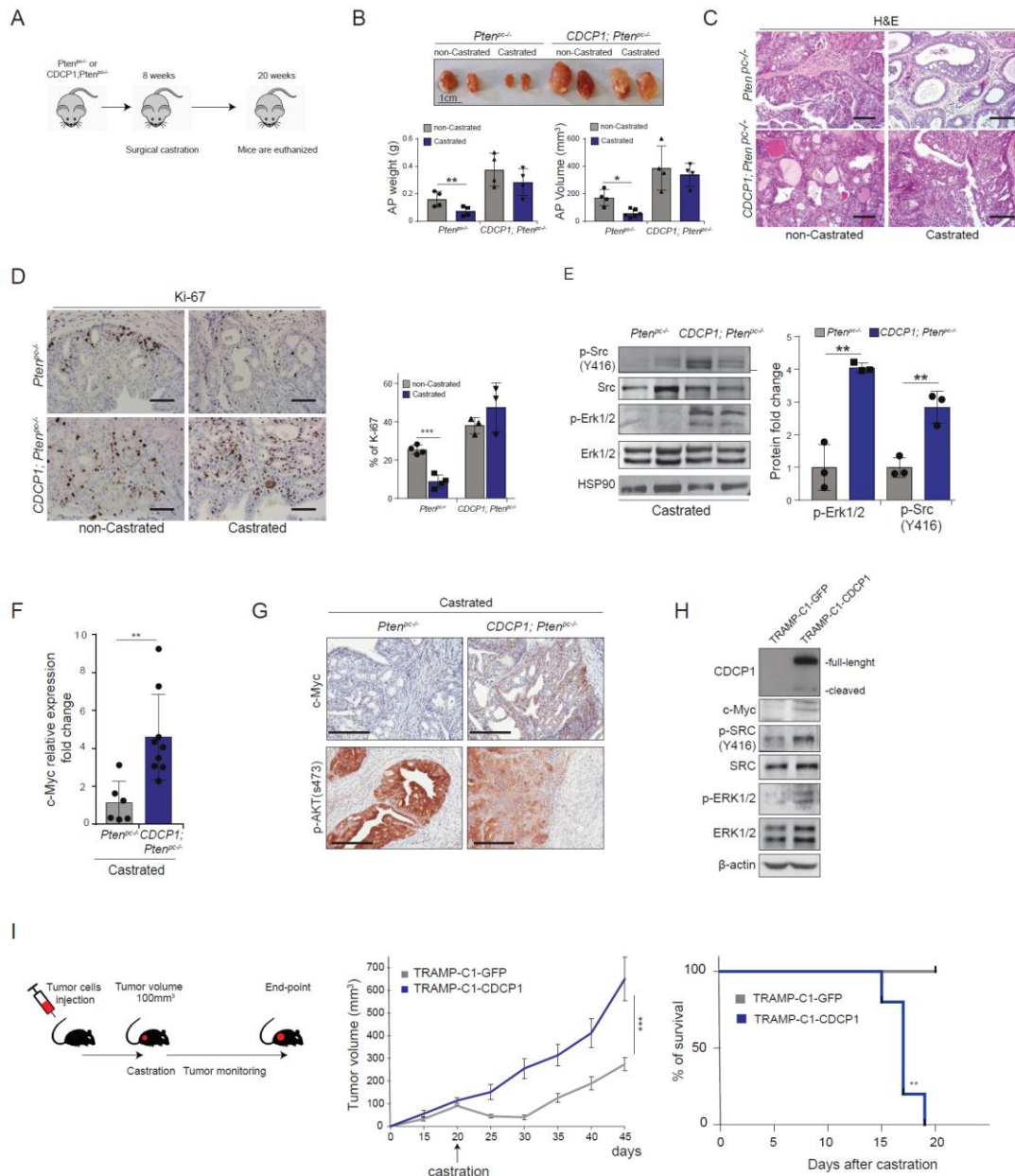


**Figure 14: CDCP1 overexpression in *Pten*-loss context drive to CRPC.**

A) Schematic representation of mice castration experiment. B) Representative images and weights quantification of anterior prostate of *Pten*<sup>pc-/-</sup> and *CDCP1*; *Pten*<sup>pc-/-</sup> non-castrated and castrated animals. Scale 1 cm (n=4). C) Representative images of H&E staining of *Pten*<sup>pc-/-</sup> and *CDCP1*; *Pten*<sup>pc-/-</sup> anterior prostate of non-castrated and castrated mice. Scale bar represents 5 mm length. D) Representative images with quantification of KI67 staining of *Pten*<sup>pc-/-</sup> and *CDCP1*; *Pten*<sup>pc-/-</sup> anterior prostate of non-castrated and castrated mice. Scale bar represents 5 mm length (n=3-4). (E) Western blot analysis and protein fold change quantification of indicated protein in the anterior prostate of *Pten*<sup>pc-/-</sup> and *CDCP1*; *Pten*<sup>pc-/-</sup> castrated mice at 20 weeks of age. F) c-Myc relative expression fold change in *Pten*<sup>pc-/-</sup> and *CDCP1*; *Pten*<sup>pc-/-</sup> castrated mice. G) Representative image of IHC staining of c-Myc and p-AKT (s473) in *Pten*<sup>pc-/-</sup> and *CDCP1*; *Pten*<sup>pc-/-</sup> castrated mice. Scale bar represents 200  $\mu$ m. H) Western blot analysis of CDCP1, c-Myc, p-Src, Src, p-Erk1/2 and Erk1/2 in TRAMP-C1-GFP and TRAMP-C1-CDCP1 mouse prostate cancer cell lines. I) Left panel, representative scheme of TRAMP-C1 allograft experiment. Middle panel, Allograft tumors volume (mm<sup>3</sup>) of TRAMP-C1-GFP and TRAMP-C1-CDCP1 cells. (n=5 in both groups). Right panel, percentage of cumulative survival of TRAMP-C1-GFP and TRAMP-C1-CDCP1 allografts. Error bars indicate standard deviation (SD). \*P<0.05; \*\*P<0.01; \*\*\*P<0.001. Statistic tests used: two-tailed t-test for panels A, D, E, F and I (middle panel), log-rank (mantel-cox) test for panel I.

### 3.4 CDCP1 overexpression leads to senescence evasion

Previous evidence demonstrated that *Pten*<sup>pc-/-</sup> mice develop indolent tumors characterized by a senescence response, which acts as an intrinsic barrier that constrains prostate cancer progression<sup>36,52</sup>. Since CDCP1 accelerates tumor progression in *Pten*<sup>pc-/-</sup> mice, we tested whether CDCP1 overexpression in this genetic background could promote senescence evasion both *in vitro* and *in vivo*, leading to metastasis. Prostate sections of the various genotypes (WT, CDCP1, *Pten*<sup>pc-/-</sup> and CDCP1; *Pten*<sup>pc-/-</sup>) were analyzed for senescence response by performing Senescence associated  $\beta$ -galactosidase (SA- $\beta$ -gal) and p-HP1 $\gamma$ , staining, two markers of senescence *in vivo*<sup>59</sup>. While *Pten*<sup>pc-/-</sup> tumors exhibit a strong cellular senescence response, CDCP1; *Pten*<sup>pc-/-</sup> tumors stained negative for both SA- $\beta$ -gal and p-HP1 $\gamma$  and positive for Cyclin D1, a marker of cell proliferation, thereby demonstrating that CDCP1 bypasses the senescence response driven by *Pten*-loss (Figure 15A). CDCP1; *Pten*<sup>-/-</sup> MEFs also stained negative for SA- $\beta$ -gal and exhibited increased cell proliferation with an elongated phenotype compared to *Pten*<sup>-/-</sup> MEFs (Figure 15B).

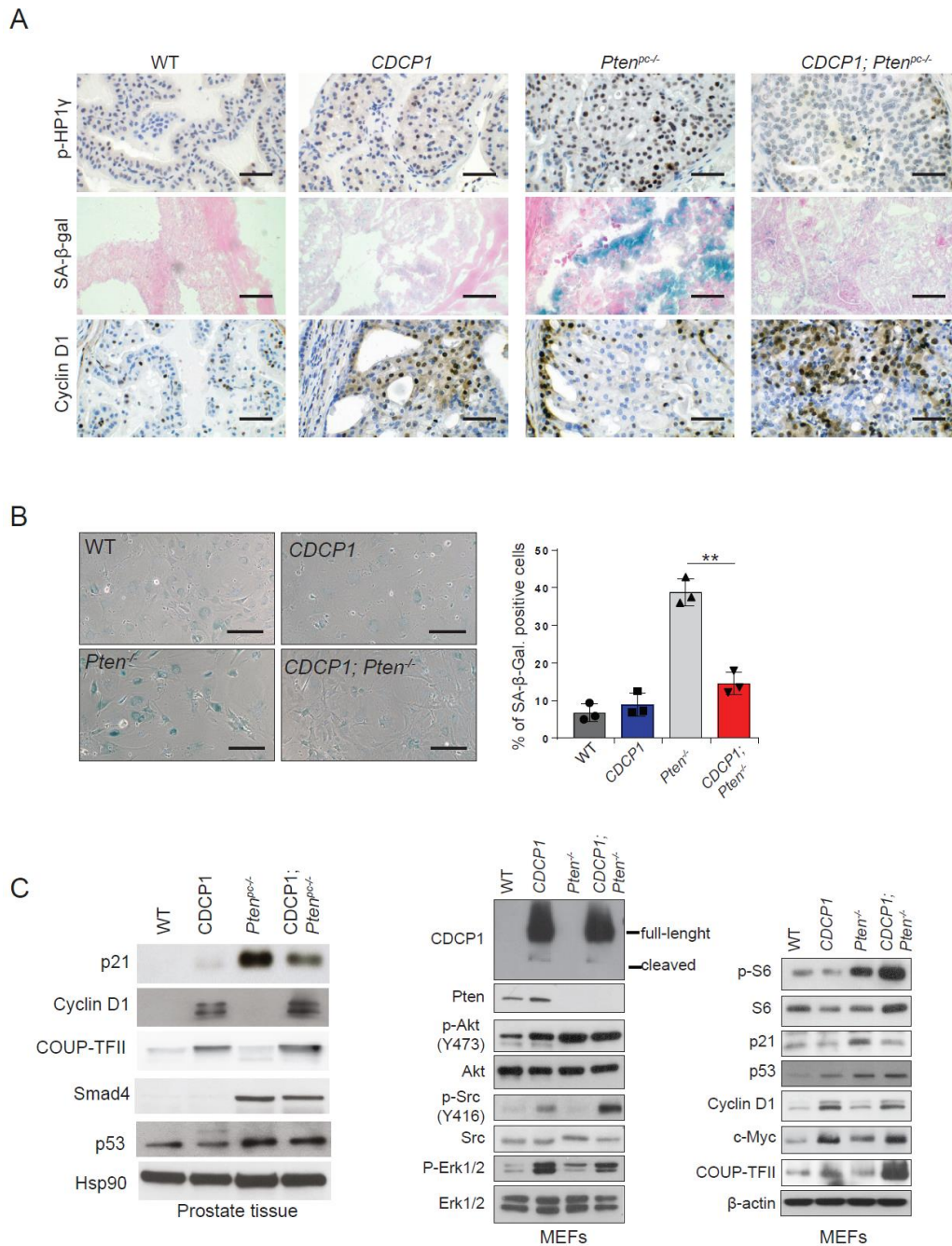


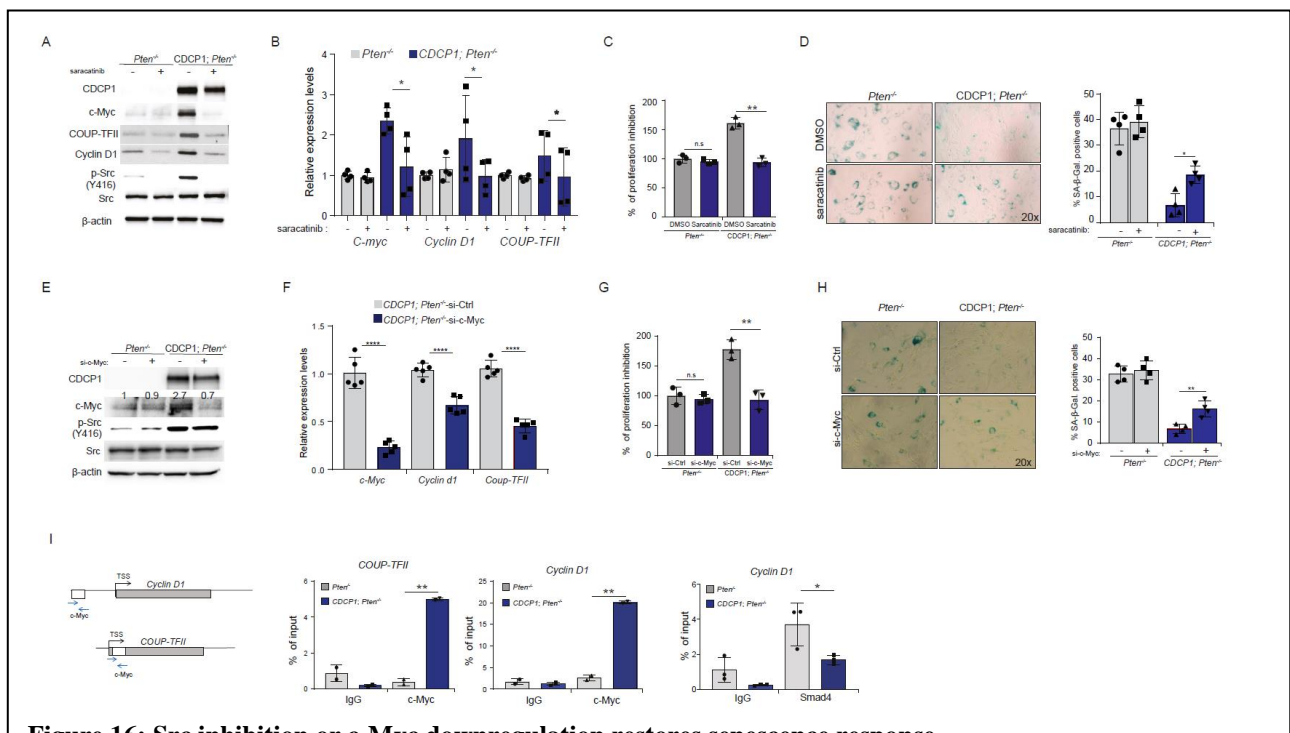
**Figure 15: CDCP1 overexpression lead to senescence evasion**

A) Representative images of p-HP1 $\gamma$ , Sa- $\beta$ -gal and Cyclin D1 in WT, *CDCP1*, *Pten<sup>pc/pc</sup>* and *CDCP1; Pten<sup>pc/pc</sup>* mice anterior prostates. Scale Bar represents 5 mm. B) Representative images and quantification of SA- $\beta$ -Gal staining in WT, *CDCP1*, *Pten<sup>pc/pc</sup>* and *CDCP1; Pten<sup>pc/pc</sup>* MEFs (n=3). Scale bar represents 5 mm length. C) Western blot analysis in mouse prostate tissues and MEFs of the indicated markers. Error bars indicate standard deviation (SD). \*\*P<0.01. Statistic tests used: two-tailed t-test for panel B.

Two recent independent reports showed that TGF $\beta$ /Smad4 pathway upregulation triggered by PTEN loss constrains prostate cancer progression by blocking Cyclin D1 transcription<sup>46,54</sup>. Of interest, overexpression of COUP-TFII, which inhibits Smad4-dependent transcription, promotes senescence

evasion by releasing Cyclin D1 expression in *Pten* null cells<sup>46,54</sup>. Thus, we compared the status of several components involved in these pathways such as p53, p21, Smad4, Cyclin D1 and COUP-TFII in *Pten*<sup>pc-/-</sup> and *CDCP1; Pten*<sup>pc-/-</sup> tumor samples. While our analysis showed that Smad4 and p53 expression did not change in *CDCP1; Pten*<sup>-/-</sup> MEFs and tumors compared to control groups, Cyclin D1 and COUP-TFII levels were significantly altered (Figure 15C). These data suggest that CDCP1 allows *Pten*-null benign tumors to acquire metastatic potential through the evasion of the TGFβ-induced senescence barrier by increasing the level of COUP-TFII.

We next moved to understand the mechanism by which CDCP1 controlled COUP-TFII levels. Interestingly, COUP-TFII, c-Myc and Cyclin D1 mRNA and protein levels were significantly

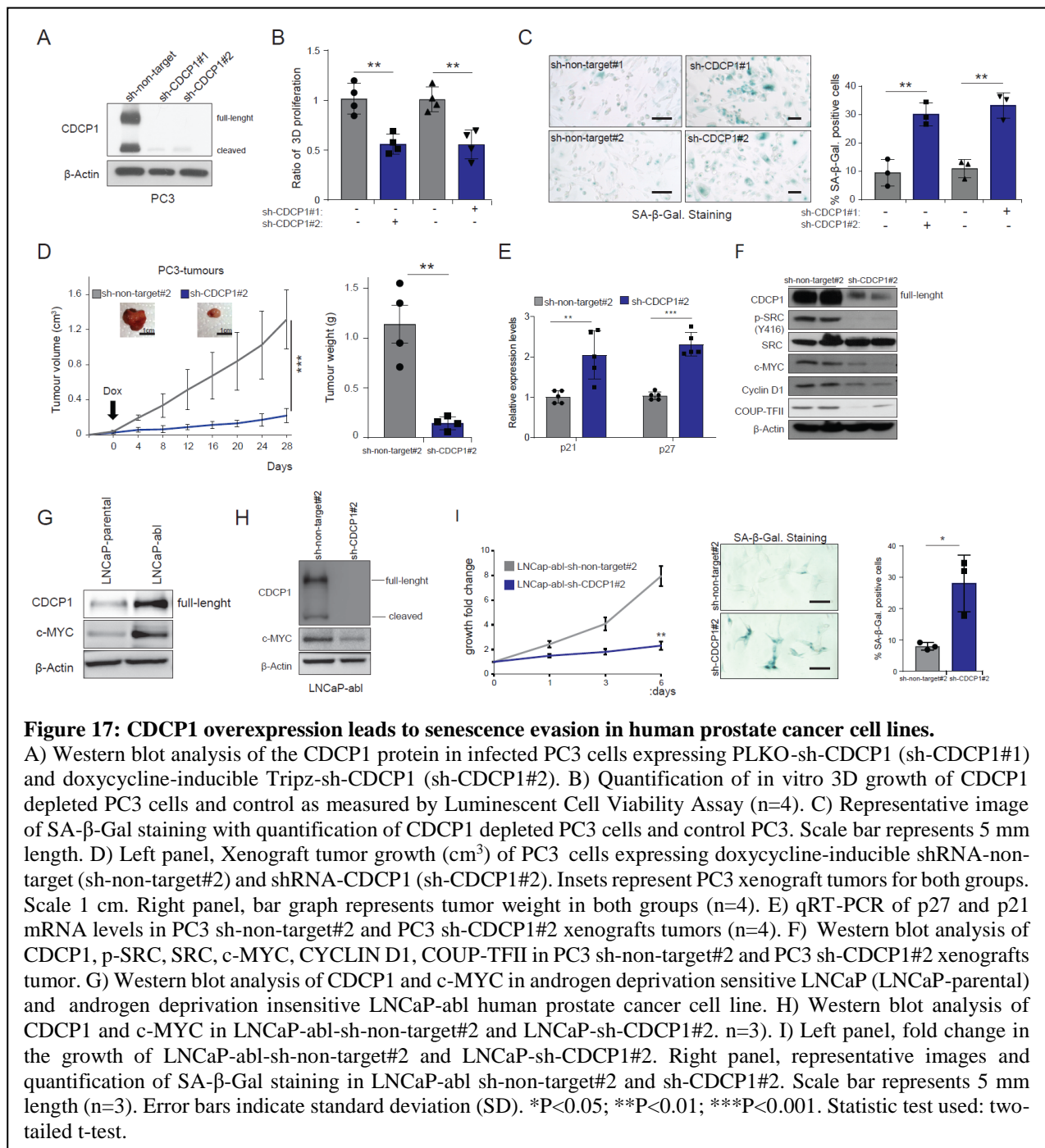


reduced in *CDCP1*; *Pten*<sup>-/-</sup> MEFs upon treatment with saracatinib, a selective inhibitor of Src (Figures 16A, B)<sup>60</sup>.

Of note, the saracatinib treatment led to a profound arrest in the proliferation and the reactivation of senescence in *CDCP1*; *Pten*<sup>-/-</sup> MEFs (Figure 16C, D). Since Src controls the levels of c-Myc, we next checked whether c-Myc could regulate COUP-TFII levels. We found that c-Myc inactivation in *CDCP1*; *Pten*<sup>-/-</sup> MEFs phenocopied the results obtained with the Src inhibitor (Figures 16E-H). In line with this evidence, the analysis of the COUP-TFII promoter revealed the presence of multiple MYC-binding sites. Chromatin immunoprecipitation (ChIP) assays confirmed that c-Myc specifically binds to the promoters of COUP-TFII in *CDCP1*; *Pten*<sup>-/-</sup> but not to that of *Pten*<sup>-/-</sup> MEFs. Additional ChIP analysis showed increased binding of c-Myc on Cyclin D1 promoter and reduced Smad4 binding affinity to the promoter of Cyclin D1 in *CDCP1*; *Pten*<sup>-/-</sup> MEFs compared to *Pten*<sup>-/-</sup> (Figure 16I). Altogether, these data demonstrate that in *CDCP1*; *Pten*<sup>pc/-</sup> tumors, increased c-Myc promotes activation of COUP-TFII that prevents Smad4 from binding the promoter of Cyclin D1.

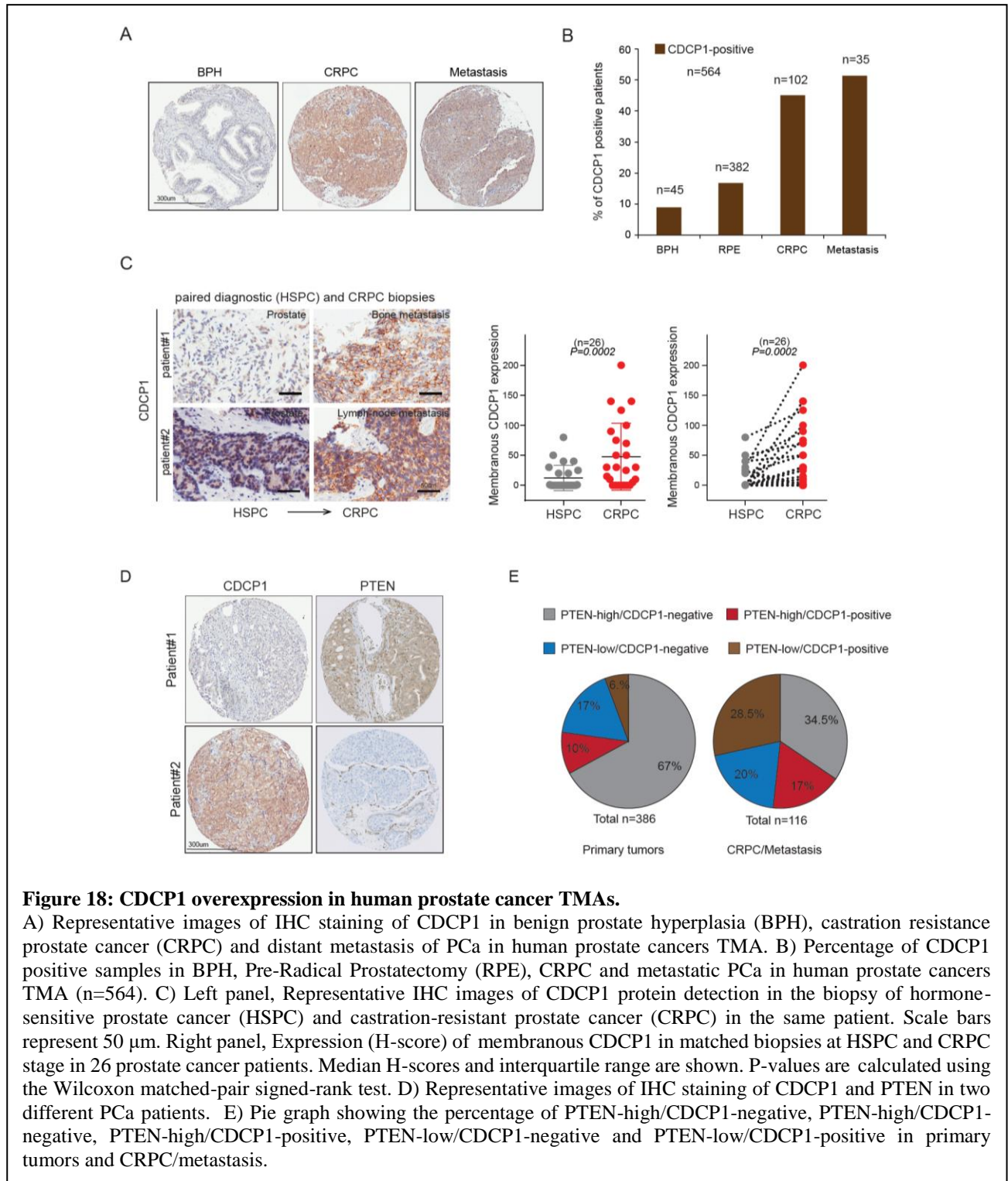
To further assess the relevance of these findings in human prostate cancer cells, we checked whether inhibition of CDCP1 could drive senescence activation in prostate cancer harboring elevated levels of CDCP1. We, therefore, depleted CDCP1 in PC3, a PTEN; TP53-deficient human prostate cancer cell line, by using two independent sh-RNAs (Figure 17A). Remarkably, CDCP1 silencing inhibited the 3D proliferation of PC3 cells (Figure 17B) and promoted senescence (Figure 17C). These results were also validated *in vivo* by injecting PC3 sh-CDCP1 and control cells in SCID mice (Figure 17D). Of note, CDCP1 depleted PC3-tumors showed a significant increase in mRNA levels of p21 and p27 that are two senescence markers and a decrease in c-MYC, COUP-TFII, and CYCLIN D1 levels in parallel with the reduction of SRC phosphorylation (Figure 17E, F). Together, these data demonstrate that CDCP1 inhibition promotes senescence by suppressing c-MYC levels in human prostate cancer cells. Downregulation of CDCP1 in LNCaP-abl cells, which present an increased level of CDCP1

compared with LNCaP parental cells, decreased proliferation and increased senescence (Figure 17G-I).



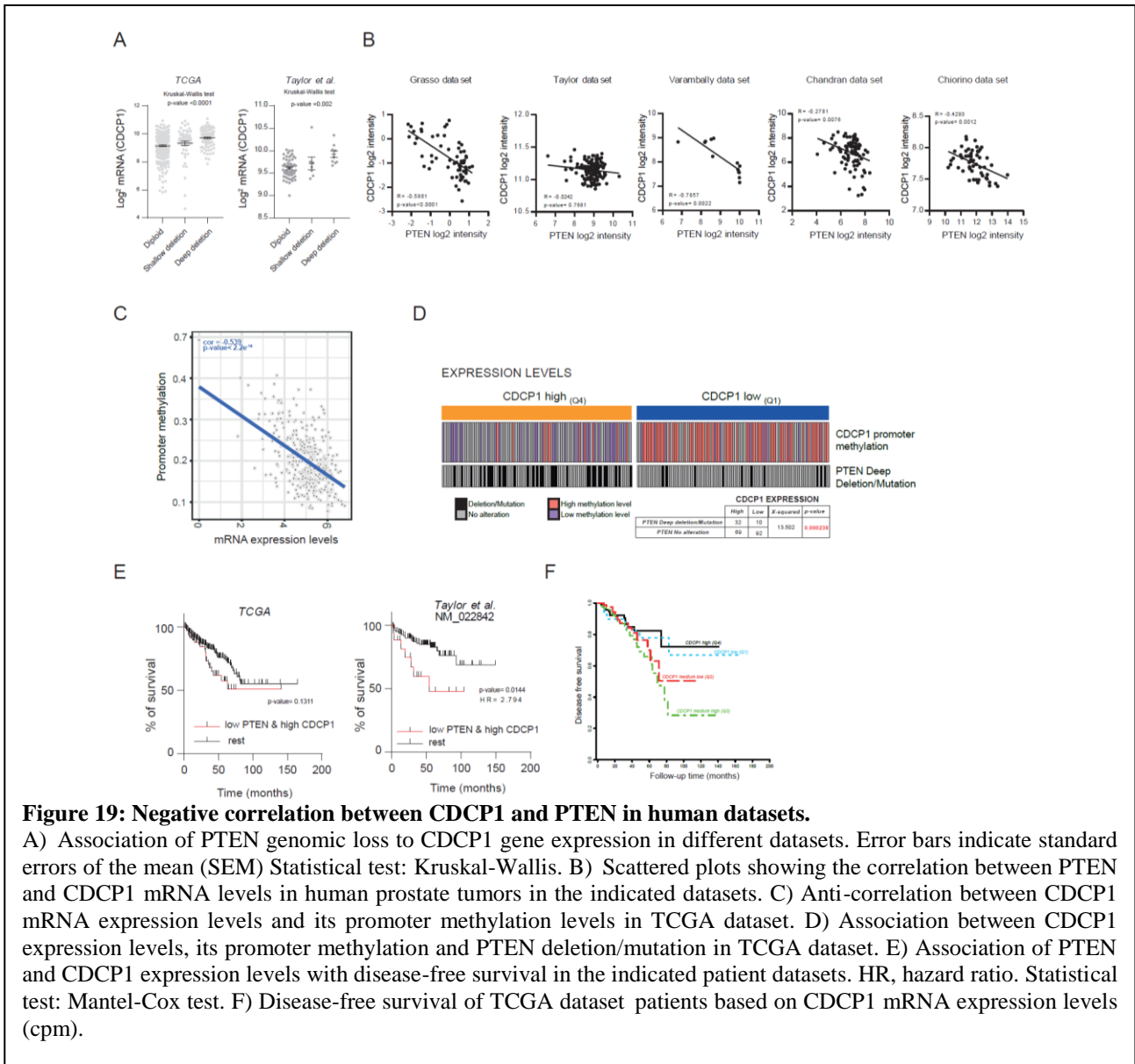
### 3.5 CDCP1 overexpression in human prostate cancer TMA

To assess the clinical relevance of CDCP1 in human prostate cancer (PCa), we examined two different tumor microarrays (TMAs), including a total of 990 cases spanning from benign, primary and metastatic PCa<sup>61-63</sup>. Immunohistochemical (IHC) analysis showed that while a large portion of



prostate tumors analyzed did not express CDCP1, a subset (48%) of CRPC and metastatic tumor samples expressed high levels of CDCP1 (Figures 18A, B). In line with these findings, analysis of consecutive tumor samples from a longitudinal study revealed that, in PCa patients, CDCP1 was upregulated during the transition from hormone-sensitive to CRPC (Figure 18C). Intriguingly, high levels of CDCP1 correlated with decreased levels of PTEN in both primary, CRPC and metastatic prostate tumor samples (Figure 18D, E). *PTEN* is one of the most frequently altered tumor suppressor genes in human PCa, where it accounts for prostate tumor initiation and progression<sup>53</sup>. The frequency of tumors displaying a low level of PTEN and high levels of CDCP1 increased in CRPCs and metastatic tumors compared to primary tumors, thereby validating the clinical relevance of this anti-correlation (Figures 18E). Additionally, bioinformatics analysis evaluating different datasets confirmed the existence of an anti-correlation between *PTEN* and *CDCP1* mRNA levels (Figure 19A). Elevated levels of CDCP1 expression were also significantly associated with PTEN genetic deletions and low CDCP1 promoter methylation in different independent data sets of PCa (Figure 19B-D).

Although patients affected by prostate tumors harboring high levels of CDCP1 had a similar disease-free survival (DFS) than patients with low CDCP1, patients with tumors expressing low levels of PTEN and increased level of CDCP1 had a significantly shorter DFS than patients of the other categories (Figure 19E, F). Taken together, these data validate the clinical relevance of CDCP1 and suggest that CDCP1 could cooperate with the loss of PTEN to promote highly aggressive prostate cancer.

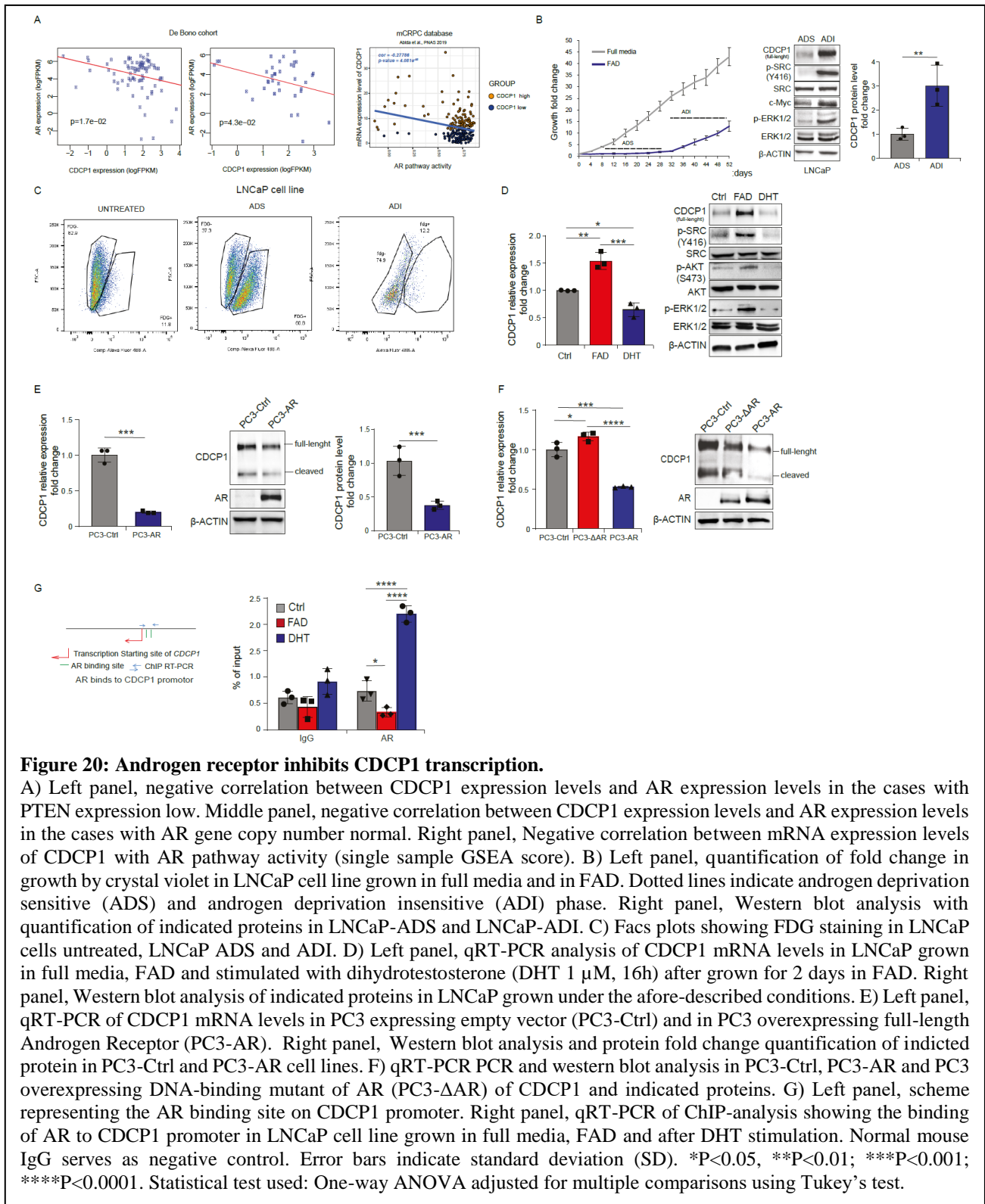


### 3.6 Androgen deprivation induces CDCP1 expression in PTEN deficient cells

Since PTEN deficient CRPCs tumors display high CDCP1 levels, and PTEN can regulate the levels and transcriptional activity of AR<sup>64</sup>, we hypothesized that AR could control the levels of CDCP1. Bioinformatics analysis in CRPC cases revealed that AR expression and AR activity inversely correlated with CDCP1 expression in prostate tumors (Figure 20A).

To further validate these data *in vitro*, we cultured the androgen-sensitive PTEN null LNCaP cell line in full androgen deprivation (FAD) condition (absence of androgens and presence of Enzalutamide)

for more than 40 days, and we waited until these cells developed resistance (Figure 20B). CDCP1 levels increased in cells resistant to Enzalutamide (androgen deprivation insensitive, ADI) compared to Enzalutamide sensitive cells (androgen deprivation sensitive, ADS).



This upregulation was associated with the concomitant activation of p-SRC, p-ERK1/2 and c-MYC and to evasion of senescence driven by enzalutamide treatment (Figure 20B, C)<sup>65</sup>.

These results prompted us to investigate whether AR could regulate the mRNA expression of CDCP1. While FAD treatment enhanced CDCP1 levels, Dihydrotestosterone (DHT) stimulation reduced its expression at mRNA and protein levels in LNCaP ADS cells (Figure 20D).

In addition, overexpression of AR reduced the mRNA and protein level of CDCP1 in the AR negative prostate cancer cell line PC3 (Figures 20E). In contrast, overexpression of a mutated form of AR, which lacked the DNA binding domain in PC3 failed to promote the downregulation of CDCP1 (Figure 20F). ChIP–quantitative PCR (ChIP-qPCR) analysis in LNCAP cells showed that the AR could bind to the CDCP1 proximal promoter, where it inhibited CDCP1 transcription (Figure 20G).

We next investigated whether loss of PTEN was needed for CDCP1 upregulation in cells kept in FAD. Indeed, CDCP1 levels increased in PTEN null LNCaP cells, but not in the PTEN wild-type LAPC4 and VCaP cell lines kept in FAD (Figure 21A). In line with these findings, we found that in the ADT insensitive cell lines PC3 and 22RV1, FAD did not upregulate CDCP1 levels (Figure 21B). Interestingly, inhibition of PI3K in LNCaP cells, but not in 22RV1 cells, promoted the downregulation of CDCP1 in cells kept in FAD (Figure 21C, D). This was associated with the concomitant upregulation of AR levels in the same cells. These data are coherent with previous findings demonstrating that PTEN loss leads to reciprocal feedback inhibition of AR activity (47). Thus, inhibition of PI3K leads to increased AR levels that promote the following down-regulation of CDCP1.

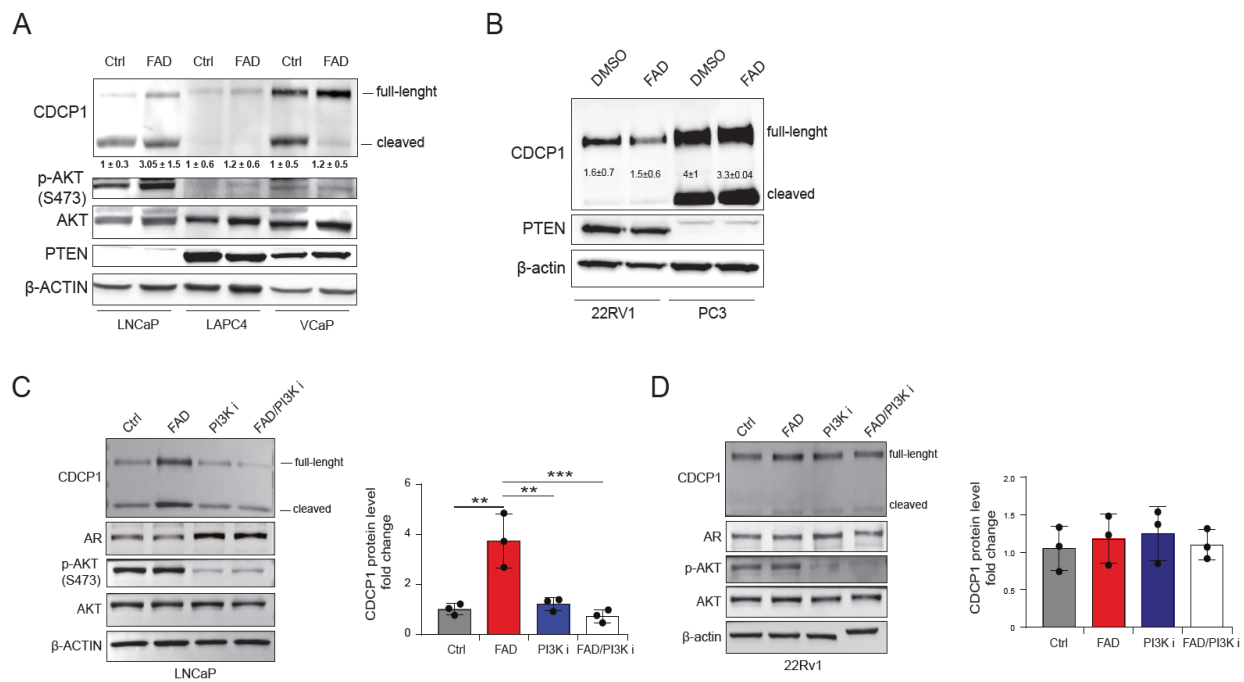


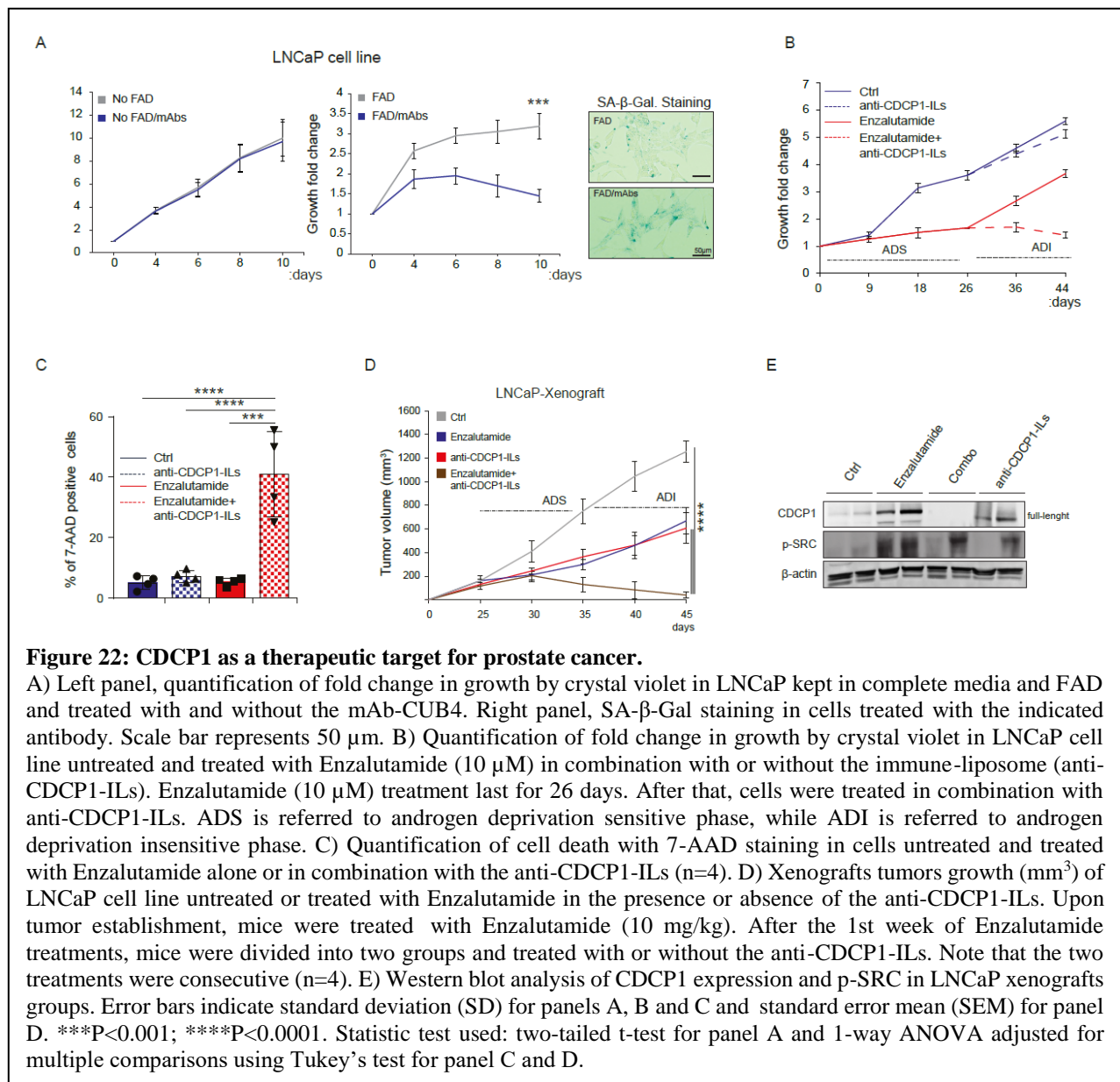
**Figure 21: Androgen deprivation induces CDCP1 overexpression in PTEN deficient cells.**

A) Western blot analysis of indicated protein in LNCaP, LAPC4 and VCaP cell lines kept in normal condition and in FAD. B) Western blot analysis of indicated protein in 22RV1 and PC3 kept in normal condition and in FAD. C) Right panel, western blot analysis of indicated proteins in LNCaP treated with PI3K inhibitor in normal conditions or in FAD. Right panel, quantification of fold change in CDCP1 protein levels in LNCaP untreated or treated with PI3K inhibitor in normal conditions and in FAD (n = 3). D) Right panel, western blot analysis of indicated proteins in 22RV1 treated with PI3K inhibitor in normal conditions or in FAD. Right panel, quantification of fold change in CDCP1 protein levels in 22RV1 untreated or treated with PI3K inhibitor in normal conditions and in FAD (n = 3). Error bars indicate standard deviation (SD). \*\*P<0.01; \*\*\*P<0.001. Statistical test used: One-way ANOVA adjusted for multiple comparisons using Tukey's test.

### 3.7 CDCP1 as a therapeutic target for prostate cancer

Given that androgen deprivation conditions elevate CDCP1 expression in ADS tumor cell lines, we postulated that compounds that block or degrade CDCP1 could be ideally used in combination with ADTs to prevent the emergence of ADI prostate tumors cells. To assess this hypothesis, we used the anti-CDCP1 monoclonal antibody CUB4, which binds the N-terminal domain of human CDCP1 and promotes CDCP1 internalization and degradation<sup>24</sup>. Co-treatment of LNCaP cells with CUB4 and enzalutamide strongly abolished cell proliferation by inducing senescence. In contrast, enzalutamide untreated cells were only slightly affected by the anti-CDCP1 antibody due to the low basal levels of CDCP1 in LNCaP cells (Figure 22A).

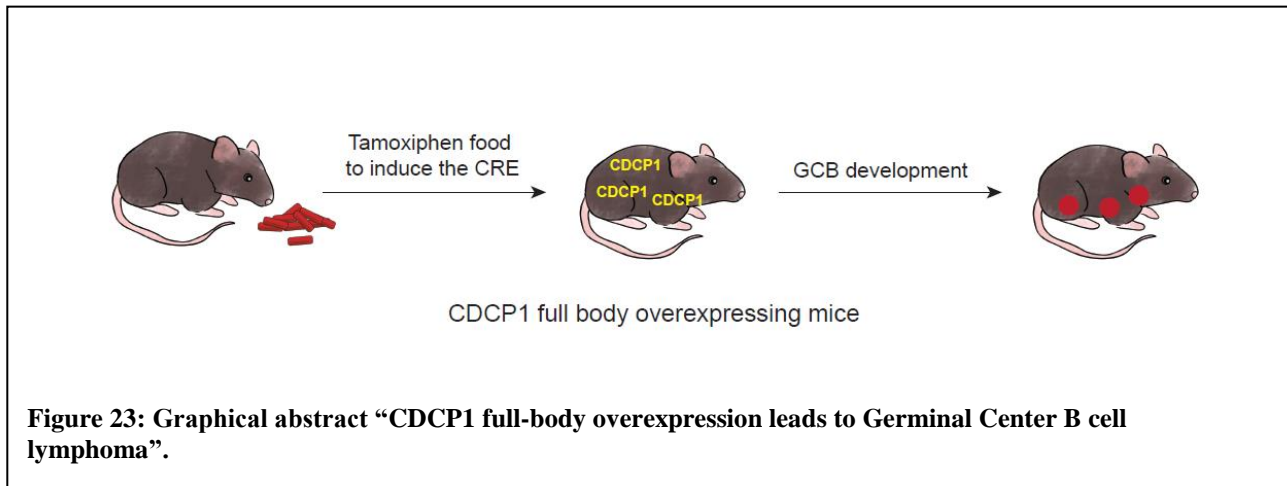
We next reasoned that tumor cells eradication rather than senescence induction could be a preferable outcome of CDCP1 targeting therapies<sup>66</sup>. Therefore, we developed an anti-CDCP1 ILs carrying doxorubicin to eliminate CDCP1 overexpressing prostate tumor cells induced by the enzalutamide treatment. Note that the anti-CDCP1 IL was generated by using the FAB of the CUB4 antibody (27). To allow the selective delivery of doxorubicin to the tumor cells, the anti-CDCP1 ILs were designed with a size of 120 nm. This size allows the preferential delivery of immunoliposome in tumor tissues due to the enhanced permeability and retention (EPR) effect of the cancer blood vessels<sup>67-69</sup>.



Enzalutamide treatment, in combination with anti-CDCP1 ILs, induced a strong apoptotic response and blocked the emergence of CDCP1+ ADI cells in a time-course experiment (Figure 22B, C). In line with the previous experiments, treatment with anti-CDCP1 ILs affected the proliferation of LNCaP cells only in the presence of Enzalutamide treatment. To validate these results *in vivo*, LNCaP cells were injected subcutaneously into SCID-mice, and upon tumor establishment, mice were treated with Enzalutamide (10mg/kg) with or without anti-CDCP1 ILs. While Enzalutamide showed minor effects on tumor growth, the combination of Enzalutamide and anti-CDCP1 ILs significantly affected tumor growth (Figure 22D). Of note, western blot analysis showed a significant increase in the levels of CDCP1 upon Enzalutamide treatment *in vivo*, which was abolished upon combination treatment (Figure 22E). These data suggest that CDCP1 targeting agents are effective when used in combination with ADTs.

## 4. Results: CDCP1 full-body overexpression leads to Germinal Center B cell lymphoma

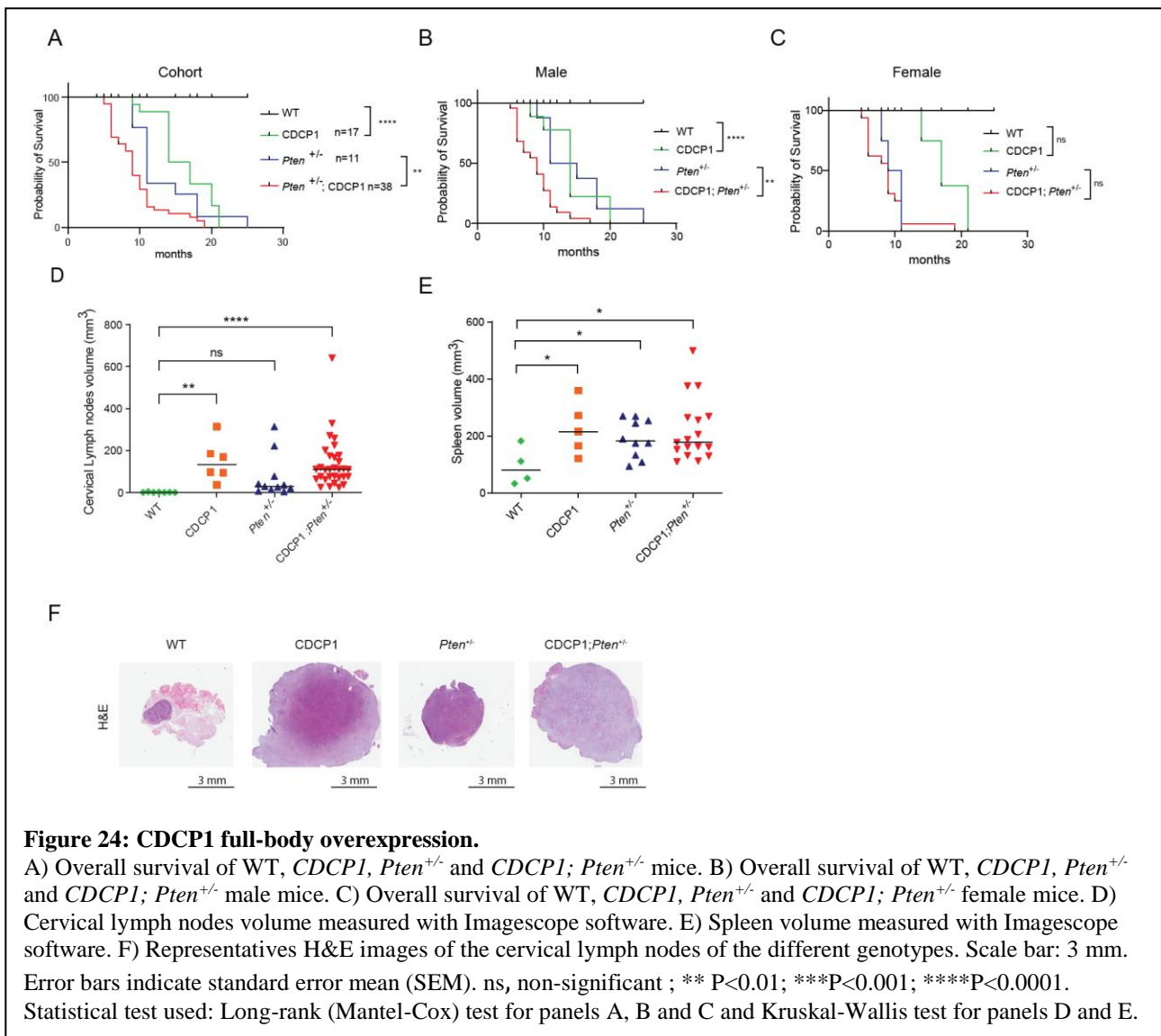
### B cell lymphoma



#### 4.1 CDCP1 full-body overexpression

To assess CDCP1 oncogenic potential, we further crossed our *CDCP1* and *CDCP1; Pten<sup>loxP/loxP</sup>* transgenic mouse model with the Cre-ER mice to get the Cre-recombinase activated by administering tamoxifen food to the mice for two weeks. Those animals were monitored, tracking survival and behavior.

We observed that  $CDCP1^+$  mice (hereafter referred to as  $CDCP1$ ) died at 10 months of age, while  $PTEN^{+/-}; CDCP1^+$  mice (hereafter referred to as  $CDCP1; Pten^{+/-}$ ) at 5-6 months (Figure 24A-C). The preponderant phenotype was the enlargement of the cervical lymph nodes and spleen (Figure 24D-F), which ultimately led to mouse death (Figure 24A-C). Histopathological analysis of the cervical lymph nodes of these mice confirmed that  $CDCP1$  mice develop lymphoma at 10 months of age, while  $CDCP1; Pten^{+/-}$  mice at 5-6 months of age (Figure 24F). Full-body  $Pten^{+/-}$  mice are known to develop non-cancerous lymphadenopathy; thus overexpression of  $CDCP1$  shifts the benign phenotype developed by  $Pten^{+/-}$  mice into an aggressive lymphoma<sup>70-72</sup>.



## 4.2 CDCP1 overexpression drives B cell lymphoma development

To better characterize the lymphoma developed by CDCP1 overexpression in mice, we performed IHC analysis of CD19 and CD3, well-known markers for B and T cells, respectively. CDCP1 overexpression, either alone or in *Pten*<sup>+/-</sup> context, leads to B cell expansion in the cervical lymph nodes (Figure 25A, B). FACS analysis confirmed a significant accumulation of CD19<sup>+</sup>B220<sup>+</sup> B cells in the cervical lymph nodes of CDCP1 full-body overexpressing mice (Figure 25C). Of note, both IHC and FACS analysis demonstrated that CD3<sup>+</sup> T cells were not differently enriched between the different genotypes (Figure 25A-C). In order to discriminate whether CDCP1-overexpressing mice develop B-cell lymphoma or leukemia, we performed FACS analysis of the bone marrow. We observed no difference in B cells maturation in CDCP1 overexpressing mice compared to the WT ones, thereby confirming is the B-cell lymphoma nature of this malignancy (Figure 25D).

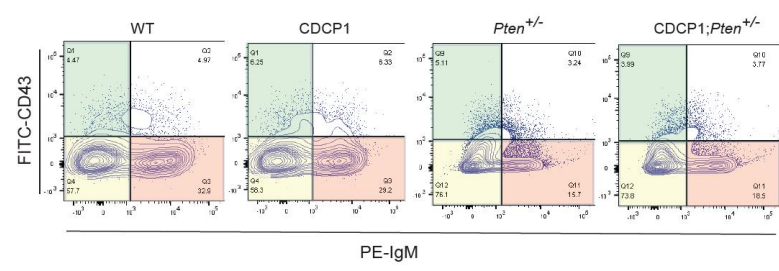
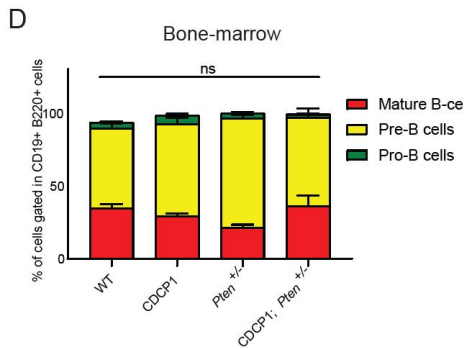
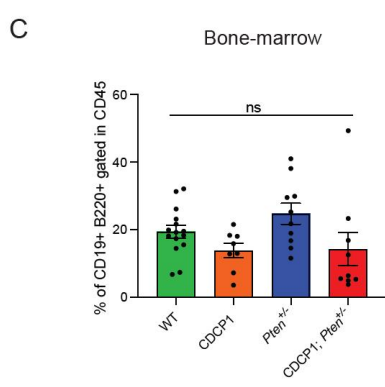
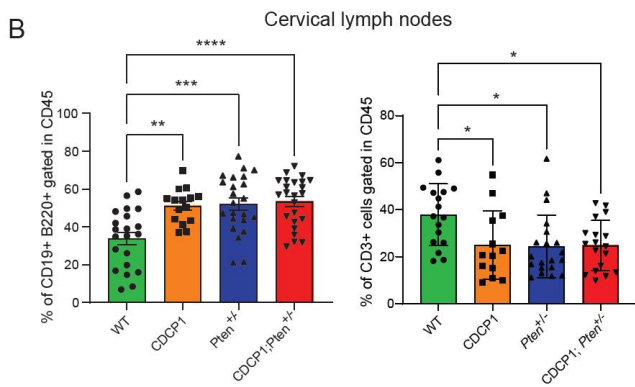
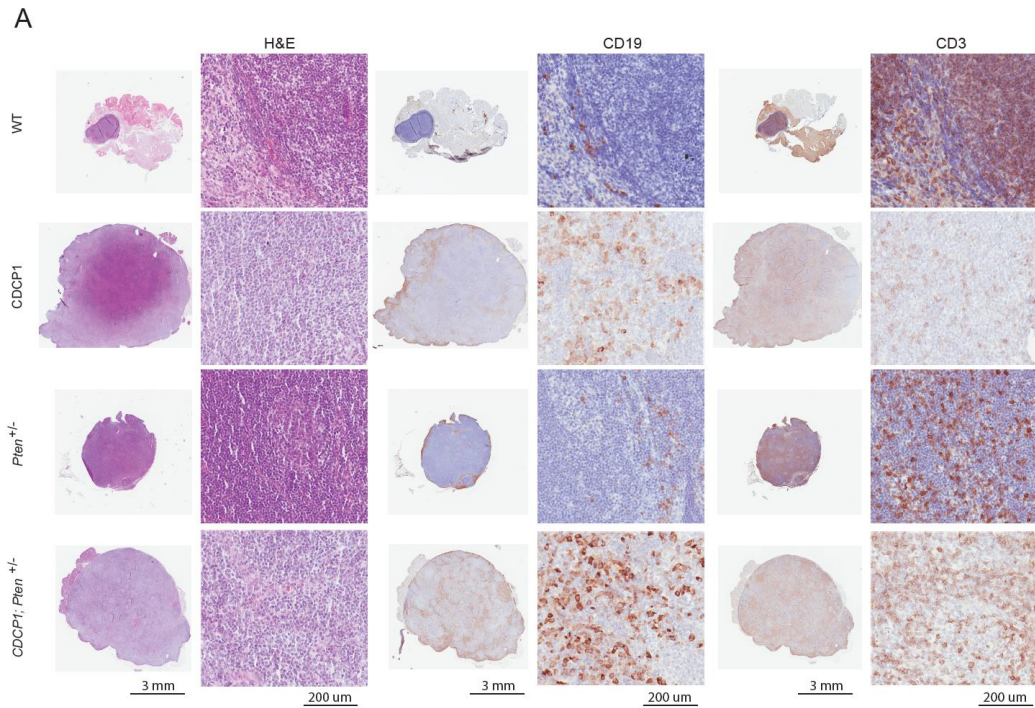


**Figure 25: CDCP1 overexpression leads to B cell lymphoma development.**

A) Representative images of H&E, CD19 and CD3 staining of cervical lymph nodes of WT, *CDCP1*, *Pten*<sup>+/-</sup> and *CDCP1*; *Pten*<sup>+/-</sup> mice. B) Quantification of CD19 and CD3 IHC staining. C) FACS analysis of CD19<sup>+</sup> B220<sup>+</sup> cells and CD3<sup>+</sup> cells gated in the CD45<sup>+</sup> cells of the cervical lymph nodes of WT, *CDCP1*, *Pten*<sup>+/-</sup> and *CDCP1*; *Pten*<sup>+/-</sup> mice. D) FACS analysis of Pro-B, Pre-B and Mature B cells in the bone marrow of WT, *CDCP1*, *Pten*<sup>+/-</sup> and *CDCP1*; *Pten*<sup>+/-</sup> mice. Error bars indicate standard error mean (SEM). ns, non-significant; \*P<0.05; \*\* P<0.01; \*\*\*P<0.001; \*\*\*\*P<0.0001. Statistical test used: One-way ANOVA adjusted for multiple comparisons using Tukey's test.

### 4.3 CDCP1 overexpression leads to GCB development

Next, we decided to characterize the B cell lymphoma type developed by our transgenic mouse models. For this reason, we performed FACS analysis for different B cell markers: PNA, CD95, IgM, and IgD<sup>73</sup>. Previous studies showed that B cells PNA<sup>+</sup>CD95<sup>+</sup> are the germinal center B cells, the IgM<sup>+</sup>IgD<sup>+</sup> B cells represent the follicular B cells, and the IgM<sup>+</sup> B cells are the marginal zone B cells. FACS staining of the cervical lymph nodes of the CDCP1 overexpressing mice showed the expansion of the PNA<sup>+</sup>CD95<sup>+</sup> B cell compartment (Figure 26A-E)<sup>73</sup>.

To confirm these data, we performed IHC analysis for PNA in the spleen of WT, *CDCP1*, *Pten*<sup>+/-</sup> and *CDCP1*; *Pten*<sup>+/-</sup>. PNA stains only the germinal center. This staining allows us to measure the area of the germinal center (Figure 26F). CDCP1 overexpressing mice showed an increase in the area of the germinal center in the spleen. Another confirmation of the phenotype is obtained by BCL6 staining in the cervical lymph nodes of the mice (Figure 26G)<sup>73</sup>.

Our data demonstrate that CDCP1 can induce Germinal center B cell lymphoma (GCB) development and that this phenotype appears earlier in *Pten* heterozygous contexts.

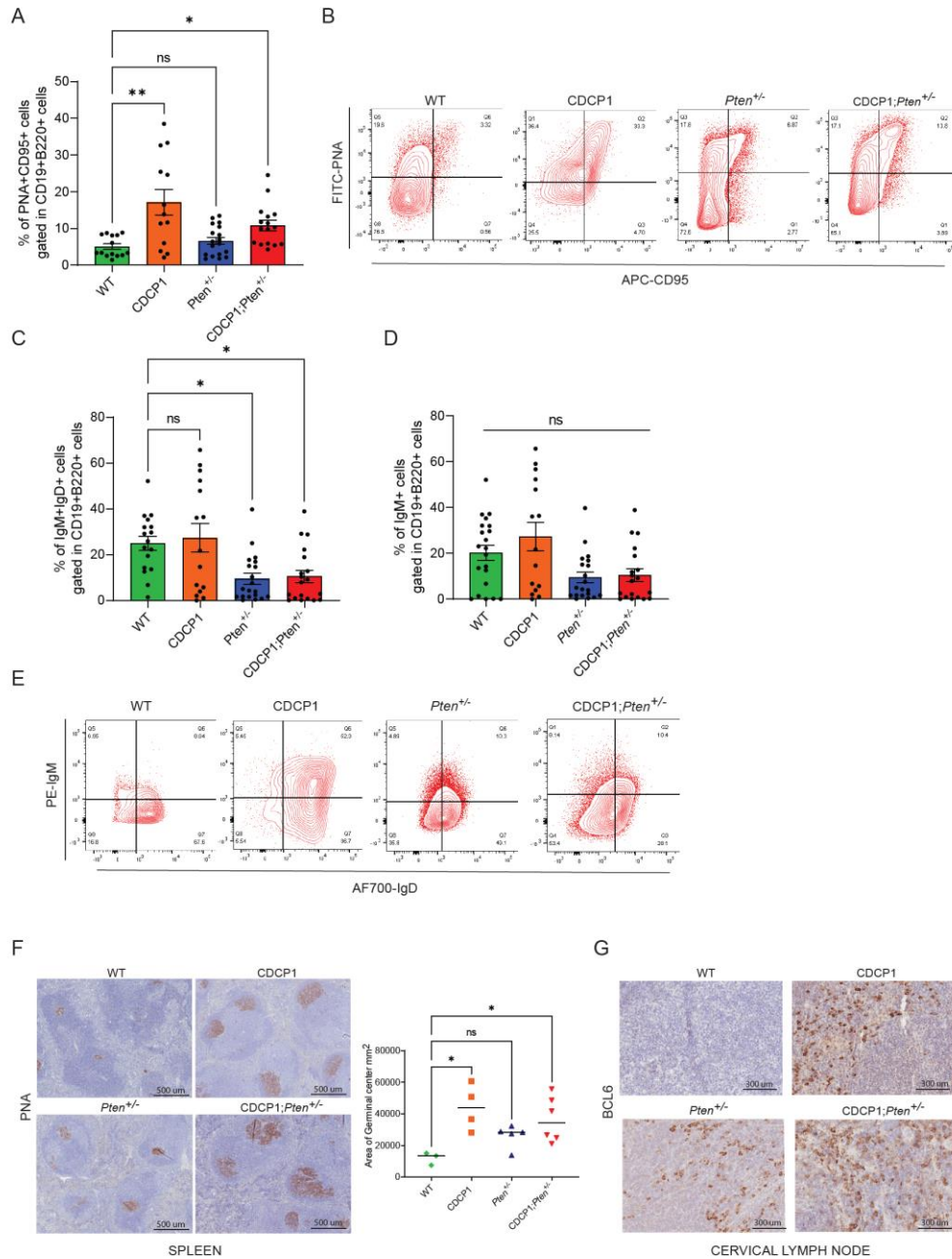
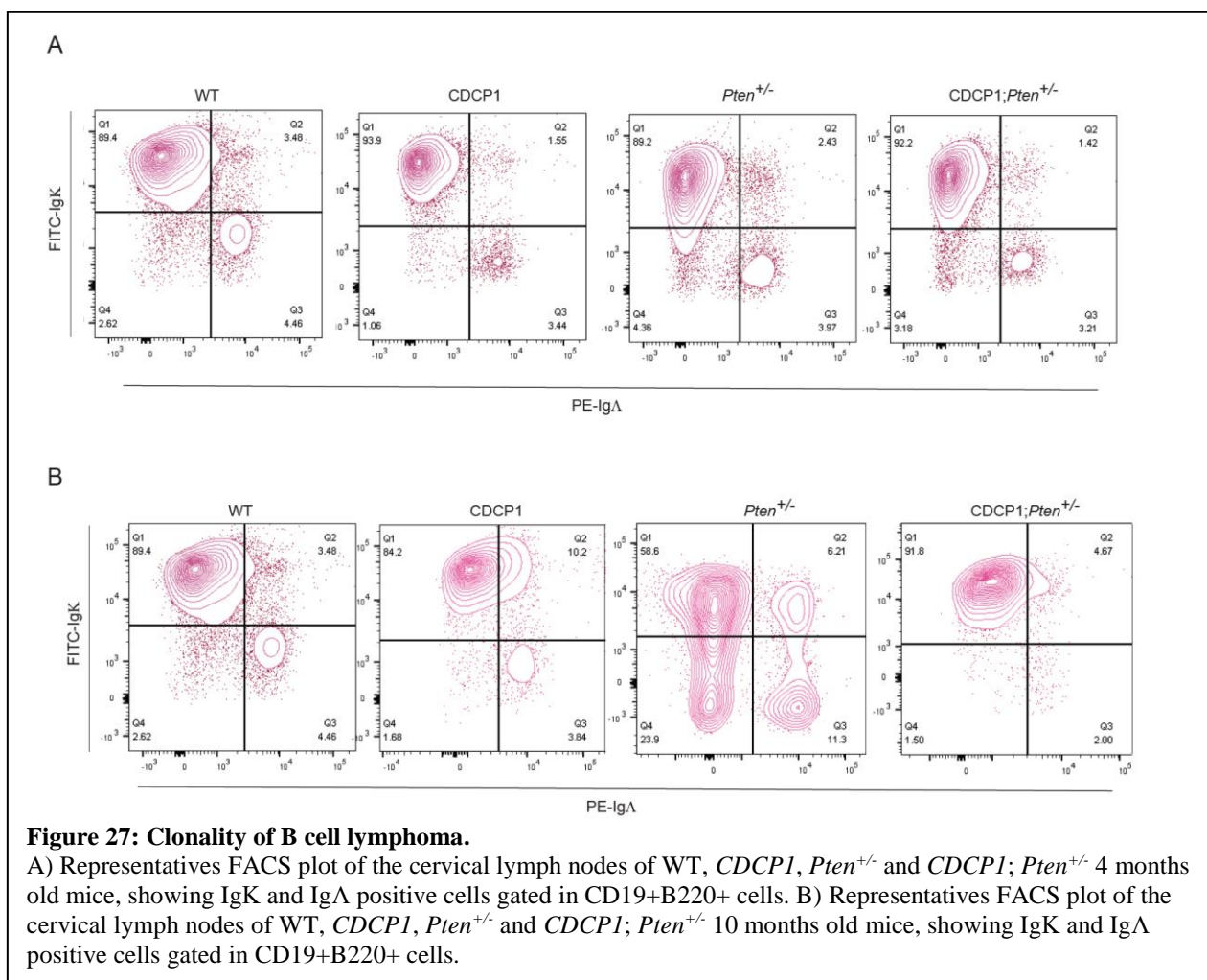


**Figure 26: CDCP1 overexpression leads to GCB development.**

A) FACS analysis of CD95+ and PNA+ B cells in the cervical lymph nodes of WT, *CDCP1*, *Pten*<sup>+/-</sup> and *CDCP1*; *Pten*<sup>+/-</sup> mice. B) Representative FACS plots of CD95+ and PNA+ B cells in the cervical lymph nodes of the mice genotypes mentioned above. C) FACS analysis of IgM+ and IgD+ B cells and D) of IgM+ B cells in the cervical lymph nodes of WT, *CDCP1*, *Pten*<sup>+/-</sup> and *CDCP1*; *Pten*<sup>+/-</sup> mice. E) Representative FACS plots of IgM+ and IgD+ B cells in the cervical lymph nodes of the mice genotypes mentioned above. F) Left panel, representative images of PNA staining in the Spleen of WT, *CDCP1*, *Pten*<sup>+/-</sup> and *CDCP1*; *Pten*<sup>+/-</sup> mice. Right panel, measure of the area of the germinal center in the spleen of the mice mentioned above. G) Bcl-6 staining of the cervical lymph nodes of WT, *CDCP1*, *Pten*<sup>+/-</sup> and *CDCP1*; *Pten*<sup>+/-</sup> mice. Error bars indicate standard error mean (SEM). ns, non-significant; \*P<0.05; \*\* P<0.01. Statistical test used: One-way ANOVA adjusted for multiple comparisons using Tukey's test.

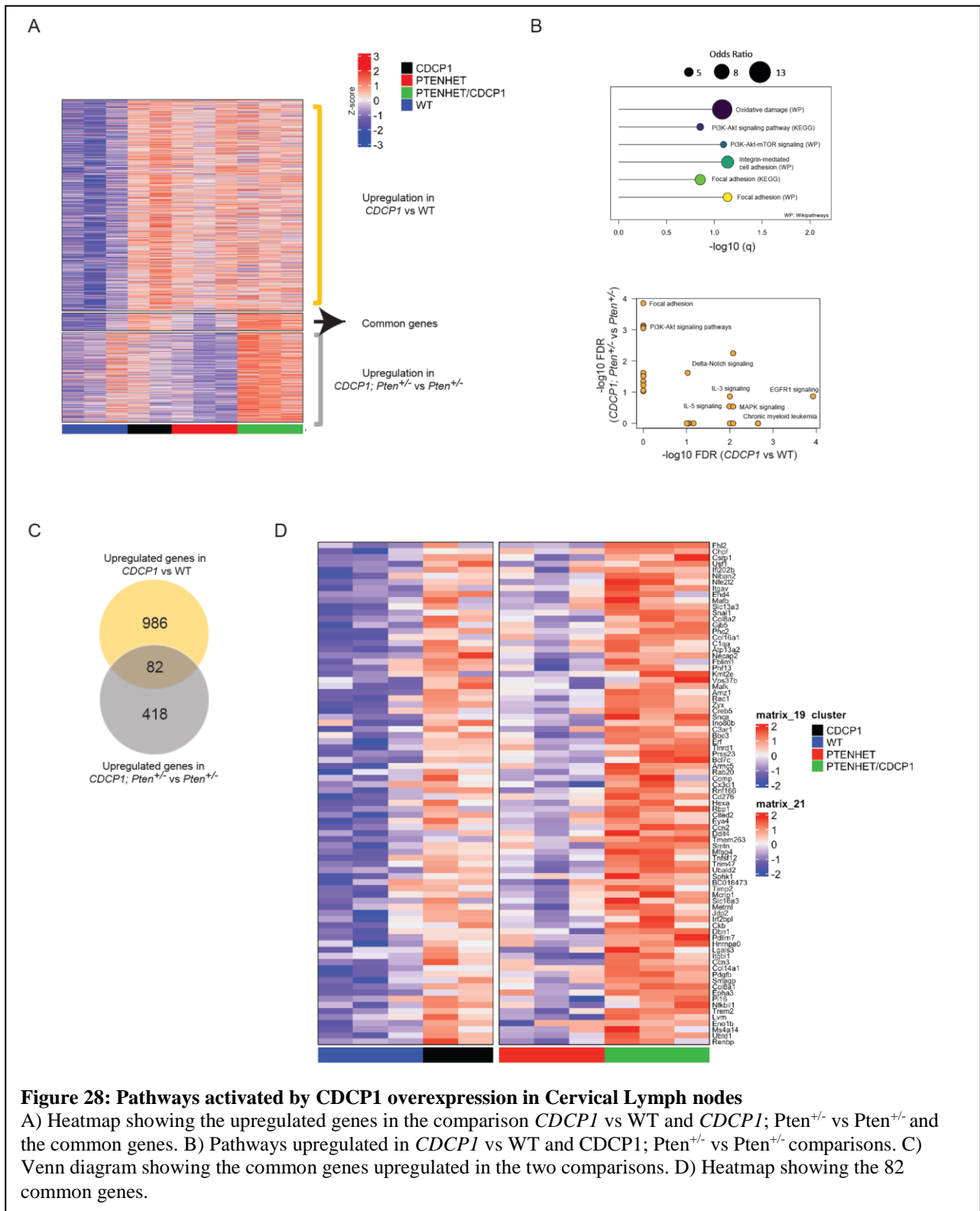
The detection of gene rearrangements in immunoglobulin (Ig), a specific marker of B lymphocyte clones, represents an essential tool for diagnosing B cell lymphoma<sup>74</sup>. To better understand if CDCP1 overexpression drives a clonal expansion of a specific B cell clone, we performed FACS analysis of the IgK and IgA markers in the B cells within the neoplastic lymph nodes. Intriguingly, no difference was observed between the four different genotypes at 4 months of age. However, at a later time (10 months of age), *CDCP1; Pten*<sup>+/-</sup> mice showed an expansion of the IgK<sup>+</sup> B cell clones (Figure 27A, B).



#### **4.4 CDCP1 overexpression in Cervical Lymph nodes triggers several oncogenic pathways**

In order to characterize the contribution of CDCP1 in lymphoma development, we performed RNA-sequencing of WT, *CDCP1*, *Pten*<sup>+/-</sup> and *CDCP1*; *Pten*<sup>+/-</sup> mice neoplastic lymph nodes. *CDCP1* and *CDCP1*; *Pten*<sup>+/-</sup> mice were compared respectively to WT and *Pten*<sup>+/-</sup>. (Figure 28A). 1892 genes were found differentially expressed in CDCP1 when compared to WT mice. Among them, 1068 genes were (56.4%) upregulated in the *CDCP1* mice. When comparing *CDCP1*; *Pten*<sup>+/-</sup> to *Pten*<sup>+/-</sup> mice, 792 genes were differentially expressed and mainly upregulated (N=500, 63%).

Of note, in both the comparisons, the most upregulated genes were belonging to EGFR1 ( $q <$



0.001), MAPK ( $q = 0.008$ ), and interleukin signaling pathways (IL-1, IL-2, IL-3, IL-5, IL-6,  $q < 0.05$ ), PI3K-Akt-mTOR-signaling ( $q < 0.001$ ), inflammation ( $q = 0.045$ ) and Notch-signaling ( $q = 0.006$ ) (Figure 28B).

To highlight the role of CDCP1 in these lymphoma models, we further focused on the common genes upregulated in both the comparisons (*CDCP1* vs WT and *CDCP1; Pten<sup>+/-</sup>* vs *Pten<sup>+/-</sup>*). Notably, we found 82 genes known to be involved in the PI3K-Akt pathway and the MAPK signaling pathway (Figure 28C and D).

#### **4.5 CDCP1 overexpression and targeting in different human lymphoma cell lines**

We then assessed the role of CDCP1 overexpression in human lymphoma cells, taking advantage of two human B cell lymphoma lines, HBL1 and U2932 (Figure 29A, D). Of note, CDCP1 overexpression promoted proliferation in both the cell lines (Figure 29B, C, E and F). Next, we tested *in vitro* the efficacy of mAbs (mAb1 and mAb2) targeting CDCP1 in combination with Ibrutinib, a drug already used in the clinic to treat B cell lymphoma, using the Incucyte system.

We evaluated the effects of these antibodies, either alone or in combination, and we saw that in all the two cell lines overexpressing CDCP1, the combination of Ibrutinib (5 $\mu$ M for U2932, 1  $\mu$ M for HBL1) with the anti-CDCP1 mAbs (10 ng/mL) was more effective in decreasing cells proliferation than the single treatment alone (Figure 29C and F). These *in vitro* results must be confirmed *in vivo* but indicate that CDCP1 represents a therapeutic target for lymphoma.

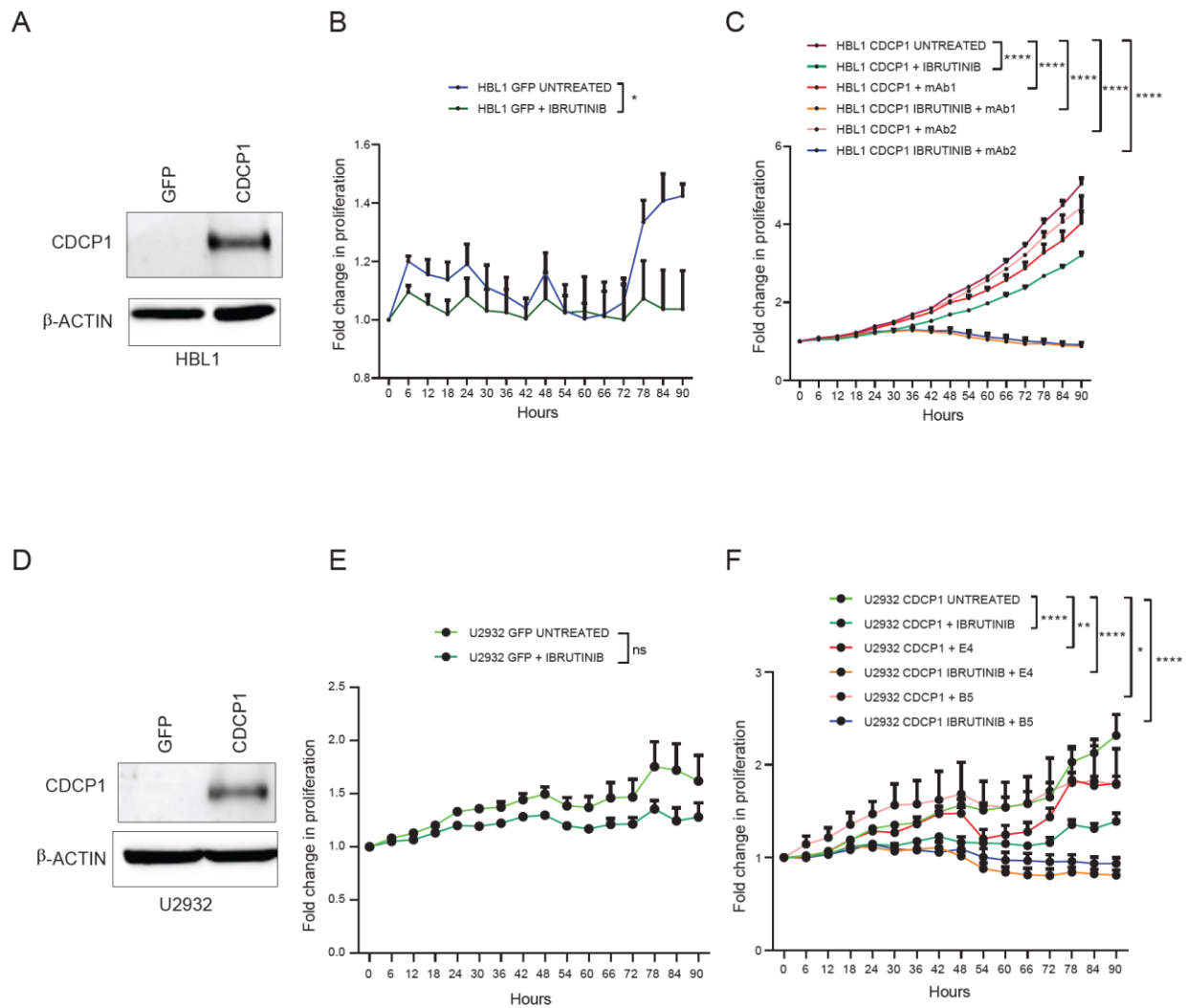


**Figure 29: CDCP1 overexpression and targeting in different human lymphoma cell lines.**

A) Western blot showing CDCP1 overexpression in HBL1 cell lines. B) Incucyte proliferation assay of HBL1 GFP cell lines after treatment with ibrutinib C) Incucyte proliferation assay of HBL1 CDCP1 cell lines after treatment with ibrutinib and two different mAb targeting CDCP1. D) Western blot showing CDCP1 overexpression in U2932 cell lines. B) Incucyte proliferation assay of U2932 GFP cell lines after treatment with ibrutinib C) Incucyte proliferation assay of U2932 CDCP1 cell lines after treatment with ibrutinib and two different mAb targeting CDCP1. Error bars indicate standard error mean (SEM). ns not significant; \* $P < 0.05$ ; \*\*\*  $P < 0.001$ ; \*\*\*\* $P < 0.0001$ . Statistical test used: One-way ANOVA adjusted for multiple comparisons using Tukey's test.

## 5. Discussion

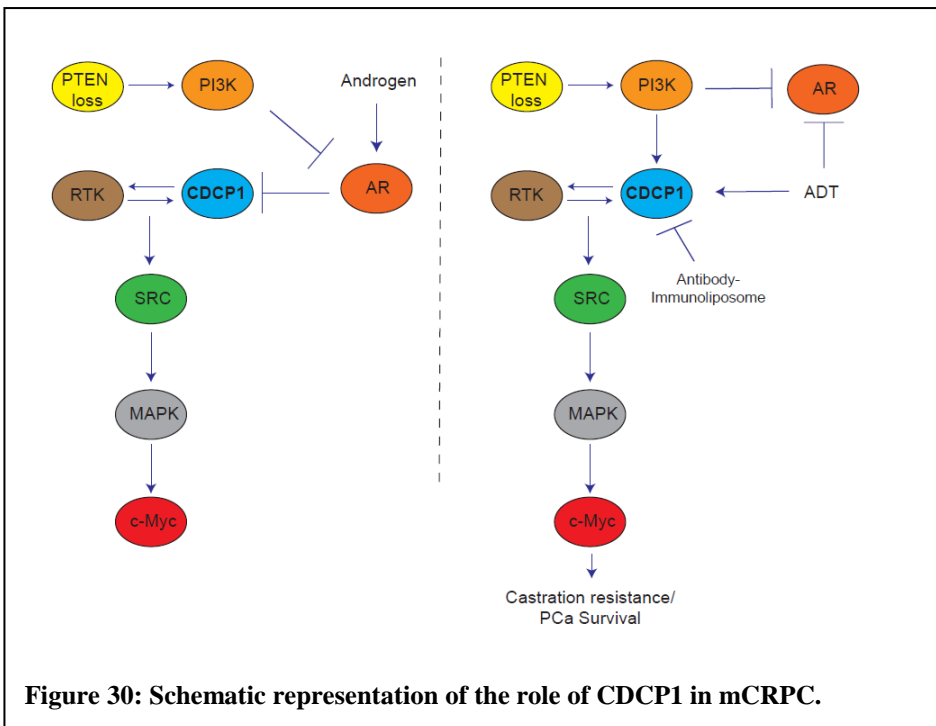
The present study highlights the crucial role of CDCP1 in promoting tumorigenesis.

CDCP1, a transmembrane protein that acts as a substrate for SRC family kinases, is overexpressed in various tumors and has been associated with cancer development, invasion, and metastasis<sup>8,77</sup>. In prostate cancer, the role of CDCP1 has remained poorly characterized due to the lack of *in vivo* model. Previous reports have demonstrated that CDCP1 overexpression increases cell proliferation in two human prostate cancer cell lines; however, validation of its elevated expression has been done in a limited number of primary prostate tumor samples<sup>25,78</sup>. In an attempt to clarify the function of CDCP1 in the context of prostate cancer, we have generated the first prostate-specific CDCP1 overexpressing transgenic mouse model and assessed the level of CDCP1 in different prostate cancer TMAs, including more than 990 cases spanning from benign, primary and metastatic prostate cancer. We have demonstrated that CDCP1 is overexpressed in a subset of advanced and metastatic prostate cancers, frequently associated with loss of PTEN. PTEN is one of the most frequently altered tumor suppressor genes in human prostate cancer, while complete loss of PTEN is frequently observed in metastatic prostate cancer<sup>79</sup>. Previous evidence demonstrated that *Pten*<sup>pc/-</sup> mice develop indolent tumors characterized by a senescence response that, acting as an intrinsic barrier, constrains prostate cancer progression<sup>36,52</sup>. However, the mechanism by which PTEN null benign tumors acquire metastatic potential has not yet been clarified<sup>36,46,54</sup>.

Here, we show in *in vivo* models that CDCP1 cooperates with PTEN loss to promote the emergence of metastases and CRPC through the upregulation of the MAPK pathway. Previous evidence demonstrates that patients that develop resistance to ADTs present tumors with elevated levels of MAPK pathway and that activation of the MAPK pathway cooperate with PTEN deficiency to promote mCRPC<sup>45,80</sup>. Mechanistically, we show that CDCP1 overexpression increases c-Myc levels in a Src-dependent manner. This, in turn, promotes the activation of COUPTF-II that further inhibits Smad4-dependent transcription. As a result, Cyclin D1 gets upregulated and

*CDCP1*; *Pten*<sup>pc/-</sup> tumors bypass senescence and progress towards a metastatic phenotype.

Of note, we have found that *CDCP1* mRNA and protein levels increase in PTEN-deficient cells treated with enzalutamide, a standard of therapy for CRPC patients. Finally, we have provided evidence that the AR can suppress the transcription of *CDCP1*, particularly in cells carrying the loss of PTEN (Figure 30).



Overexpression of the AR in AR-negative prostate cancer cell lines significantly decreases *CDCP1* levels, thus validating our observations. The Reciprocal feedback regulation of PI3K and androgen receptor signaling in PTEN-

deficient prostate cancer can explain the observed PTEN-*CDCP1* dependency (Figure 29)<sup>64</sup>. Therapeutically, we have demonstrated that *CDCP1* inhibition, in combination with ADT, might represent an interesting new therapeutic approach in prostate cancer. Indeed, we showed that inhibition of *CDCP1* in combination with Enzalutamide has the potential for prostate cancer treatment. Treatment of PTEN-deficient human prostate tumor cells with Enzalutamide promoted the upregulation of *CDCP1* levels. This treatment rendered PTEN null cells more sensitive to *CDCP1* targeting agents.

On the other hand, Enzalutamide untreated cells did not respond to *CDCP1* targeting agents. Moreover, we demonstrated *in vivo* that the combination of enzalutamide with a new *CDCP1*

immuno-liposome carrying doxorubicin inhibits tumor progression by inducing a strong apoptotic response. These findings demonstrate that CDCP1-targeting therapies should be combined with ADT to maximize the efficacy of this standard of treatment. Therapeutically, the use of an anti-CDCP1 ILs containing doxorubicin has several advantages:

- Liposomes loaded with doxorubicin are already in the clinic and are well tolerated by cancer patients.
- The size of anti-CDCP1 ILs allows its extravasation and accumulation preferentially at the tumor site due to the EPR effect<sup>67-69</sup>.
- The conjugation of the liposomes with the human FAB of the CDCP1 antibody increases the specificity and permanence of the IL in tumors overexpressing CDCP1, increasing its anti-cancer efficacy.

On the negative side, since the anti-CDCP1 ILs have been generated with an antibody that recognizes human CDCP1, our experiments in mice cannot exclude the risk of systemic toxicities of the ILs, and further experiments should be carried on by using a mouse antibody.

Furthermore, the generation of a full-body mouse model overexpressing CDCP1, either alone or in combination with heterozygous loss of *Pten*, allowed us to demonstrate that CDCP1 might act as a potent driver oncogene in other tumor contexts. In particular, full-body overexpression of CDCP1 leads to the spontaneous development of a B cell lymphoma phenotype. FACS analysis of the B cells in the cervical lymph nodes of these mice showed that CDCP1 overexpression sustains the expansion of the germinal center B cells compartment. Further, the analysis of mouse B cells maturation markers in the bone marrow showed no alteration of the B cells development, thus excluding a leukemic phenotype.

Mechanistically, we showed that CDCP1 overexpression, either alone or in *Pten*<sup>+/-</sup> context, drives upregulation of several signaling pathways, such as PI3K, Delta-Notch signaling, EGFR and MAPKs pathway, that have been reported to play critical roles in lymphoma development<sup>81</sup>.

Since CDCP1 significantly drives lymphoma development and it is a transmembrane protein, we reasoned that it could be a good therapeutic target for other malignancies.

Hence, we decided to take advantage of several human lymphoma cell lines to overexpress CDCP1.

The first important results obtained were that, in the lymphoma cell lines, CDCP1 overexpression was able to increase cell proliferation, thus confirming the critical role of CDCP1 in human settings.

Then, we decided to assess the efficacy of CDCP1 targeting in combination with Ibrutinib, a drug already used in the clinic for B cell lymphoma treatment. We tested two monoclonal antibodies targeting CDCP1 (mAb1 and mAb2) alone or in combination with Ibrutinib and we found that the combination therapy was significantly more effective than the single treatment with Ibrutinib or mAbs in decreasing cell proliferation.

These results indicate that CDCP1 could be used as a therapeutic target for this kind of disease.

However, further investigations are still needed to validate our findings *in vivo*, using both xenografts and transgenic mouse models.

In the future, we will also characterize CDCP1 levels in lymphoma TMAs to better understand its expression in human patients and its correlation to disease progression and response to therapy.

In conclusion, thanks to our novel mouse models, we demonstrated that CDCP1 can drive cancer initiation and progression and it represents a relevant clinical therapeutic target for two different tumors. Notably, the CDCP1 transmembrane structure offers several advantages for the development of effective therapeutic drugs. However, as CDCP1 is also expressed in other tissues at lower levels, caution should be taken to ensure therapeutic success with negligible systemic toxicity.

## 6. Materials and Methods

### 6.1 Acquisition of MEFs

Primary MEFs were prepared as described previously from individual embryos of various genotypes<sup>36</sup>. Briefly, all genotypes MEFs were obtained by crossing male wild type and *Pten*<sup>lox-lox</sup> with female *CDCP1*<sup>lox-stop-lox</sup> mice. A pregnant mouse at 13- or 14-day post-coitum was sacrificed by cervical dislocation. Embryos were harvested and the individual MEFs were cultured in DMEM containing 10% fetal bovine serum and 1% PenStrep. Primary *Pten*<sup>lox/lox</sup> MEFs were infected with retroviruses expressing either pMSCV-CRE-PURO-IRES-GFP or pMSCV-PURO-IRES-GFP for 48 h and selected with Puromycin at a concentration of 3 ug/ml and as previously described. All mice were maintained under specific pathogen-free conditions in the animal facilities of the IRB institute, and the experiments were performed according to the state guidelines and approved by the local ethical committee.

### 6.2 Cell culture and reagents

Human prostate carcinoma cell lines were purchased from ATCC and maintained according to the supplier's recommendation. Cells were transduced with PLKO or TRIPZ doxycycline-inducible lentiviral construct, against human CDCP1 gene or empty Vector, obtained by Thermo Scientific, Waltham, MA, USA (CloneIDs: V3THS\_329377 and V2THS\_191307). LNCaP-abl and LAPC4 cells were a gift from Dr. Jean-Philippe Theurillat (Institute of Oncology Research (IOR), Bellinzona). PC3-AR were generated by infecting them with retroviruses expressing full-length human AR (provided by Dr. Jean-Philippe Theurillat). PC3-ΔAR were generated using the expression of human AR with the deletion of amino acids 538-614, deletion of AR DNA binding domain (Addgene, Catalog #89107). LNCaP-ADI cells were generated from parental LNCaP by growing them in RPMI 1640 containing 10% charcoal-stripped FBS. Androgen stimulation experiments were performed using 1 nM of the 5α-Dihydrotestosterone (DHT) (Sigma, Catalog #521-18-6). Full

androgen deprivation (FAD) experiment was performed culturing the cells in RPMI with Charcoal-stripped FBS and Enzalutamide. Enzalutamide (APEX BIO Catalog #A3003) was dissolved in DMSO at a concentration of 10  $\mu$ M.

Tramp-C1 mouse prostate cancer cell line were purchased from ATCC and maintained according to the supplier's recommendation. To induce CDCP1 overexpression, these cells were infected using MIG-GFP and MIG-GFP-CDCP1 plasmid.

Silencing of c-Myc in MEFs was done using c-Myc siRNA and negative control siRNA, purchased from Sigma (Catalog #8024873724-000050; #8024873724-000060). The cells were transfected with Lipofectamine RNAiMAX (Catalog #13778-030; Invitrogen) according to the manufacturer's protocol.

Human lymphoma cell lines were purchased from ATCC and maintained according to the supplier's recommendation. Cells were transduced with MIG-GFP and MIG-GFP-CDCP1 plasmid to induce CDCP1 overexpression. Ibrutinib (MedChemExpress Catalog #936563-96-1) was dissolved in DMSO and was administered to the cells at the concentration of 5  $\mu$ M for SUDHL16 and U2932 and 1  $\mu$ M for HBL1. mAbs are dissolved in PBS and administered at the concentration of 10 ng/mL.

### **6.3 CDCP1 protein expression in human prostate cancer TMAs**

The first group of TMAs was composed of two TMAs (Figure 18A, B, D and E). The first TMA, include benign prostate tissue and prostate cancer at different stages (n=237), as previously reported<sup>63</sup>. Spots with metastases were not included in the analysis to avoid false-negative results due to poor fixation of tissue (mostly material from autopsies). The second TMA (n=192) consisted of locally advanced, inoperable, mostly metastatic prostate cancer including CRPC and hormone naïve (untreated) prostate cancer, as previously reported<sup>63</sup>. For distant metastasis, CDCP1 staining was performed on 6 regular histological sections of distant and lymph node prostate cancer metastases. The second group of TMAs (Figures 1A-1D and Table 1A and 1B) was composed of three different

TMA as previously described<sup>61,62</sup>. Briefly, the first TMA includes 201 samples of BHP, RPE, CRPC and metastasis samples. The second TMA includes 323 PCa samples of TUP-P and RPE samples. The third TMA include 82 CRPC samples. H-Score: the intensity of membrane CDCP1 staining on a scale of 0 (no staining), 1+ (weak staining), 2+ (moderate staining), and 3+ (strong staining) multiplied by the percentage of positive tumor cells. In the second group of TMAs PTEN status was determined FISH or IHC analysis as previously described (30). The use of the clinical samples for TMA construction was approved by the Ethical Committee of the University of Basel and the University of Zürich. For Paired diagnostic (HSPC) and CRPC biopsies (Figure 18C): Patients were identified from a population of men with mCRPC treated at the Royal Marsden NHS Foundation Trust. All patients provided written informed consent and were enrolled in institutional protocols approved by the Royal Marsden NHS Foundation Trust Hospital (London, UK) ethics review committee (reference no. 04/Q0801/60). Twenty-five patients with a diagnosis of prostate adenocarcinoma with sufficient formalin-fixed, paraffin-embedded (FFPE), matched diagnostic (archival) hormone-sensitive prostate cancer (HSPC) and CRPC tissue for CDCP1 immunohistochemistry were selected. HSPC tissue demonstrated adenocarcinoma and was obtained from either prostate needle biopsy (21 cases), transurethral resection of the prostate (TURP; 3 cases) or bone biopsy (1 case). CRPC tissue was obtained from the same patients through biopsies of bone (19 cases), lymph node (5 cases) or liver (1 case). All tissue blocks were freshly sectioned and only considered for IHC analyses if adequate material was present ( $\geq 50$  tumor cells; reviewed by D.N.R.).

#### **6.4 Bioinformatic analysis**

Correlation between CDCP1 and PTEN in prostate cancer data sets<sup>53,80,82-84</sup> was carried out using Spearman's correlation which estimates a correlation coefficient value 'R' and a significant P-value. We retrieved gene-expression and DNA-methylation from The Cancer Genome Atlas (TCGA) and performed a correlation analysis between the mRNA expression level and the methylation profile of

CDCP1 (Pearson correlation). Methylation level of CDCP1 was determined as the mean of  $\beta$ -values within +/- 1000 bp distance from the transcription start site (TSS). Samples were classified into quartiles (Q1-Q4) based on mRNA expression level of CDP1 or according to its methylation. Dependency between CDCP1 expression and PTEN deletions/mutations was determined using  $\chi$ -squared test. Survival analysis has been performed using Kaplan-Meier estimator and Cox-regression model.

## 6.5 Immunoblotting

Tissue and cell lysates were prepared with RIPA buffer (Catalog #9806, Cell Signaling Technology) with PMSF (Phenylmethanesulfonyl fluoride; Catalog #329-98-6, Sigma). Protein concentrations of the lysates were measured by Pierce BCA Protein Assay Kit (Catalog #23225, Thermo Scientific). The lysates were then resolved by SDS-PAGE and immunoblotted with the indicated antibodies. For analysis of fly tissue, wandering third-instar larvae were rinsed in PBS, salivary glands were dissected out, washed in PBS and homogenized in SDS sample buffer. The following antibodies were used for Western Blotting: PTEN (Catalog #9552S; Cell Signaling Technology, 1:1000); HSP90 (Catalog #4877S; Cell Signaling Technology, 1:1000); c-Myc (Catalog #A713(G-4), Santa Cruz Biotechnology, 1:500); p21 (Catalog #ab107099, Abcam, 1:1000);  $\beta$ -actin (Catalog #A5316; Sigma, 1:5000); Cyclin D1 (Catalog #2978S, Cell Signaling Technology, 1:1000); COUP-TFII (Catalog #PP-H7147-00; Perseus Proteomics, 1:1000); SMAD4 (Catalog #E0615, Santa Cruz Biotechnology, 1:500); p-SRC-Tyr416 (Catalog #6943S, Cell Signaling Technology, 1:1000); SRC (Catalog #2123S, Cell Signaling Technology, 1:1000); AKT (Catalog #9272S, Cell Signaling Technology, 1:1000); p-AKT-S473 (Catalog #9171S, Cell Signaling Technology, 1:1000); p53 (Catalog #ab131442, Abcam, 1:1000); CDCP1 (Catalog #4115, Cell Signaling Technology, 1:1000); Erk1/2 (Catalog #4695S, Cell Signaling Technology, 1:1000); p-Erk1/2-T202/Y204 (Catalog #4370S, Cell Signaling Technology, 1:1000); S6 (Catalog #2317S, Cell Signaling Technology, 1:1000); p-S6-Ser235/236 (Catalog

#4857, Cell Signaling Technology, 1:1000); AR (N-20) (Catalog #SC-816 Santa Cruz Biotechnology, 1:500).

## **6.6 Autopsy and Histopathology**

Animals were autopsied, and all tissues were examined regardless of their pathological status.

Normal and tumor tissue samples were fixed in 10% neutral-buffered formalin (ThermoScientific, Cat No. 5701) for 24-36 hrs after which the Formalin was removed under running tap water and the tissues were kept in either 1x PBS or 70% Ethanol solution until to process. Tissues were processed by ethanol dehydration and embedded in paraffin according to standard protocols, using the following steps:

1. Ethanol 70% - 10 mins (20 mins for bigger tissues)
2. Ethanol 80% - 10 mins (20 mins for bigger tissues)
3. Ethanol 95% - 10 mins (15 mins for bigger tissues)
4. Ethanol 95% - 10 mins (15 mins for bigger tissues)
5. Ethanol 100% - 10 mins (20 mins for bigger tissues)
6. Ethanol 100% - 10 mins (20 mins for bigger tissues)
7. Ethanol 100% - 10 mins (10 mins for bigger tissues)
8. Xylol - 15 mins (30 mins for bigger tissues)
9. Xylol - 10 mins (Same time of processing for the bigger tissues too)
10. Xylol - 10 mins (Same time of processing for the bigger tissues too)
11. Paraffin - 35 mins (Same time of processing for the bigger tissues too)
12. Paraffin - 35 mins (Same time of processing for the bigger tissues too)

Sections (5µm) were prepared for antibody detection and Haematoxylin and Eosin (H&E) staining (C0303, Diapath) and (C0363, Diapath) respectively. The following antibodies were used: Ki-67 (clone SP6, Catalog #RM-9106-R7; Rabbit Polyclonal; Unmask Water bath 98°C pH 6 20'; Lab

vision, Dilution Ready To Use); CDCP1 (Catalog #4115, Rabbit Polyclonal; Unmask Water bath 98°C pH 6 20'; Cell Signaling Technology, 1:50); p-HP1 $\gamma$ -Ser83 (Catalog #2600, Unmask Water bath 98°C pH 6 20'; Cell Signaling Technology, 1:50), Cyclin D1 (Catalog #2978S, Cell Signaling Technology); AR (N-20) (Catalog #SC-816, Rabbit Polyclonal; Unmask Water bath 98°C pH 6 20'; Santa Cruz Biotechnology, 1:300); Wide Spectrum Cytokeratin (Pankeratin) (Catalog #Z0622; Rabbit Polyclonal; Unmask Water bath 98°C pH 9 20'; DAKO, 1:2000); CD3 (Catalog #A0452 Dako; Rabbit Polyclonal; Unmask water bath 98°C pH 9 20'; Dako, 1:800); CD19 (Catalog #ab25232, abcam; Rat Monoclonal 6D5; Unmask water bath 98°C pH 9 20'; 1:200); BCL6 (Catalog #sc-7388, Santa Cruz Biotechnology; Mouse monoclonal; Unmask water bath 98°C pH 9 20'; 1:300).

## 6.7 RNA extraction for RNA-sequencing

Cervical lymphonodes were smashed mechanically with in TRIzol® (Catalog# 12183555, Life technologies). After the stratification with chloroform, the transparent phases were transferred in filter and the RNA was extracted using the RNeasy Plus Mini Kit (Cat. No. #74126, Qiagen) according to the manufacturer's instructions.

## 6.8 RNA-sequencing analysis

RNA-sequencing was performed on the cervical lymphonodes of WT, CDCP1, *Pten*<sup>+/-</sup> and CDCP1;*Pten*<sup>+/-</sup> mice. Two samples were excluded after Quality Check of alignment.

RNA sequencing was performed at the Institute of Oncology Research using the NEBNext Ultra Directional II RNA library preparation kit for Illumina and sequenced on the Illumina NextSeq500 with single-end, 75 base pair long reads. The overall quality of sequencing reads was evaluated using a variety of tools, namely FastQC, RSeQC<sup>85</sup>, AfterQC<sup>86</sup> and Qualimap<sup>87</sup>. Sequence alignments to the reference mouse genome (GRCm38) was performed using STAR (v.2.5.2a)<sup>88</sup>. Gene-expression was quantified at gene level by using the comprehensive annotations made available by Gencode<sup>89</sup>.

Genes were considered not expressed and filtered out when at least 2 samples had a counts per million (CPM) value less than 2, resulting in only 14099 genes used for a downstream analysis. Counts were normalized using the trimmed mean of M values (TMM) method in the edgeR package in R<sup>90</sup>. Log2-CPM values were used for downstream analysis and visualization.

Differential expression analysis was performed using the limma package<sup>91</sup> and a gene was considered significantly differentially expressed with a p-value lower than 0.1.

Gene set enrichment was performed using the EnrichR online tool considering KEGG and Wikipathways murine databases<sup>92</sup> and statistical significance of the pathways was determined by adjusted p-value ( $q < 0.05$ ).

## 6.9 Quantitative real-time PCR

RNA was extracted using TRIzol® Plus RNA Purification Kit (Catalog# 12183555, Life technologies). 1 ug of total RNA was used for cDNA synthesis using SuperScript® III Platinum® One-Step qRT-PCR Kit (Catalog# 11732-020, Life technologies). Quantitative Real-Time PCR (q-RT-PCR) was performed as previously described(12). Primers used are listed in Table 2 and 3. All qRT-PCR data presented was normalized using GAPDH, HRPT or 18S rRNA.

<b>Table 1: Primers for RT-PCR (Mouse)</b>	
<i>p16Ink4a</i> forward	5'-CGCAGGTTCTTGGTCACTGT-3'
<i>p16Ink4a</i> reverse	5'-TGTTTCACGAAAGCCAGAGCG-3'
<i>p21</i> forward	5'-GGGCGCACGATGTTTCAGAA-3'
<i>p21</i> reverse	5'-CACCACCAGGTCGAAATGGG-3'
<i>p27</i> forward	5'-GCAAAACAAAAGGGCCAACA-3'
<i>p27</i> reverse	5'-GGGCGTCTGCTCCACAGT-3'
<i>Gapdh</i> forward	5'-AGGTCGGTGTGAACGGATTTG-3'
<i>Gapdh</i> reverse	5'-TGTAGACCATGTAGTTGAGGT-3'
<i>Rn18S</i> forward	5'-ACCGCAGCTAGGAATAATG-3'

<i>Rn18S</i> reverse	5'-GCCTCAGTTCCGAAAACCA -3'
<i>COUP-TF II</i> forward	5'-TCAACTGCCACTCGTACCTG-3'
<i>COUP-TF II</i> reverse	5'-CATGATGTTGTTAGGCTG-3'
<i>Cyclin D1</i> forward	5'-GCGTACCCTGACACCAATC-3'
<i>Cyclin D1</i> reverse	5'-CTCCTCTTCGCACTTCTGCTC-3'
<i>c-Myc</i> forward	5'-CTGGACCAGGGAGTGGAGT-3'
<i>c-Myc</i> reverse	5'-ACGTAGTAGTCGGTTCTCA-3'

<b>Table 2: Primers for RT-PCR (Human)</b>	
<i>p21</i> forward	5'-TGTCCGTCAGAACCCATGC-3'
<i>p21</i> reverse	5'-AAAGTCGAAGTTCCATCGCTC-3'
<i>p27</i> forward	5'-TAATTGGGGCTCCGGCTAACT-3'
<i>p27</i> reverse	5'- TGCAGGTCGCTTCCTTATTCC-3'
<i>GAPDH</i> forward	5'-AATCCCATCACCATCTTCCA-3'
<i>GAPDH</i> reverse	5'-TGGACTCCACGACGTACTION-3'
<i>c-MYC</i> forward	5'-CGGAACTCTTGTGCGTAAGG-3'
<i>c-MYC</i> reverse	5'-CTCAGCCAAGGTTGTGAGGT-3'
<i>CDCPI</i> forward	5'-TGGTTCCACCCAGAAATGT-3'
<i>CDCPI</i> reverse	5'-GATGATGCACAGACGTTTTAT-3'

## 6.10 FACS staining

Tumours were disaggregated and digested in collagenase D and DNase for 30 min at 37 °C to obtain a single-cell suspension. Bone marrows were flushed from the femurs of the mice with RPMI using 21-gauge needle. The obtained cell suspension from both tumors and bone marrows was filtered with cell strainer (40 µm). After neutralization of unspecific binding with anti-CD16/CD32 antibody (Biolegend, Cat. no. 101305), single-cell suspensions were stained with specific monoclonal antibodies (primary antibodies directly conjugated) to assess the phenotype and diluted 1:200. The antibodies used were: CD45 (clone 30-F11, Cat no. Biolegend, 103139); CD4 (clone GK1.5, Cat no. Biolegend, 100414); PNA (Vector lab, Cat no. FL-1071), CD43 (clone S7, Cat no. BD Bioscience, 553270); CD3 (clone 145-2-C11, Cat no. Biolegend, 100307), CD95 (clone SA367H8, Cat no.

Biolegend, 152603), IgM (clone RMM-1, Cat. No. Biolegend, 406507); IgD (clone 11-26c-2a, Cat. No. Biolegend, 405729); CD19 (clone 1D3, Cat. No. Invitrogen, 25-0193-82); CD8 (clone 53-6-7, Cat.no. Biolegend, 100742); B220 (Clone RA3-6B2, Cat. No. Biolegend, 103255). For flow gating, we used isotype controls of fluorescence minus one controls. Samples were acquired on a BD Fortessa flow cytometer (BD Biosciences). Data were analysed using FlowJo software (TreeStar). For IgA (Southern Biotech, Cat. No. 1175-09) and IgK (Southern Biotech, Cat. No. 1170-02) detection, cells were permeabilized with the Fix/perm kit (Life technologies, Cat. No. GAS004) according to the manufacturer instruction

### **6.11 ChIP assay**

Cells were cultured to a confluence of 90–95% and were cross-linked with 1% formalin for 10 min followed by the addition of 2.5 M glycine for 5 min at room temperature. The culture medium was aspirated and the cells were washed twice with ice-cold phosphate-buffered saline. Nuclear extracts were sonicated using a Misonix 3,000 model sonicator to sheer crosslinked DNA to an average fragment size of ~500 bp. Sonicated chromatin was incubated for 16 h at 4 °C on a rotor with  $\gamma$ -bind Plus sepharose beads (Catalog# 17-0886-01, GE Healthcare) conjugated with either anti-c-Myc ((9E10)x L0815) anti-SMAD4 ((B-8) Catalog #E0615; Santa Cruz) or Mouse-IgG antibody (Catalog #92590 Millipore). After incubation, beads were washed thoroughly and then centrifuged. The chromatin was eluted from the beads, and crosslinks were removed by incubation at 56 °C for 12 h. DNA was then purified using the QIAquick PCR Purification Kit (Catalog# 28104, Qiagen). The binding of the transcription factor, c-Myc, on Cyclin D1 promoter was determined using SABiosciences' proprietary database (DECODE, DECipherment of DNA Elements). The primer mix used for ChIP assay in MEFs: 1) to detect Smad4 binding site (SBE) on Cyclin D1 promotor were: SBEChIPf 5'-CCGCTTAGTCCCCATTCTAAAG-3' and SBEChIPr: 5'-GGCATCTCCATTCTTAATCCAG-3'; 2) to detect c-Myc binding on Coup-tfII promotor: COUP-

TFIICHIPf 5'-GTGCGGGGACAAGTCGAGCGG-3' and COUP-TFIICHIPr 5'-GCGGTGGTGCTGGTTCGATGGG-3'; 3) to detect c-Myc binding on Cyclin D1 promoter we use EpiTect ChIP qPCR Primer Assay For Mouse Ccnd1, NM\_007631.2 (-)04Kb (Catalog #GPM1053924(-)04A). The primer mix used for ChIP assay in LNCaP to detect AR binding site on CDCP1 promoter were: f 5'-GAATTTGTCCTCGATTCAG-3' and r 5'-GCCAGAGGTCTGTTGGAC-3'. ChIP qPCR was performed using KAPA SYBR FAST ABI qPCR Master Mix solution (Catalog# 07959389001, KAPA Biosystem, Roche) on Step One Real-Time PCR systems (Applied Biosystems).

### **6.12 Proliferation and senescence assays**

Proliferation assay in MEFs was performed by plating  $10^4$  cells per well in a 24-well plate in triplicate while that in human prostate cancer cell lines was performed by plating  $1-2 \times 10^4$  cells per well of 24-well plate in triplicate. Cell proliferation was monitored at days 0, 3, 6 and 9 whereby cells were fixed for 15 min in a solution of 10% buffered formalin washed with phosphate-buffered saline (pH 7.2) and subsequently stained with 0.01% Crystal violet solution. Excessive staining was removed by washing the plates with distilled water and by drying them overnight. Crystal violet-stained cells were dissolved in 10% acetic acid solution for 30 min on a shaker and the extracted dye was read with a spectrophotometer at 590 nm. Cellular senescence in vitro was assessed using the Senescence  $\beta$ -Galactosidase Staining Kit (Catalog #9860; Cell Signaling) as per manufacturer's instructions and the quantification was done counting the total number of cells with Hoechst 3342, trihydrochloride, trihydrate (Catalog #953557; Invitrogen).

### **6.13 Liposomes formulation**

Stealth liposomes (SL) were prepared using HSPC:CHOL:mPEG<sub>5kDa</sub>-DSPE at a the 18:9:1 molar ratio. The lipid film, obtained evaporating a chloroform solution of the components, was hydrated

with a solution of 250 mM ammonium sulfate (pH 5.5) and then extruded at 60°C until reaching the vesicle size of ~100nm. The external buffer was exchanged to PBS pH 7.4 by a PD-10 desalting column. Doxorubicin (DXR) was encapsulated by remote loading (DXR: HSPC 0.2:1 w/w) at 60°C. Free DXR was removed using a PD-10 desalting column and the drug loading was determined spectrophotometrically ( $\lambda=477$  nm) in methanol. The CUB4 Fab'-coupled PEG-phospholipid derivative was prepared by reacting the Fab' of CUB4, obtained as described below, with maleimide-PEG-DSPE and then CUB4 Fab'-PEG-DSPE was introduced on the liposome surface by post-insertion to provide stealth immunoliposomes (SIL). Briefly, CUB4 was enzymatically digested with pepsin (1:50 w/w E/S, 3 h at 37°C) in 0.1 M sodium acetate at pH 3.8, followed by FPLC analysis on a Superose 12 10/300 GL column using PBS pH 7.4 (flow-rate 0.5 ml/min). The F(ab')<sub>2</sub> fragment was collected and treated 30 minutes at RT with 10 mM cysteamine to yield the Fab' fragment, following purified by FPLC using 50 mM phosphate buffer, 150 mM NaCl and 10 mM EDTA, pH 5. By exploiting its free sulfhydryl groups, Fab' was immediately coupled (overnight at rt, pH 7.0-7.5) to the maleimide groups of mixed micelles composed of Maleimide-PEG<sub>5kDa</sub>-DSPE:mPEG<sub>5kDa</sub>-DSPE 4:1 mol/mol at a final molar ratio of 10:1 Maleimide: Fab'. Finally, these micelles were incubated 1h at 60°C with SL at a molar ratio of 0.05:1 PEG:HSPC to achieve SIL, followed by purification on a Sepharose CL-4B column using PBS pH 7.4 and Fab' quantification by BCA assay.

#### **6.14 Statistics**

All data points are presented for quantitative data, with an overlay of the mean with SD and SEM (specified in the figures legends). All statistical analysis were performed using Graph Pad Prism 8 or Microsoft Excel 2016 or R-studio. The statistic test used is the T-test 1 or 2 tailed (as specified in the figures legends). Other used statistical analysis were indicated in the figure legends.

## 6.15 Study approval

All mice were maintained under specific-pathogen-free conditions in the animal facilities of the Institute for Research in Biomedicine, in Bellinzona. Experiments were performed according to state guidelines and approved by the local ethics committee. The *Pten*<sup>loxP</sup> conditional knockout mice have been previously described (12). CDCP1 conditional overexpression was generated as described in the text. However, to check for correct targeting of the transgene DNAs from different clones were digested with SpeI and analyzed for correct targeting using an internal 840-bp PstI/XbaI the ColA1 3`probe that hybridized also with the WT allele (33). To obtain the prostate-specific overexpression of CDCP1 and deletion of Pten, female CDCP1 and/or *Pten*<sup>loxP/loxP</sup> mice were crossed with male Probasin-Cre4 (Pb-Cre4) transgenic mice (34) . For genotyping, tail derived DNA was subjected to polymerase chain reaction (PCR) analyses. For *Pten*<sup>loxP/loxP</sup> genotyping, primer 1 (5'-AAAAGTTCCCCTGATGATGATTTGT-3') and primer 2 (5'-TGTTTTTGACCAATTAAAGTAGGCTGTG-3') were used, while for detecting the allele in the prostate, primer 3 (5'-TTCTCTTGAGCACTGTTTCACAGGC-3') and primer 1 were used. For Probasin-Cre4 (Pb-Cre4), primer 1 (5'-TGATGGACATGTTTCAGGGATC-3') and primer 2 (5'-GCCACCAGTCTGCATGA-3') while for CDCP1 mice, primer 1 (5'-CAAGGGAGAAGAGAGTGCGG -3') and primer 2 (5'-CCCAACAATGGGGATGTAAG -3) were used both for genotyping and detecting the allele in the prostate. For the downregulation of CDCP1, cells were infected with PLKO-sh-CDCP1 and doxycycline-inducible pTripz-CDCP1-shRNA. As control for both vectors we used as control non-target shRNA. In the xenograft experiments, 1×10<sup>6</sup> Tripz-sh*CDCP1* or Tripz-shRNA controls PC3 cells and 1×10<sup>6</sup> LNCaP cells were injected subcutaneously (s.c.) in SCID-NOD mice. After tumor cell injection, tumor formation was monitored every three days and upon tumor onset, the mice injected with PC3 cells were fed with Doxycycline (0.2 g/L) water supplemented with 5% sucrose until the end of the experiment. Necropsies were performed on the animals, and all tissues were examined regardless of their pathological status.

Normal and tumor tissue samples were fixed in 10% neutral-buffered formalin (Catalog #HT501128, Sigma) overnight. Then, samples were processed by ethanol dehydration and embedded in paraffin according to standard protocols. Sections (5  $\mu$ m) were prepared for antibody detection and hematoxylin and eosin staining.

## References

1. Hooper, J. D. *et al.* Subtractive immunization using highly metastatic human tumor cells identifies SIMA135/CDCP1, a 135 kDa cell surface phosphorylated glycoprotein antigen. *Oncogene* **22**, 1783–1794 (2003).
2. Brown, T. A. *et al.* Adhesion or Plasmin Regulates Tyrosine Phosphorylation of a Novel Membrane Glycoprotein p80/gp140/CUB Domain-containing Protein 1 in Epithelia. *Journal of Biological Chemistry* **279**, 14772–14783 (2004).
3. Bhatt, A. S., Erdjument-Bromage, H., Tempst, P., Craik, C. S. & Moasser, M. M. Adhesion signaling by a novel mitotic substrate of src kinases. *Oncogene* **24**, 5333–5343 (2005).
4. Takeda, H., Fujimori, Y., Kai, S., Ogawa, H. & Nakano, T. CD318/CUB-domain-containing protein 1 expression on cord blood hematopoietic progenitors. *Experimental and Therapeutic Medicine* **1**, 497–501 (2010).
5. Hooper, J. D. *et al.* Subtractive immunization using highly metastatic human tumor cells identifies SIMA135/CDCP1, a 135 kDa cell surface phosphorylated glycoprotein antigen. *Oncogene* **22**, 1783–1794 (2003).
6. Miyazawa, Y. *et al.* CDCP1 Regulates the Function of MT1-MMP and Invadopodia-Mediated Invasion of Cancer Cells. *Molecular Cancer Research* **11**, 628–637 (2013).
7. Marwa Scherl-Mostageer *et al.* Identification of a novel gene, CDCP1, overexpressed in human colorectal cancer. *Oncogene* **20**, 4402–4408 (2001).
8. Wortmann, A., He, Y., Deryugina, E. I., Quigley, J. P. & Hooper, J. D. The cell surface glycoprotein CDCP1 in cancer-Insights, opportunities, and challenges. *IUBMB Life* **61**, 723–730 (2009).
9. Gu, C. *et al.* Characterization of Neuropilin-1 Structural Features That Confer Binding to Semaphorin 3A and Vascular Endothelial Growth Factor 165. *Journal of Biological Chemistry* **277**, 18069–18076 (2002).

10. Predes, D., Cruz, J. V. R., Abreu, J. G. & Mendes, F. A. CUB domain-containing protein 1 (CDCP1) binds transforming growth factor beta family members and increase TGF- $\beta$ 1 signaling pathway. *Experimental Cell Research* **383**, 111499 (2019).
11. Uekita, T. *et al.* CUB Domain-Containing Protein 1 Is a Novel Regulator of Anoikis Resistance in Lung Adenocarcinoma. *Molecular and Cellular Biology* **27**, 7649–7660 (2007).
12. Benes, C. H. *et al.* The C2 Domain of PKC $\delta$  Is a Phosphotyrosine Binding Domain. *Cell* **121**, 271–280 (2005).
13. Law, M. E. *et al.* CUB domain-containing protein 1 and the epidermal growth factor receptor cooperate to induce cell detachment. *Breast Cancer Research* **18**, (2016).
14. Alajati, A. *et al.* Interaction of CDCP1 with HER2 Enhances HER2-Driven Tumorigenesis and Promotes Trastuzumab Resistance in Breast Cancer. *Cell Reports* **11**, 564–576 (2015).
15. Law, M. E. *et al.* Glucocorticoids and histone deacetylase inhibitors cooperate to block the invasiveness of basal-like breast cancer cells through novel mechanisms. *Oncogene* **32**, 1316–1329 (2013).
16. Casar, B. *et al.* Blocking of CDCP1 cleavage in vivo prevents Akt-dependent survival and inhibits metastatic colonization through PARP1-mediated apoptosis of cancer cells. *Oncogene* **31**, 3924–3938 (2012).
17. Awakura, Y. *et al.* Microarray-based identification of CUB-domain containing protein 1 as a potential prognostic marker in conventional renal cell carcinoma. *Journal of Cancer Research and Clinical Oncology* **134**, 1363–1369 (2008).
18. Ikeda, J. *et al.* Epigenetic regulation of the expression of the novel stem cell marker CDCP1 in cancer cells. *The Journal of Pathology* **210**, 75–84 (2006).
19. Bühring, H.-J. *et al.* CDCP1 identifies a broad spectrum of normal and malignant stem/progenitor cell subsets of hematopoietic and nonhematopoietic origin. *Stem cells* **22**, 334–343 (2004).

20. Uekita, T. *et al.* CUB-Domain-Containing Protein 1 Regulates Peritoneal Dissemination of Gastric Scirrhous Carcinoma. *The American Journal of Pathology* **172**, 1729–1739 (2008).
21. Conze T. *et al.* CDCP1 is a novel marker for Hematopoietic stem cells. *Ann. N.Y. Accademy of Science* **996**, 222-226 (2003).
22. Gioia, R. *et al.* Quantitative phosphoproteomics revealed interplay between Syk and Lyn in the resistance to nilotinib in chronic myeloid leukemia cells. *Blood* **118**, 2211–2221 (2011).
23. Boyer, A. P., Collier, T. S., Vidavsky, I. & Bose, R. Quantitative Proteomics with siRNA Screening Identifies Novel Mechanisms of Trastuzumab Resistance in HER2 Amplified Breast Cancers. *Molecular & Cellular Proteomics* **12**, 180–193 (2013).
24. Kollmorgen, G. *et al.* Antibody mediated CDCP1 degradation as mode of action for cancer targeted therapy. *Molecular Oncology* **7**, 1142–1151 (2013).
25. Siva, A. C. *et al.* Targeting CUB Domain-Containing Protein 1 with a Monoclonal Antibody Inhibits Metastasis in a Prostate Cancer Model. *Cancer Research* **68**, 3759–3766 (2008).
26. Beard, C., Hochedlinger, K., Plath, K., Wutz, A. & Jaenisch, R. Efficient method to generate single-copy transgenic mice by site-specific integration in embryonic stem cells. *genesis* **44**, 23–28 (2006).
27. Trotman, L. C. *et al.* Pten Dose Dictates Cancer Progression in the Prostate. *PLoS Biology* **1**, e59 (2003).
28. Monvoisin, A. *et al.* VE-cadherin-CreER<sup>T2</sup> transgenic mouse: A model for inducible recombination in the endothelium. *Developmental Dynamics* **235**, 3413–3422 (2006).
29. Jones, L. P. *et al.* Promotion of mammary cancer development by tamoxifen in a mouse model of Brca1-mutation-related breast cancer. *Oncogene* **24**, 3554–3562 (2005).
30. McMenamin *et al.* Loss of PTEN Expression in Paraffin-embedded Primary Prostate Cancer Correlates with High Gleason Score and Advanced Stage. *Cancer research* **59**, 4291-4296 (1999).

31. Di Cristofano *et al.* Pten is essential for embryonic development and tumour suppression. *Nature genetics* **19**, 348-355 (1998).
32. Carracedo, A., Alimonti, A. & Pandolfi, P. P. PTEN Level in Tumor Suppression: How Much Is Too Little?: Figure 1. *Cancer Research* **71**, 629–633 (2011).
33. Phin, S., Moore, M. W. & Cotter, P. D. Genomic Rearrangements of PTEN in Prostate Cancer. *Frontiers in Oncology* **3**, (2013).
34. Recine F. *et al.* Hormonal therapy and chemotherapy in hormone-naive and castration resistant prostate cancer. *Translational Andrology and Urology* **4(3)**, 355-364 (2015).
35. Wang X. *et al.* Clinical Significance of *PTEN* deletion, mutation, and Loss of PTEN expression in *De Novo* Diffuse large B-cell Lymphoma. *Neoplasia* **20**, 574-593 (2018).
36. Chen *et al.* Crucial role of p53-dependent cellular senescence in suppression of Pten-deficient tumorigenesis. *Nature* **436(7051)**, 725-730 (2005).
37. Borg. Hereditary prostate cancer:a new piece of the puzzle. *Nature publishing group* **7**, 153-155 (2001).
38. Wolf M. D. *et al.* American cancer society guide for the early detection of prostate cancer. *Cncer journal of clinicians* **60**, 70-98 (2010).
39. Trotman L. *et al.* Identification of a tumour suppressor network opposing nuclear Akt function. *Nature* **441(7092)**, 523-527 (2006).
40. Bubendorf, L. *et al.* Metastatic patterns of prostate cancer: An autopsy study of 1,589 patients. *Human Pathology* **31**, 578–583 (2000).
41. Logothetis, C. J. & Lin, S.-H. Osteoblasts in prostate cancer metastasis to bone. *Nature Reviews Cancer* **5**, 21–28 (2005).
42. Sharma P. *et al.* Mouse models of prostate cancer. *Oncogene* **18**, 5349-5355 (1998).
43. Shen, M. M. & Abate-Shen, C. Molecular genetics of prostate cancer: new prospects for old challenges. *Genes & Development* **24**, 1967–2000 (2010).

44. Salmena, L., Carracedo, A. & Pandolfi, P. P. Tenets of PTEN Tumor Suppression. *Cell* **133**, 403–414 (2008).
45. Mulholland, D. J. *et al.* Pten Loss and RAS/MAPK Activation Cooperate to Promote EMT and Metastasis Initiated from Prostate Cancer Stem/Progenitor Cells. *Cancer Research* **72**, 1878–1889 (2012).
46. Ding, Z. *et al.* SMAD4-dependent barrier constrains prostate cancer growth and metastatic progression. *Nature* **470**, 269–273 (2011).
47. Donnou, S. *et al.* Murine Models of B-Cell Lymphomas: Promising Tools for Designing Cancer Therapies. *Advances in Hematology* **2012**, 1–13 (2012).
48. Ekström-Smedby, K. Epidemiology and etiology of non-Hodgkin lymphoma – a review. *Acta Oncologica* **45**, 258–271 (2006).
49. Lenz G. *et al.* Molecular subtypes of diffuse large B-cell lymphoma arise by distinct genetic pathways. *PNAS* **105**, 13520-13525 (2008).
50. Pasqualucci, L. Molecular pathogenesis of germinal center-derived B cell lymphomas. *Immunological Reviews* **288**, 240–261 (2019).
51. Basso, K. & Dalla-Favera, R. Germinal centres and B cell lymphomagenesis. *Nature Reviews Immunology* **15**, 172–184 (2015).
52. Alimonti, A. *et al.* A novel type of cellular senescence that can be enhanced in mouse models and human tumor xenografts to suppress prostate tumorigenesis. *Journal of Clinical Investigation* **120**, 681–693 (2010).
53. Taylor, B. S. *et al.* Integrative Genomic Profiling of Human Prostate Cancer. *Cancer Cell* **18**, 11–22 (2010).
54. Qin, J. *et al.* COUP-TFII inhibits TGF- $\beta$ -induced growth barrier to promote prostate tumorigenesis. *Nature* **493**, 236–240 (2013).

55. Furstoss O. *et al.* c-Abl is an effector of Src for growth factor-induced c-myc expression and DNA synthesis. *The EMBO journal* **21**, 514-524 (2002).
56. Jain, S. *et al.* Src Inhibition Blocks c-Myc Translation and Glucose Metabolism to Prevent the Development of Breast Cancer. *Cancer Research* **75**, 4863–4875 (2015).
57. Barone M. V. *et al.* Myc but not Fos rescue of PDGF signaling block caused by kinase-inactive Src. *Nature* **378**, 509-512 (1995).
58. Lunardi, A. *et al.* A co-clinical approach identifies mechanisms and potential therapies for androgen deprivation resistance in prostate cancer. *Nature Genetics* **45**, 747–755 (2013).
59. Di Mitri, D. *et al.* Tumour-infiltrating Gr-1+ myeloid cells antagonize senescence in cancer. *Nature* **515**, 134–137 (2014).
60. Hennequin, L. F. *et al.* N -(5-Chloro-1,3-benzodioxol-4-yl)-7-[2-(4-methylpiperazin-1-yl)ethoxy]-5- (tetrahydro-2 H -pyran-4-yloxy)quinazolin-4-amine, a Novel, Highly Selective, Orally Available, Dual-Specific c-Src/Abl Kinase Inhibitor. *Journal of Medicinal Chemistry* **49**, 6465–6488 (2006).
61. Cima, I. *et al.* Cancer genetics-guided discovery of serum biomarker signatures for diagnosis and prognosis of prostate cancer. *Proceedings of the National Academy of Sciences* **108**, 3342–3347 (2011).
62. Fankhauser C. D. *et al.* Comprehensive Immunohistochemical analysis of PDL-1 shows scarce expression in castration-resistant prostate cancer. *Oncotarget* **9**, 10284-10293 (2018).
63. Zellweger, T. *et al.* Estrogen receptor  $\beta$  expression and androgen receptor phosphorylation correlate with a poor clinical outcome in hormone-naïve prostate cancer and are elevated in castration-resistant disease. *Endocrine-Related Cancer* **20**, 403–413 (2013).
64. Carver *et al.* Reciprocal feedback regulation of PI3K and androgen receptor signaling in PTEN-deficient prostate cancer. *Cancer cell* **19(5)**, 575-586 (2011).
65. Burton, D. G. A. *et al.* Androgen Deprivation-Induced Senescence Promotes Outgrowth of

- Androgen-Refractory Prostate Cancer Cells. *PLoS ONE* **8**, e68003 (2013).
66. Campisi, J. Aging and cancer: the double-edged sword of replicative senescence. *Journal of the American Geriatrics Society* **45**, 482–488 (1997).
67. Jain, R. K. Normalization of Tumor Vasculature: An Emerging Concept in Antiangiogenic Therapy. *Science* **307**, 58–62 (2005).
68. Maeda, H., Nakamura, H. & Fang, J. The EPR effect for macromolecular drug delivery to solid tumors: Improvement of tumor uptake, lowering of systemic toxicity, and distinct tumor imaging in vivo. *Advanced Drug Delivery Reviews* **65**, 71–79 (2013).
69. Maeda, H., Tsukigawa, K. & Fang, J. A Retrospective 30 Years After Discovery of the Enhanced Permeability and Retention Effect of Solid Tumors: Next-Generation Chemotherapeutics and Photodynamic Therapy-Problems, Solutions, and Prospects. *Microcirculation* **23**, 173–182 (2016).
70. Shojaee, S. *et al.* PTEN opposes negative selection and enables oncogenic transformation of pre-B cells. *Nature Medicine* **22**, 379–387 (2016).
71. Alimonti, A. *et al.* Subtle variations in Pten dose determine cancer susceptibility. *Nature Genetics* **42**, 454–458 (2010).
72. Di Cristofano *et al.* Impaired Fas Response and Autoimmunity in Pten<sup>+/-</sup> Mice. *Science* **285**, 2122-2125 (1999).
73. Brescia, P. *et al.* MEF2B Instructs Germinal Center Development and Acts as an Oncogene in B Cell Lymphomagenesis. *Cancer Cell* **34**, 453–465.e9 (2018).
74. Lu, C. *et al.* The value of detecting immunoglobulin gene rearrangements in the diagnosis of B-cell lymphoma. *Oncotarget* **8**, 77009 (2017).
75. Zheng X. *et al.* Different sensitivity of germinal center B-cell like diffuse large B cell lymphoma cells towards ibrutinib treatment. *Cancer cell international* **14**, 2-9 (2014).

76. Jacobs L. *et al.* Functional imaging in combination with mutation status aids prediction of response to inhibiting B-cell receptor signaling in lymphoma. *Oncotarget* **8**, 78917-78929 (2017).
77. Uekita, T. & Sakai, R. Roles of CUB domain-containing protein 1 signaling in cancer invasion and metastasis. *Cancer Science* **102**, 1943–1948 (2011).
78. Yang L. *et al.* Dysregulated expression of cell surface glycoprotein CDCP1 in prostate cancer. *Oncotarget* **6**, 43743- 43758 (2015).
79. Jamaspishvili, T. *et al.* Clinical implications of PTEN loss in prostate cancer. *Nature Reviews Urology* **15**, 222–234 (2018).
80. Chandran, U. R. *et al.* Gene expression profiles of prostate cancer reveal involvement of multiple molecular pathways in the metastatic process. *BMC Cancer* **7**, (2007).
81. Revandkar, A. *et al.* Inhibition of Notch pathway arrests PTEN-deficient advanced prostate cancer by triggering p27-driven cellular senescence. *Nature Communications* **7**, (2016).
82. Varambally, S. *et al.* Integrative genomic and proteomic analysis of prostate cancer reveals signatures of metastatic progression. *Cancer Cell* **8**, 393–406 (2005).
83. Grasso, C. S. *et al.* The mutational landscape of lethal castration-resistant prostate cancer. *Nature* **487**, 239–243 (2012).
84. Lefort K. *et al.* Dual tumor suppressing and promoting function of Notch1 Signaling in human prostate cancer. *Oncotarget* **7**, 48011-48026 (2016).
85. Wang, L., Wang, S. & Li, W. RSeQC: quality control of RNA-seq experiments. *Bioinformatics* **28**, 2184–2185 (2012).
86. Chen, S. *et al.* AfterQC: automatic filtering, trimming, error removing and quality control for fastq data. *BMC Bioinformatics* **18**, (2017).
87. Garcia-Alcalde F. *et al.* Qualimap: evaluating next-generation sequencing alignment data. *Bioinformatics* **28**, 2678-2679 (2012).

88. Dobin, A. *et al.* STAR: ultrafast universal RNA-seq aligner. *Bioinformatics* **29**, 15–21 (2013).
89. Harrow, J. *et al.* GENCODE: The reference human genome annotation for The ENCODE Project. *Genome Res.* **22**, 1760–1774 (2012).
90. Robinson, M. D., McCarthy, D. J. & Smyth, G. K. edgeR: a Bioconductor package for differential expression analysis of digital gene expression data. *Bioinformatics* **26**, 139–140 (2010).
91. Ritchie, M. E. *et al.* limma powers differential expression analyses for RNA-sequencing and microarray studies. *Nucleic Acids Research* **43**, e47–e47 (2015).
92. Kuleshov, M. V. *et al.* Enrichr: a comprehensive gene set enrichment analysis web server 2016 update. *Nucleic Acids Research* **44**, W90–W97 (2016).

## Annex 1

**Figure 6:** The Pb-Cre CDCP1<sup>loxP/loxP</sup> transgenic mouse model was generated from a former Pos-doc while I was involved since the beginning in the generation of the full-body mouse model.

**Figure 11:** I performed the RT-PCR and the western blots in panels B, C, and D.

**Figure 12:** I performed the western blots and quantification in panels D and E.

**Figure 13:** I helped to sacrifice the mice used for pathological and survival analysis. I performed the western blots and quantification in panel F.

**Figure 14:** I performed surgical castration both in transgenic mice and in TC1 mice. I sacrificed and analyzed mice. I performed western blots and RT-PCRs present in the figures.

**Figure 15:** I performed SA- $\beta$ -gal staining both in tissues and in MEFs. I performed all the western blots present in the figures.

**Figure 16:** I performed all the experiments in this figure.

**Figure 17:** I performed all the *in vitro* experiments present in this figure.

**Figure 20:** I performed all the experiments in the figure (except panel A).

**Figure 21:** I performed experiments and western blots present in panels A and B.

**Figure 22:** I performed the *in vitro* experiment with the immune-liposome in panels B and C and the *in vivo* experiment in panels D and E with a former Pos-doc of the lab.

**Figure 23-29:** I performed all the experiments presented in the figure with the help of a master student that I supervised and a lab technician, under the supervision of my PI Andrea Alimonti.

## Annex 2

# CDCP1 overexpression drives prostate cancer progression and can be targeted in vivo

**Abdullah Alajati,<sup>1,2</sup> Mariantonietta D'Ambrosio,<sup>1,2,3</sup> Martina Troiani,<sup>1,2</sup> Simone Mosole,<sup>1,2</sup> Laura Pellegrini,<sup>1,2</sup> Jingjing Chen,<sup>1,2,3</sup> Ajinkya Revandkar,<sup>1,2,3</sup> Marco Bolis,<sup>1,2</sup> Jean-Philippe Theurillat,<sup>1,2</sup> Ilaria Guccini,<sup>1,2</sup> Marco Losa,<sup>1,2</sup> Arianna Calcinotto,<sup>1,2</sup> Gaston De Bernardis,<sup>1,2</sup> Emiliano Pasquini,<sup>1,2</sup> Rocco D'Antuono,<sup>4</sup> Adam Sharp,<sup>5</sup> Ines Figueiredo,<sup>5,6</sup> Daniel Nava Rodrigues,<sup>5,6</sup> Jonathan Welti,<sup>5,6</sup> Veronica Gil,<sup>5,6</sup> Wei Yuan,<sup>5,6</sup> Tatjana Vlajnic,<sup>7</sup> Lukas Bubendorf,<sup>7</sup> Giovanna Chiorino,<sup>8</sup> Letizia Gnetti,<sup>9</sup> Verónica Torrano,<sup>10,11,12</sup> Arkaitz Carracedo,<sup>10,11,12,13</sup> Laura Campese,<sup>14</sup> Susumu Hirabayashi,<sup>14</sup> Elena Canato,<sup>15</sup> Gianfranco Pasut,<sup>15</sup> Monica Montopoli,<sup>15</sup> Jan Hendrik Rüschoff,<sup>16</sup> Peter Wild,<sup>16</sup> Holger Moch,<sup>16</sup> Johann De Bono,<sup>5,6</sup> and Andrea Alimonti<sup>1,2,3,17,18</sup>**

1 Institute of Oncology Research (IOR), Oncology Institute of Southern Switzerland (IOSI), Bellinzona, Switzerland.

2 Università della Svizzera Italiana, Lugano, Switzerland.

3 Faculty of Biology and Medicine, University of Lausanne UNIL, Lausanne, Switzerland.

4 Institute for Research in Biomedicine (IRB), Bellinzona, Switzerland.

5 Division of Clinical Studies, Institute of Cancer Research, London, United Kingdom.

6 Royal Marsden NHS Foundation Trust, London, United Kingdom.

7 Institute for Pathology, University Hospital Basel, Basel, Switzerland.

8 Fondazione Edo ed Elvo Tempia, Via Malta, Biella, Italy.

9 Pathology Unit, University Hospital of Parma, Parma, Italy.

10 Center for Cooperative Research in Biosciences (CIC bioGUNE), Basque Research and Technology Alliance (BRTA), Derio, Spain.

11 Biochemistry and Molecular Biology Department, University of the Basque Country (UPV/EHU), Bilbao, Spain.

12 Centro de Investigación Biomédica en Red Cáncer (CIBERONC), Madrid, Spain.

13 Ikerbasque: Basque Foundation for Science, Bilbao, Spain.

14 MRC London Institute of Medical Sciences (LMS), Imperial College London, London, United Kingdom.

15 Department of Pharmaceutical and Pharmacological Sciences, University of Padua, Padua, Italy.

16 Institute of Pathology and Molecular Pathology, University Hospital Zurich, Zurich, Switzerland. 17 Department of Medicine, University of Padua, Padua, Italy.

18 Department of Health Sciences and Technology, Eidgenössische Technische Hochschule Zürich (ETH), Zurich, Switzerland.

## CDCP1 overexpression drives prostate cancer progression and can be targeted in vivo

Abdullah Alajati, ... , Johann De Bono, Andrea Alimonti

*J Clin Invest.* 2020;130(5):2435-2450. <https://doi.org/10.1172/JCI131133>.

Research Article

Oncology

The mechanisms by which prostate cancer shifts from an indolent castration-sensitive phenotype to lethal castration-resistant prostate cancer (CRPC) are poorly understood. Identification of clinically relevant genetic alterations leading to CRPC may reveal potential vulnerabilities for cancer therapy. Here we find that CUB domain-containing protein 1 (CDCP1), a transmembrane protein that acts as a substrate for SRC family kinases (SFKs), is overexpressed in a subset of CRPC. Notably, CDCP1 cooperates with the loss of the tumor suppressor gene PTEN to promote the emergence of metastatic prostate cancer. Mechanistically, we find that androgens suppress CDCP1 expression and that androgen deprivation in combination with loss of PTEN promotes the upregulation of CDCP1 and the subsequent activation of the SRC/MAPK pathway. Moreover, we demonstrate that anti-CDCP1 immunoliposomes (anti-CDCP1 ILs) loaded with chemotherapy suppress prostate cancer growth when administered in combination with enzalutamide. Thus, our study identifies CDCP1 as a powerful driver of prostate cancer progression and uncovers different potential therapeutic strategies for the treatment of metastatic prostate tumors.

Find the latest version:

<https://jci.me/131133/pdf>



# CDCP1 overexpression drives prostate cancer progression and can be targeted in vivo

Abdullah Alajati,<sup>1,2</sup> Mariantonietta D'Ambrosio,<sup>1,2,3</sup> Martina Troiani,<sup>1,2</sup> Simone Mosole,<sup>1,2</sup> Laura Pellegrini,<sup>1,2</sup> Jingjing Chen,<sup>1,2,3</sup> Ajinkya Revandkar,<sup>1,2,3</sup> Marco Bolis,<sup>1,2</sup> Jean-Philippe Theurillat,<sup>1,2</sup> Ilaria Guccini,<sup>1,2</sup> Marco Losa,<sup>1,2</sup> Arianna Calcinotto,<sup>1,2</sup> Gaston De Bernardis,<sup>1,2</sup> Emiliano Pasquini,<sup>1,2</sup> Rocco D'Antuono,<sup>4</sup> Adam Sharp,<sup>5</sup> Ines Figueiredo,<sup>5,6</sup> Daniel Nava Rodrigues,<sup>5,6</sup> Jonathan Welti,<sup>5,6</sup> Veronica Gil,<sup>5,6</sup> Wei Yuan,<sup>5,6</sup> Tatjana Vlajnic,<sup>7</sup> Lukas Bubendorf,<sup>7</sup> Giovanna Chiorino,<sup>8</sup> Letizia Gnetti,<sup>9</sup> Verónica Torrano,<sup>10,11,12</sup> Arkaitz Carracedo,<sup>10,11,12,13</sup> Laura Complesse,<sup>14</sup> Susumu Hirabayashi,<sup>14</sup> Elena Canato,<sup>15</sup> Gianfranco Pasut,<sup>15</sup> Monica Montopoli,<sup>15</sup> Jan Hendrik Rüschoff,<sup>16</sup> Peter Wild,<sup>16</sup> Holger Moch,<sup>16</sup> Johann De Bono,<sup>5,6</sup> and Andrea Alimonti<sup>1,2,3,17,18</sup>

<sup>1</sup>Institute of Oncology Research (IOR), Oncology Institute of Southern Switzerland (IOSI), Bellinzona, Switzerland. <sup>2</sup>Università della Svizzera Italiana, Lugano, Switzerland. <sup>3</sup>Faculty of Biology and Medicine, University of Lausanne UNIL, Lausanne, Switzerland. <sup>4</sup>Institute for Research in Biomedicine (IRB), Bellinzona, Switzerland. <sup>5</sup>Division of Clinical Studies, Institute of Cancer Research, London, United Kingdom. <sup>6</sup>Royal Marsden NHS Foundation Trust, London, United Kingdom. <sup>7</sup>Institute for Pathology, University Hospital Basel, Basel, Switzerland. <sup>8</sup>Fondazione Edo ed Elvo Tempia, Via Malta, Biella, Italy. <sup>9</sup>Pathology Unit, University Hospital of Parma, Parma, Italy. <sup>10</sup>Center for Cooperative Research in Biosciences (CIC bioGUNE), Basque Research and Technology Alliance (BRTA), Derio, Spain. <sup>11</sup>Biochemistry and Molecular Biology Department, University of the Basque Country (UPV/EHU), Bilbao, Spain. <sup>12</sup>Centro de Investigación Biomédica en Red Cáncer (CIBERONC), Madrid, Spain. <sup>13</sup>Ikerbasque: Basque Foundation for Science, Bilbao, Spain. <sup>14</sup>MRC London Institute of Medical Sciences (LMS), Imperial College London, London, United Kingdom. <sup>15</sup>Department of Pharmaceutical and Pharmacological Sciences, University of Padua, Padua, Italy. <sup>16</sup>Institute of Pathology and Molecular Pathology, University Hospital Zurich, Zurich, Switzerland. <sup>17</sup>Department of Medicine, University of Padua, Padua, Italy. <sup>18</sup>Department of Health Sciences and Technology, Eidgenössische Technische Hochschule Zürich (ETH), Zurich, Switzerland.

**The mechanisms by which prostate cancer shifts from an indolent castration-sensitive phenotype to lethal castration-resistant prostate cancer (CRPC) are poorly understood. Identification of clinically relevant genetic alterations leading to CRPC may reveal potential vulnerabilities for cancer therapy. Here we find that CUB domain-containing protein 1 (CDCP1), a transmembrane protein that acts as a substrate for SRC family kinases (SFKs), is overexpressed in a subset of CRPC. Notably, CDCP1 cooperates with the loss of the tumor suppressor gene PTEN to promote the emergence of metastatic prostate cancer. Mechanistically, we find that androgens suppress CDCP1 expression and that androgen deprivation in combination with loss of PTEN promotes the upregulation of CDCP1 and the subsequent activation of the SRC/MAPK pathway. Moreover, we demonstrate that anti-CDCP1 immunoliposomes (anti-CDCP1 ILs) loaded with chemotherapy suppress prostate cancer growth when administered in combination with enzalutamide. Thus, our study identifies CDCP1 as a powerful driver of prostate cancer progression and uncovers different potential therapeutic strategies for the treatment of metastatic prostate tumors.**

## Introduction

Castration-resistant prostate cancer (CRPC) is the second leading cause of death among men in developed countries (1). Although second-generation androgen-deprivation therapies (ADTs) have been successfully used to treat CRPC, patients develop resistance and eventually succumb to the disease (2). Mechanisms of resistance in CRPCs include, among others, activation of androgen receptor (AR) (i.e., AR amplification, mutations, or splicing variants) and upregulation of signaling pathways promoting AR independent growth, such as the PI3K/AKT and MAPK pathways that are mutually deregulated in CRPCs (3–6). Although in metastatic prostate cancers the PI3K signaling pathway is activated by the loss or mutations of the tumor suppressor PTEN (7), the mecha-

nism by which the MAPK pathway is upregulated remains partially unknown. Interestingly, activation of the MAPK pathway by K-RAS in a PTEN-deficient prostate cancer mouse model leads to the development of metastatic prostate cancer (8). However, mutations of either KRAS or BRAF account for only a minority of human prostate cancer cases (5, 9, 10). Thus, the identification of new regulators of this pathway, in the context of PTEN-null prostate cancers, would open the way to new effective therapies for the treatment of this disease. The *Pten*-null prostate conditional mouse model provides an excellent tool to study prostate tumorigenesis. *Pten* deficiency in the mouse prostate epithelium leads to benign prostate tumors characterized by a senescence response that opposes tumor progression (11, 12). Therefore, this model can be used to identify pathways or genes that serve as the “second hit” for the evasion of senescence, acquisition of metastatic potential, and the preclinical validation of new therapies in this setting (12–14).

CUB domain-containing protein 1 (CDCP1), also known as SIMA135 (15), gp140 (16), CD318 (17), or Trask (18), is a transmembrane protein that is frequently overexpressed in a variety of human cancers (19–21). Several papers demonstrate that CDCP1 is a potent oncogene that drives cancer development, invasion,

**Authorship note:** A. Alajati and MD contributed equally to this work.

**Conflict of interest:** A. Alimonti is a cofounder of and owns stock in OncoSense.

**Copyright:** © 2020 Alajati et al. This is an open access article published under the terms of the Creative Commons Attribution 4.0 International License.

**Submitted:** June 18, 2019; **Accepted:** January 22, 2020; **Published:** April 6, 2020.

**Reference information:** *J Clin Invest.* 2020;130(5):2435–2450.

<https://doi.org/10.1172/JCI131133>.

**Table 1. CDCP1-positive samples in BPH, RPE, CRPC, and metastatic PCa in human prostate cancers**

	BPH	RPE	CRPC	Metastasis
Total	45	382	102	35
CDCP1-positive	4	65	45	18

For TMA1,  $n = 564$ .

and metastases. In cells cultured in adherent conditions, CDCP1 overexpression promotes the activation of Src-family members (SFKs), phosphorylation of protein kinase C delta (PKC- $\delta$ ), and the upregulation of the MAPK/ERK pathway (22). In contrast with these results, recent studies reported that loss of CDCP1, in cells kept in nonadherent conditions, supports tumor cells proliferation by differentially regulating SRC activity (23–25). Interestingly, CDCP1 targeting, either with monoclonal antibodies or small molecule inhibitors, has demonstrated effectiveness at inhibiting tumor growth and metastasis in vivo (26–28). Since treatments with either SRC or MAPK inhibitors have been associated with poor tolerability in the clinic (29), CDCP1 targeting could represent an excellent and alternative therapeutic option. In the present manuscript, we show that CDCP1 is overexpressed in a subset of advanced human CRPCs, and cooperates with loss of PTEN to promote the emergence of this disease. Moreover, we have found that AR represses CDCP1 transcription, whereas ADTs promote the upregulation of CDCP1 in tumor cells harboring PTEN deletions, thereby increasing the activation of the SRC/MAPK pathway. Notably, treatment of anti-CDCP1 ILs loaded with chemotherapy in combination with enzalutamide substantially inhibits prostate tumor progression. Our results introduce what we believe is a previously unknown and exciting therapeutic strategy to treat PTEN-deficient prostate cancer patients.

## Results

*CRPC and metastatic prostate tumors exhibit elevated expression of CDCP1, and overexpression of CDCP1 correlates with PTEN loss.* To assess the clinical relevance of CDCP1 in human prostate cancer (human PCa), we examined 2 different tumor microarrays (TMAs), including a total of 990 cases spanning benign, primary, and metastatic PCa (30–32). Immunohistochemical (IHC) analysis showed that while a large portion of prostate tumors analyzed did not express CDCP1, a subset (48%) of CRPC and metastatic tumor samples expressed a high level of CDCP1 (Figure 1, A and B, Supplemental Figure 1A, and Tables 1 and 2; supplemental material available online with this article; <https://doi.org/10.1172/JCI131133DS1>). In line with these findings, analysis of consecutive tumor samples from a longitudinal study revealed that CDCP1 was upregulated in PCa patients during the transition from hormone-sensitive to CRPC (Supplemental Figure 1B). Intriguingly, high levels of CDCP1 correlated with decreased levels of PTEN in both primary, CRPC, and metastatic prostate tumor samples (Figure 1, C and D, and Tables 3 and 4). PTEN is one of the most frequently altered tumor suppressor genes in PCa, where it accounts for prostate tumor initiation and progression (5). The frequency of tumors displaying a low level of

PTEN and high levels of CDCP1 increased in CRPCs and metastatic tumors when compared with primary tumors, thereby validating the clinical relevance of this anti-correlation (Figure 1, C and D, and Tables 3 and 4). Additionally, bioinformatics analysis evaluating different data sets confirmed the existence of an anti-correlation between PTEN and CDCP1 mRNA levels (Supplemental Figure 1, C and D). Elevated levels of CDCP1 expression were also significantly associated with PTEN genetic deletions and low CDCP1 promoter methylation in different independent data sets of PCa (Figure 1E and Supplemental Figure 1, E and F). Although patients affected by prostate tumors harboring a high level of CDCP1 had a similar disease-free survival (DFS) as patients with low CDCP1, patients with tumors expressing low levels of PTEN and an increased level of CDCP1 had a significantly shorter DFS than patients in the other categories (Figure 1F and Supplemental Figure 1G). Taken together, these data validate the clinical relevance of CDCP1 and suggest that CDCP1 could cooperate with the loss of PTEN to promote highly aggressive prostate cancer.

*Conditional overexpression of CDCP1 in the mouse prostate and Drosophila melanogaster initiates tumorigenesis.* To model CDCP1 overexpression in cancer, we generated a CDCP1 transgenic mouse model. At first, we constructed a pCAGGS vector with a transcriptional STOP sequence flanked by loxP sites upstream of CDCP1-cDNA. The resulting pCAGGS-loxP-STOP-loxP-CDCP1 vector along with PGK-FlpO plasmid were coelectroporated into the ColA locus of modified KH2 embryonic stem cells (ref. 33 and Supplemental Figure 2A). PCR and Southern blot analysis confirmed gene integration and recombination events (Supplemental Figure 2B). Next, we crossed CDCP1 with PB-Cre4 mice for prostate-specific expression of CDCP1 (34). IHC, reverse transcription PCR (RT-PCR), and Western blot analyses were performed on prostate tissues of 10-week-old CDCP1<sup>Pb-Cre</sup> mice (CDCP1<sup>pcLSL/+</sup>, hereafter referred to as CDCP1<sup>+</sup>) and confirmed the prostate-specific expression of CDCP1 (Supplemental Figure 2, C–E). Of note, the expression of CDCP1 in a panel of human prostate tumor cell lines, patient-derived prostate cancer xenografts (PDXs), and tumors collected from CDCP1<sup>+</sup> mice did not show significant differences in CDCP1 levels (Supplemental Figure 2F), thereby demonstrating that overexpression of CDCP1 in the mouse model is similar to the CDCP1 levels in human tumors. Next, we examined tumor incidence in CDCP1 mice over 24 months. CDCP1 mice developed prostate hyperplasia between 4 and 6 months of age at 50% penetrance. CDCP1 mice between 7 and 9 months of age developed a high penetrance of PIN (prostatic intraepithelial neoplasia) lesions characterized by multilayered epithelial cells with features of nuclear atypia. These mice further developed high-

**Table 2. CDCP1 membranous staining in TMA1 tumors from BPH/RPE and CRPC/metastasis patients**

	Total	CDCP1-positive
BPH/RPE	427	69
CRPC/metastasis	137	63

The  $\chi^2$  test was used for statistical analysis.  $\chi^2 = 29.9301$ .  $P < 0.00001$ . The result is significant at  $P < 0.05$ .

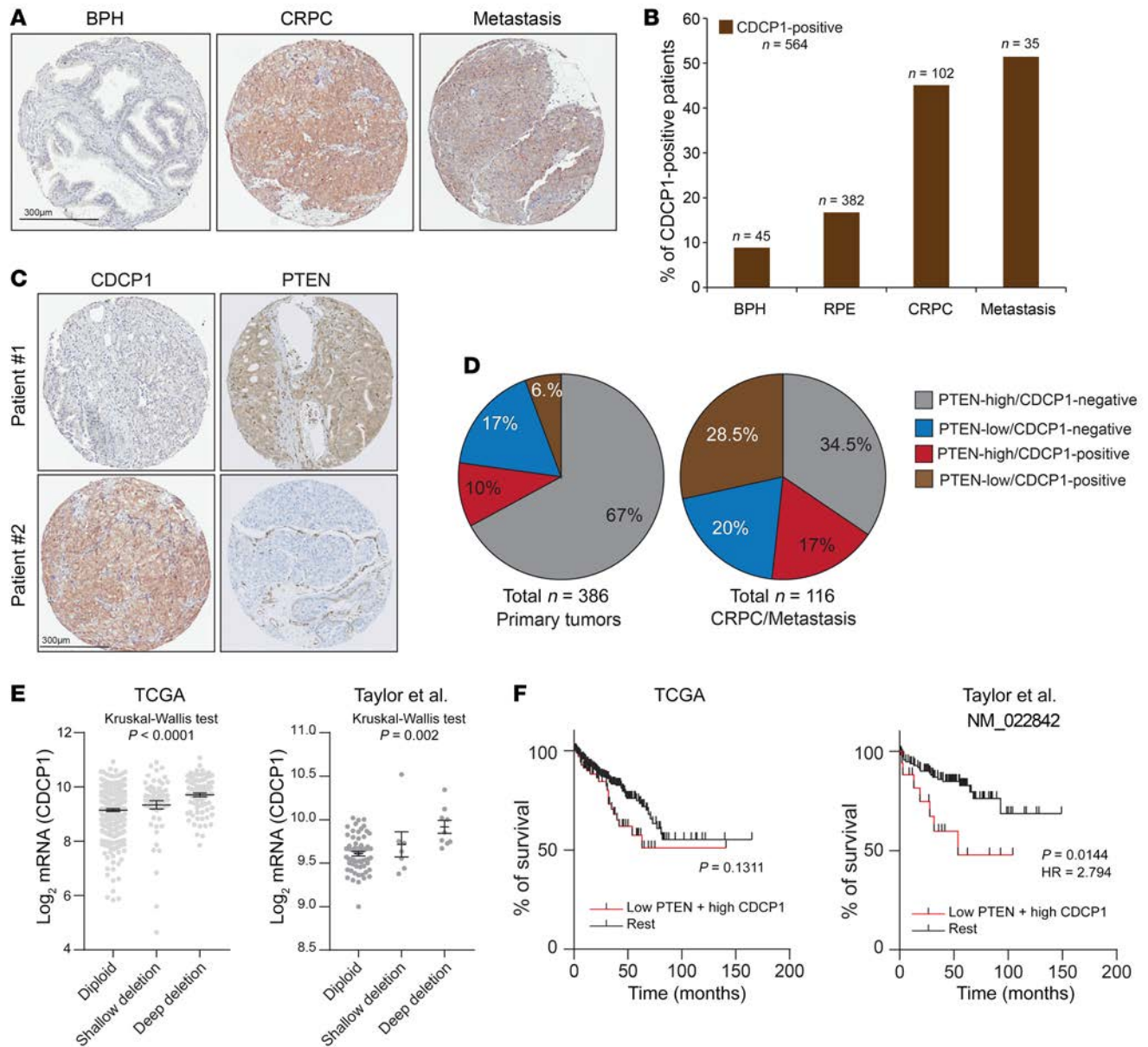


**Figure 1. Advanced and metastatic prostate tumors exhibit elevated expression of CDCP1 and overexpression of CDCP1 correlate with PTEN loss. (A)** Representative images of IHC staining of CDCP1 in benign prostate hyperplasia (BPH), CRPC, and distant metastasis of PCa in human prostate cancer TMA1. Scale bar: 300  $\mu$ m. **(B)** Percentage of CDCP1-positive samples in BPH, preradical prostatectomy (RPE), CRPC, and metastatic PCa in human prostate cancer TMA1 (n = 564). **(C)** Representative images of IHC staining of CDCP1 and PTEN in 2 different PCA patients. Scale bar: 300  $\mu$ m. **(D)** Pie graph showing the percentage of PTEN-high/CDCP1<sup>-</sup>, PTEN-high/CDCP1<sup>+</sup>, PTEN-low/CDCP1<sup>-</sup> and PTEN-low/CDCP1<sup>+</sup> in primary tumors and CRPC/metastasis. **(E)** Association of PTEN genomic loss to CDCP1 gene expression in TCGA (left panel) and Taylor data set (right panel) (5). Error bars indicate SEM; statistical test: Kruskal-Wallis. **(F)** Association of PTEN and CDCP1 expression levels with disease-free survival in the indicated patient data sets. In the Taylor data set, low PTEN indicates patients with expression signal lower than 8.74, and high CDCP1 indicates patients with expression signal higher than 11.19. In TCGA, low PTEN indicates patients with expression signal lower than 10.19, and high CDCP1 indicates patients with expression signal higher than 9.49. HR, hazard ratio. Statistical test: Mantel-Cox.

grade PIN (HGPIN) lesions after 14 months of age with 100% penetrance and showed high Ki67 expression (Figure 2, A–D, and Supplemental Figure 2G). In parallel, Western blot analysis revealed a significant increase of Src and Erk1/2 phosphorylation in the prostatic epithelium of *CDCP1* mice and *CDCP1*<sup>+</sup> mouse embryonic fibroblast (MEFs) derived from this model (Figure 2, E and F). To further validate these findings in a different model, we overexpressed both WT human CDCP1 (CDCP1-WT) and an inactive

form of CDCP1 (CDCP1-delta) lacking Src-phosphorylation sites (35, 36) in *Drosophila melanogaster*. The *Drosophila* larval imaginal discs are a monolayer epithelium that is considered morphologically comparable to mammalian epithelia and therefore constitutes an ideal system in which to model cancer progression in vivo (37). Increased EGFR/Ras signaling has been previously shown to promote the formation of bristles located on the dorsal part of the fly thorax (notum) (also referred to as macrochaetae formation),

**Table 3. PTEN and CDCP1 membranous staining in primary TMA1 tumors from PCa patients**

	CDCP1-negative	CDCP1-positive
PTEN-normal	259	39
PTEN-low	66	22

To shear cross-linked DNA to an average fragment, the  $\chi^2$  statistical test was used.  $\chi^2 = 7.246$ .  $P < 0.007106$ . The result is significant at  $P < 0.05$ .

a tumor-like phenotype (35, 36). We found that overexpression of CDCP1-WT, but not CDCP1-delta, promoted extra macrochaetae formation. Note that both CDCP1 isoforms localized at the cell membrane of the salivary gland of the fly, as assessed by costaining of E-cadherin, and presented similar expression levels (Supplemental Figure 3, A–C, arrows). Interestingly, loss of 1 allele (50% reduction) of *src42A* and *src64B* (35, 38, 39), the 2 Src homologs in *Drosophila*, suppressed extra macrochaetae formation driven by the overexpression of CDCP1-WT, demonstrating that this phenotype is Src-dependent (Supplemental Figure 3D). Collectively, this cross-species genetic approach demonstrates that CDCP1 overexpression in vivo initiates tumorigenesis.

*CDCP1 cooperates with Pten loss to drive prostate cancer progression and metastasis.* To further model the interplay existing between PTEN and CDCP1 in vivo, we crossed *CDCP1* mice with *Pten*-null prostate conditional mice (*Pten<sup>pc-/-</sup>*) to obtain *CDCP1 Pten<sup>pc-/-</sup>* double mutant mice. Although monoallelic loss or mutations in *PTEN* is associated with benign prostate tumors (34, 40), complete loss of *PTEN* is frequently observed in human metastatic prostate cancer (5). However, complete loss of *Pten* in the mouse is not sufficient to promote metastatic prostate cancer and additional genetic hits are needed to promote the onset of metastases (12). Strikingly, by the age of 25 weeks, *CDCP1 Pten<sup>pc-/-</sup>* mice developed focally invasive adenocarcinoma, which progressed to highly aggressive carcinoma at later time points, a phenotype that is never observed in *Pten<sup>pc-/-</sup>* mice (Figure 3A). Notably, the macroscopic analysis showed a significant increase in weight and volume of *CDCP1 Pten<sup>pc-/-</sup>* tumor compared with its counterparts (Figure 3B). Importantly, histopathological analysis of *CDCP1 Pten<sup>pc-/-</sup>* mice revealed metastatic spread of epithelial tumor nodules, positive for Pan-Cytokeratin (PanK), CDCP1, and AR, to draining lumbar lymph nodes in 50% ( $n = 4/8$ ) and to the lung in 11% ( $n = 1/9$ ) of the cases analyzed (Figure 3C and Supplemental Figure 4, A and B). The histological features of these metastases resembled those of the primary prostate tumors (Supplemental Figure 4A). By contrast, *Pten<sup>pc-/-</sup>* mice did not develop metastasis, as previously reported (12–14). Moreover, MEFs derived from *CDCP1 Pten<sup>pc-/-</sup>* mice showed an increased proliferative and migratory capacity when compared with *Pten<sup>pc-/-</sup>* cells (Supplemental Figure 4, C and D). Additionally, Kaplan-Meier cumulative survival analysis showed that *CDCP1 Pten<sup>pc-/-</sup>* mice died or had to be euthanized due to extensive tumor burden at the age of 60 to 80 weeks (Figure 3D). Of note, none of the age-matched *Pten<sup>pc-/-</sup>* mice died, indicating a profound effect of CDCP1 overexpression on the survival of *Pten<sup>pc-/-</sup>* mice. Moreover, the percentage of Ki-67 positive cells was significantly higher in *CDCP1 Pten<sup>pc-/-</sup>* mice when compared with their counterpart mice (Figure 3E). At

the molecular level, Western blot analysis revealed that *CDCP1 Pten<sup>pc-/-</sup>* tumors showed elevated levels of Src and p-Erk1/2, whereas p-Akt was not changed compared with *Pten<sup>pc-/-</sup>* tumors (Figure 3F). Since activated Src is known to regulate c-Myc levels (41–43), we reasoned that CDCP1 overexpression could drive c-Myc overexpression through Src. Indeed, CDCP1-overexpressing tumors showed increased levels of c-Myc expression (Figure 3F). Furthermore, IHC analysis revealed high levels of c-Myc and pErk1/2 in *CDCP1 Pten<sup>pc-/-</sup>* tumors compared with *Pten<sup>pc-/-</sup>* tumors (Figure 3G).

We next checked whether CDCP1 could also promote resistance to androgen deprivation therapy (ADT) in the same setting. To this end, we performed surgical castration in both *Pten<sup>pc-/-</sup>* and *CDCP1 Pten<sup>pc-/-</sup>* mice. Although *Pten<sup>pc-/-</sup>* tumors responded to castration as previously reported (44), *CDCP1 Pten<sup>pc-/-</sup>* did not, as shown by tumor weight, volume, histopathological analysis, and IHC for Ki-67 (Supplemental Figure 5, A–D). Resistance to castration in *CDCP1 Pten<sup>pc-/-</sup>* tumors was associated with higher levels of p-Src, p-Erk1/2, and c-Myc when compared with *Pten<sup>pc-/-</sup>* tumors, thus explaining the emergence of CRPC in this genetic background (Supplemental Figure 5, E–G). These data were additionally validated in vivo by overexpressing CDCP1 in TRAMP-C1 mouse prostate epithelial cells injected into C57BL/6 mice (TRAMP-C1-CDCP1). Overexpression of CDCP1 in TRAMP-C1 cells significantly increased the levels of p-Src and p-Erk (Supplemental Figure 5H), accelerated the emergence of castration-resistant prostate cancer, and shortened the survival of TRAMP-C1-CDCP1 mice when compared with the control group (Supplemental Figure 5I).

*Overexpression of CDCP1 bypasses the SMAD4 senescence barrier through activation of the Src/MAPK/Myc axis.* Previous evidence demonstrated that *Pten<sup>pc-/-</sup>* mice develop indolent tumors characterized by a senescence response that acts as an intrinsic barrier to constrain prostate cancer progression (11, 12). Since CDCP1 accelerates tumor progression in *Pten<sup>pc-/-</sup>* mice, we tested whether CDCP1 overexpression in this genetic background could promote senescence evasion both in vitro and in vivo, leading to metastasis. Prostate sections of the various genotypes (*WT*, *CDCP1*, *Pten<sup>pc-/-</sup>*, and *CDCP1 Pten<sup>pc-/-</sup>*) were analyzed for senescence response by performing SA- $\beta$ -gal and p-HPI $\gamma$  staining, 2 markers of senescence in vivo (45). Although *Pten<sup>pc-/-</sup>* tumors exhibit a strong cellular senescence response, *CDCP1 Pten<sup>pc-/-</sup>* tumors stained negative for both SA- $\beta$ -gal and p-HPI $\gamma$  and positive for Cyclin D1, a marker of cell proliferation, thereby demonstrating that CDCP1 bypasses the senescence response driven by *Pten* loss (Figure 4A). *CDCP1 Pten<sup>pc-/-</sup>* MEFs also stained negative for SA- $\beta$ -gal and exhibited increased cell proliferation with an elongated phenotype when compared with *Pten<sup>pc-/-</sup>* MEFs (Supplemental Figure 6A).

**Table 4. PTEN and CDCP1 membranous staining in TMA1 tumors from CRPC/metastasis PCa patients**

	CDCP1-negative	CDCP1-positive
PTEN-normal	40	20
PTEN-negative	23	33

The  $\chi^2$  test was used for statistical analysis.  $\chi^2 = 7.6471$ .  $P < 0.005686$ . The result is significant at  $P < 0.05$ .

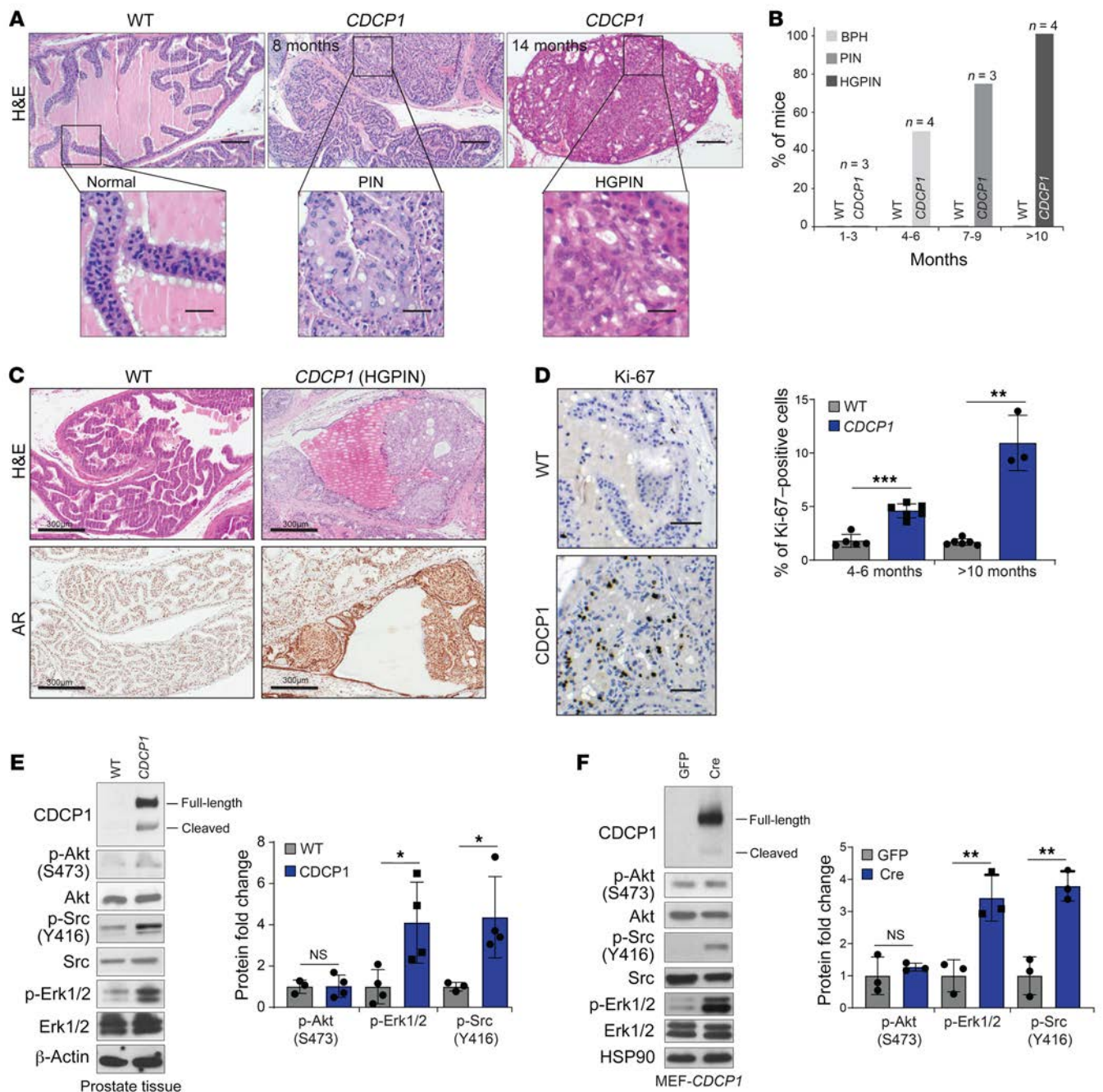


**Figure 2. Conditional overexpression of CDCP1 initiates tumorigenesis.** (A) Representative images of H&E staining of anterior prostate of WT and *CDCP1* mice. Scale bars: 500  $\mu$ m. Boxes represent regions in higher magnification in WT mice, prostatic intraepithelial neoplasia (PIN), and high-grade PIN (HGPIN) in *CDCP1* mice. Scale bars: 125  $\mu$ m. (B) Histopathological characterization and quantification of the prostate in WT and *CDCP1* mice. (C) IHC staining of H&E and AR in representative anterior prostate gland of WT and *CDCP1* mice affected by HGPIN. Scale bars: 300  $\mu$ m. (D) IHC staining of Ki-67 in representative anterior prostate of WT and *CDCP1* mice older than 10 months. Scale bars: 250  $\mu$ m. Quantification of Ki-67 staining in anterior prostate of WT and *CDCP1* mice at the indicated ages ( $n = 3-7$  for each genotype). (E) Western blot analysis of major downstream targets of CDCP1 signaling in anterior prostates of 4-month-old WT and *CDCP1* mice. Bar graph represents the fold change of normalized p-Akt, p-Erk1/2, and p-Src to their total proteins in *CDCP1* prostates compared with WT prostates ( $n = 4$ ). (F) Western blot analysis of major downstream targets of CDCP1 signaling in mouse embryonic fibroblasts (MEFs) from *CDCP1* transgenic mice infected with retroviral vector overexpressing GFP or Cre. Bar graph represents the fold change of normalized p-Akt, p-Erk1/2, and p-Src to their total proteins in transgenic MEF-*CDCP1* mice infected with GFP or Cre retro-virus vectors ( $n = 3$ ). Error bars indicate SD. \* $P < 0.05$ ; \*\* $P < 0.01$ ; \*\*\* $P < 0.001$ . Statistical test: 2-tailed  $t$  test.

Two recent independent reports showed that TGF $\beta$ /Smad4 pathway upregulation triggered by PTEN loss constrains prostate cancer progression by blocking Cyclin D1 transcription (13, 14). Of interest, overexpression of COUP-TFII, which inhibits

Smad4-dependent transcription, promotes senescence evasion by releasing Cyclin D1 expression in *Pten*-null cells (13, 14). Thus, we compared the status of several components involved in these pathways such as p53, p21, Smad4, Cyclin D1, and COUP-TFII in

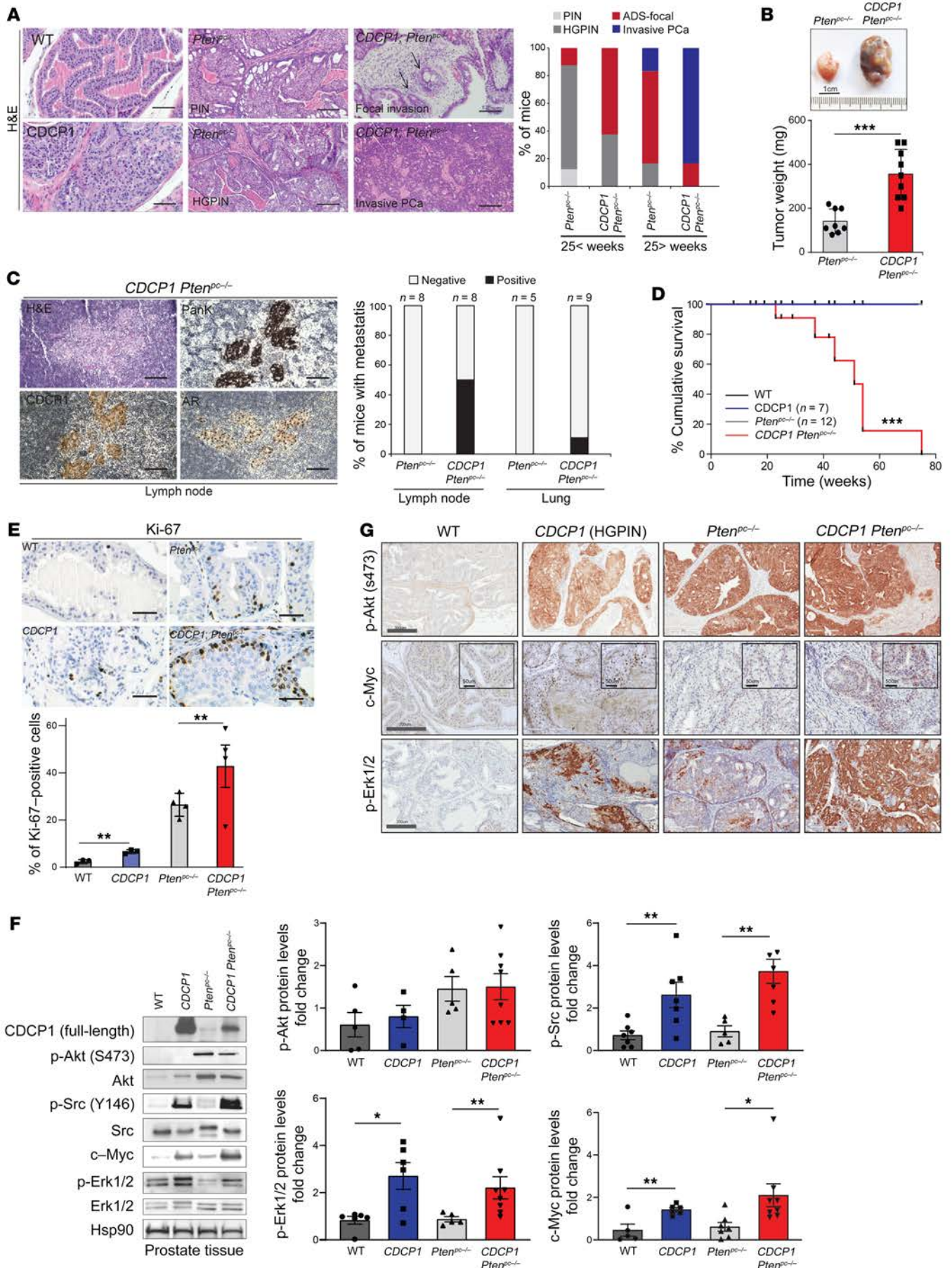


**Figure 3. CDCP1 cooperates with Pten loss to drive prostate cancer progression and metastasis.** (A) Representative images of H&E staining of anterior prostate of WT, *CDCP1*, *Pten*<sup>pc-/-</sup>, and *CDCP1 Pten*<sup>pc-/-</sup> mice at the age of 10 months. Scale bars: 500  $\mu$ m. Bar graph representing the percentage of mice with PIN, HGPIN, ADS-focal, and invasive PCa. (B) Bar graph representing tumor weight of *Pten*<sup>pc-/-</sup> and *CDCP1 Pten*<sup>pc-/-</sup> mice, insets represent anterior prostate of *Pten*<sup>pc-/-</sup> and *CDCP1 Pten*<sup>pc-/-</sup>. Scale bar: 1 cm. (C) Representative images of H&E, Pan-cytokeratin (Pank), CDCP1, and AR staining of lumbar lymph node metastases in *CDCP1 Pten*<sup>pc-/-</sup> mice at 10 months of age ( $n = 4/8$ ). Scale bars: 250  $\mu$ m. Graph shows the percentage of mice with lymph node and lung metastasis. (D) Cumulative survival of WT, *CDCP1*, *Pten*<sup>pc-/-</sup>, and *CDCP1 Pten*<sup>pc-/-</sup> mice. (E) Representative images of Ki-67 staining in anterior prostate of WT, *CDCP1*, *Pten*<sup>pc-/-</sup>, and *CDCP1 Pten*<sup>pc-/-</sup> mice (3 months old). Scale bars: 125  $\mu$ m. Quantification of Ki-67 staining in anterior prostate of indicated genotypes ( $n = 3-4$  for each genotype). (F) Western blot analysis and protein fold change quantification of specified proteins in anterior prostate glands from the indicated genotypes at 20 weeks of age. Graphs show protein fold change quantification of p-Src, p-Erk1/2, p-Akt, and c-Myc ( $n = 5-7$ ). (G) Immunohistochemistry staining of p-AKT, p-ERK1/2, and c-Myc of anterior prostates of WT, *CDCP1*, *Pten*<sup>pc-/-</sup>, and *CDCP1 Pten*<sup>pc-/-</sup> mice. Scale bars: 300  $\mu$ m (p-AKT, p-ERK1/2); 200  $\mu$ m (c-Myc); 50  $\mu$ m (inset). Error bars indicate SD for B and E and SEM for F. \* $P < 0.05$ ; \*\* $P < 0.01$ ; \*\*\* $P < 0.001$ . The following statistical tests were used: unpaired 2-tailed  $t$  test for B and E, log-rank (Mantel-Cox) test for D, and 1-tailed  $t$  test for F.

*Pten*<sup>pc-/-</sup> and *CDCP1 Pten*<sup>pc-/-</sup> tumor samples. Although our analysis showed that Smad4 and p53 expression did not change in *CDCP1 Pten*-null MEFs and tumors compared with control groups, Cyclin D1 and COUP-TFII levels were significantly altered (Figure 4, B and C, and Supplemental Figure 6, B and C). These data suggest that CDCP1 allows *Pten*-null benign tumors to acquire metastatic potential through the evasion of the TGFB-induced senescence barrier by increasing the level of COUP-TFII. We next tried to understand the mechanism by which CDCP1 controlled *COUP-TFII* levels. Interestingly, COUP-TFII, c-Myc, and Cyclin D1 mRNA and protein levels were significantly reduced in *CDCP1 Pten*<sup>-/-</sup> MEFs upon treatment with saracatinib, a selective inhibitor of Src (ref. 46, Figure 4D, and Supplemental Figure 6D). Of note, the saracatinib treatment led to a profound arrest in the proliferation and reactivation of senescence in *CDCP1 Pten*<sup>-/-</sup> MEFs (Figure 4E and Supplemental Figure 6E). Since Src controls the levels of c-Myc, we next checked whether c-Myc could regulate *COUP-TFII* levels. We found that c-Myc inactivation in *CDCP1 Pten*<sup>-/-</sup> MEFs phenocopied the results obtained with the Src inhibitor (Figure 4, F and G, and Supplemental Figure 6, F and G). In line with this evidence, the analysis of the *COUP-TFII* promoter revealed the presence of multiple MYC-binding sites (Supplemental Figure 6H). Chromatin immunoprecipitation (ChIP) assays confirmed that c-Myc specifically binds to the promoters of *COUP-TFII* in *CDCP1 Pten*<sup>-/-</sup> but not to those in *Pten*<sup>-/-</sup> MEFs. Additional ChIP analysis showed increased binding of c-Myc on *Cyclin D1* promoter and reduced Smad4 binding affinity to the promoter of *Cyclin D1* in *CDCP1 Pten*<sup>-/-</sup> MEFs compared with *Pten*<sup>-/-</sup> (Figure 4H). Altogether, these data demonstrate that in *CDCP1 Pten*<sup>pc-/-</sup> tumors, increased levels of c-Myc promote activation of COUP-TFII, which prevents Smad4 from binding to the promoter of Cyclin D1.

To further assess the relevance of these findings in human prostate cancer cells, we checked whether inhibition of CDCP1 could drive senescence activation in prostate cancer harboring

elevated levels of CDCP1. We therefore depleted CDCP1 in PC3, a PTEN TP53-deficient human prostate cancer cell line, by using 2 independent sh-RNAs (Supplemental Figure 7A). Remarkably, the silencing of CDCP1 inhibited the 3D proliferation of PC3 cells (Supplemental Figure 7B) and promoted senescence (Supplemental Figure 7, C and D). These results were also validated in vivo by injecting PC3 sh-CDCP1 and control cells in SCID mice (Supplemental Figure 7, E and F). Of note, CDCP1-depleted PC3 tumors showed a significant decrease in c-MYC, COUP-TFII, and Cyclin D1 levels in parallel with the reduction of SRC phosphorylation (Supplemental Figure 7G). Together, these data demonstrate that CDCP1 inhibition promotes senescence by suppressing c-MYC levels in human prostate cancer cells. Downregulation of CDCP1 in LNCaP-abl cells that present an increased level of CDCP1 compared with LNCaP parental cells decreased proliferation and increased senescence (Supplemental Figure 7, H-J).

*Androgen deprivation induces CDCP1 expression in PTEN-deficient cells.* Since PTEN-deficient CRPC tumors display high CDCP1 levels, and PTEN can regulate the levels and transcriptional activity of AR (47), we formed the hypothesis that AR could control the levels of CDCP1. Bioinformatics analysis in CRPC cases revealed that AR expression and AR activity inversely correlated with CDCP1 expression in prostate tumors (Supplemental Figure 8, A and B). To further validate these data in vitro, we cultured the androgen-sensitive PTEN-null LNCaP cell line in full androgen deprivation (FAD) condition (absence of androgens and presence of enzalutamide) for more than 40 days and waited until these cells developed resistance (Figure 5A). CDCP1 levels increased in cells resistant to enzalutamide (androgen deprivation insensitive, ADI) when compared with enzalutamide-sensitive cells (androgen deprivation sensitive, ADS). This upregulation was associated with the concomitant activation of p-SRC, p-ERK1/2, and c-MYC and to evasion of senescence driven by enzalutamide treatment (ref. 48, Figure 5B, and Supplemental Figure 8C). These results prompted us to investigate whether AR could regulate the mRNA expression of CDCP1. Although FAD treatment enhanced CDCP1 levels, dihydrotestosterone (DHT) stimulation reduced its expression at both mRNA and protein levels in LNCaP ADS cells (Figure 5C). In addition, overexpression of AR reduced the mRNA and protein levels of CDCP1 in the AR<sup>+</sup> prostate cancer cell line PC3 (Figure 5D and Supplemental Figure 8D). In contrast, overexpression of a mutated form of AR that lacked the DNA binding domain in PC3 failed to promote the downregulation of CDCP1 (Figure 5E). ChIP-quantitative PCR (ChIP-qPCR) analysis in LNCaP cells, showed that the AR could bind to the CDCP1 proximal promoter, where it inhibited CDCP1 transcription (Figure 5F).

We next investigated whether loss of PTEN was needed for the upregulation of CDCP1 in cells kept in FAD. Indeed, CDCP1 levels increased in PTEN-null LNCaP cells but not in the PTEN-WT LAPC4 and VCaP cell lines kept in FAD (Figure 5G). In line with these findings, we found that in the ADT-insensitive cell lines PC3 and 22RV1, FAD did not upregulate CDCP1 levels (Supplemental Figure 8E). Interestingly, inhibition of PI3K in LNCaP cells, but not in 22RV1 cells, promoted a downregulation of CDCP1 in cells kept in FAD (Figure 5H and Supplemental Figure 8F). This was associated with the concomitant upregulation of AR levels in the same cells. These data are in agreement with previous findings

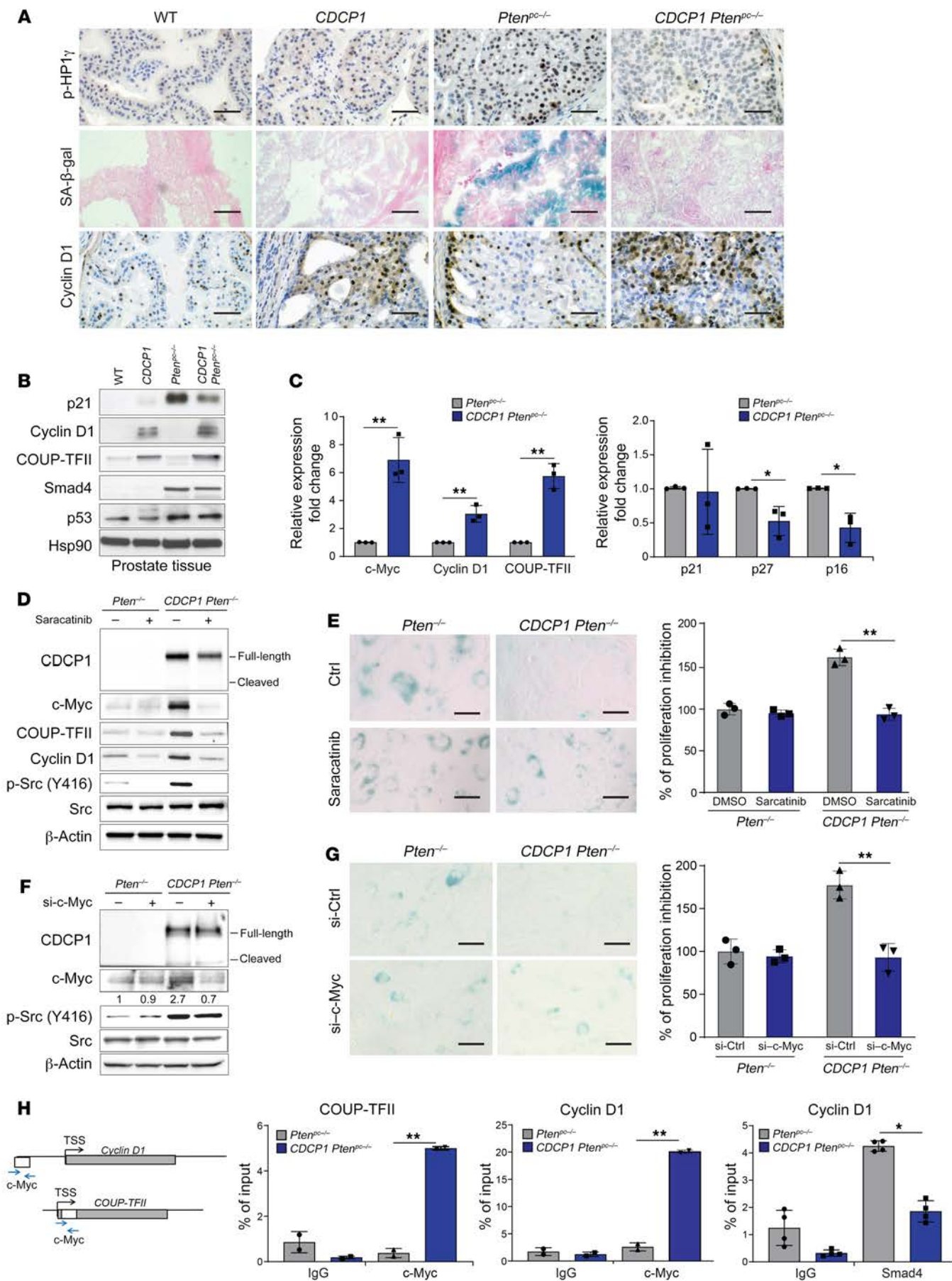


**Figure 4. Overexpression of CDCP1 overcomes Pten loss-induced cellular senescence bypassing the SMAD4 barrier through activation of the Src/MAPK/c-Myc axis.** (A) Representative images of p-HP1 $\gamma$ . Senescence associated- $\beta$ -galactosidase (SA- $\beta$ -Gal) and Cyclin D1 staining in the anterior prostates of WT, *CDCP1*, *Pten*<sup>pc/-</sup>, and *CDCP1 Pten*<sup>pc/-</sup> mice. Scale bars: 125  $\mu$ m. (B) Western blot analysis of p21, Cyclin D1, COUP-TFII, Smad4, and p53 in anterior prostate glands from the indicated genotypes. (C) qRT-PCR analysis of c-Myc, Cyclin D1, COUP-TFII, p21, p27, and p16 expression in prostates from 12- to 16-week-old *Pten*<sup>pc/-</sup> and *CDCP1 Pten*<sup>pc/-</sup> mice ( $n = 3$ ). (D) Western blot analysis of *Pten*<sup>pc/-</sup> and *CDCP1 Pten*<sup>pc/-</sup> MEFs treated with saracatinib (100 nM) for 12 hours. (E) Representative images of SA- $\beta$ -Gal staining in *Pten*<sup>pc/-</sup> and *CDCP1 Pten*<sup>pc/-</sup> MEFs treated with saracatinib (100 nM) and DMSO for 12 hours. Scale bars: 125  $\mu$ m. Bar graph shows the fold change in growth by crystal violet in *Pten*<sup>pc/-</sup> and *CDCP1 Pten*<sup>pc/-</sup> MEFs treated with saracatinib (100 nM) or DMSO as control ( $n = 3$ ). (F) Western blot analysis of *Pten*<sup>pc/-</sup> and *CDCP1 Pten*<sup>pc/-</sup> MEFs transfected with si-c-Myc and control si-scramble (si-Ctrl) after 48 hours. (G) Representative images of SA- $\beta$ -Gal staining in *Pten*<sup>pc/-</sup> and *CDCP1 Pten*<sup>pc/-</sup> MEFs transfected with si-c-Myc and si-Ctrl after 48 hours. Scale bars: 125  $\mu$ m. Bar graph shows the fold change in growth by crystal violet in *Pten*<sup>pc/-</sup> and *CDCP1 Pten*<sup>pc/-</sup> MEFs transfected with si-c-Myc and si-Ctrl ( $n = 3$ ). (H) Schemes of Cyclin D1 and COUP-TFII promoters. qRT-PCR of ChIP-analysis showing the binding of c-Myc to COUP-TFII promoter and c-Myc and Smad4 to Cyclin D1 promoters in *Pten*<sup>pc/-</sup> and *CDCP1 Pten*<sup>pc/-</sup> MEFs. Normal mouse IgG serves as negative control ( $n = 2$ ). Error bars indicate SD. \* $P < 0.05$ ; \*\* $P < 0.01$ . Statistical test: 2-tailed  $t$  test.

demonstrating that PTEN loss leads to reciprocal feedback inhibition of AR activity (47). Thus, inhibition of PI3K leads to increased AR levels that promote the following downregulation of CDCP1.

*CDCP1 targeting improves the efficacy of ADT.* Given that androgen deprivation conditions elevate CDCP1 expression in ADS tumor cell lines, we postulated that compounds that block or degrade CDCP1 could be ideally used in combination with ADTs to prevent the emergence of ADI prostate tumor cells. To assess this hypothesis, we used the anti-CDCP1 monoclonal antibody CUB4, which binds the N-terminal domain of human CDCP1 and promotes CDCP1 internalization and degradation (27). Cotreatment of LNCaP cells with CUB4 and enzalutamide strongly affected the proliferation of these cells by inducing senescence. In contrast, enzalutamide-untreated cells were only slightly affected by the anti-CDCP1 antibody due to the low basal levels of CDCP1 in LNCaP cells (Supplemental Figure 8G). We next reasoned that tumor cell eradication rather than senescence induction could be a preferable outcome of CDCP1 targeting therapies (49). Therefore, we developed an anti-CDCP1 IL carrying doxorubicin to eliminate CDCP1-overexpressing prostate tumor cells induced by the enzalutamide treatment. Note that the anti-CDCP1 IL was generated by using the FAB of the CUB4 antibody (27). To allow the selective delivery of doxorubicin to the tumor cells, the anti-CDCP1 ILs were designed with a size of 120 nm. This size allows the preferential delivery of immunoliposome in tumor tissues due to the enhanced permeability and retention (EPR) effect of the cancer blood vessels (50–52).

Enzalutamide treatment, in combination with anti-CDCP1 ILs, induced a strong apoptotic response and blocked the emergence of CDCP1<sup>+</sup> ADI cells in a time-course experiment (Figure 6, A and B). In line with the previous experiments, treatment with anti-CDCP1 ILs affected the proliferation of LNCaP cells only in the presence of enzalutamide treatment. To validate these results in vivo, LNCaP cells were injected subcutaneously into SCID

mice and upon the establishment of tumors, mice were treated with enzalutamide (10 mg/kg) with or without anti-CDCP1 ILs. Although enzalutamide showed minor effects on tumor growth, the combination of enzalutamide and anti-CDCP1 ILs significantly affected tumor growth (Figure 6, C and D). Note that Western blot analysis showed a significant increase in the levels of CDCP1 upon enzalutamide treatment in vivo, which was abolished upon combination treatment (Supplemental Figure 8H). Together these data suggest that CDCP1 targeting agents are effective when used in combination with ADT.

## Discussion

The present study highlights the crucial role of CDCP1 in promoting prostate cancer tumorigenesis and progression, and its ability to drive metastasis and CRPC in cooperation with PTEN deficiency. Since CDCP1 is highly expressed in mCRPC patients and can be easily targeted, our work opens new opportunities for combinatorial therapies. *PTEN* is one of the most frequently altered tumor suppressor genes in human prostate cancer, whereas complete loss of *PTEN* is frequently observed in metastatic prostate cancer (7). Previous evidence demonstrated that *Pten*<sup>pc/-</sup> develops indolent tumors characterized by a senescence response that, acting as an intrinsic barrier, constrain prostate cancer progression (11, 12). However, the mechanism by which *PTEN*-null benign tumors acquire metastatic potential remained poorly understood (12–14). CDCP1, a transmembrane protein that acts as a substrate for SRC family kinases, is overexpressed in a variety of tumors and has been associated with cancer development, invasion, and metastasis (20, 21). Although CDCP1 has been considered as an oncogene, recent publications demonstrate that CDCP1 inactivation accelerates mammary and skin tumorigenesis in the PyMT and SmoM2 models, respectively (25). As recently demonstrated, loss of CDCP1 can change the spectrum of SRC substrate phosphorylation in cells kept in suspension. Indeed, CDCP1 negatively regulates c-SRC and PKC $\delta$  in suspended cells by sequestering these kinases away from their canonical substrates. As a consequence, SRC can phosphorylate CDK5R1/p35, thereby triggering the loss of ITGB1/b1-integrin inside-out activation (22).

In prostate cancer, the role of CDCP1 remains poorly characterized due to the lack of an in vivo model. Previous reports demonstrate that CDCP1 overexpression increases cellular proliferation in 2 human prostate cancer cell lines with validation of its elevated expression in a limited number of primary prostate tumor samples (28, 53). In an attempt to clarify the function of CDCP1 in prostate cancer, we generated the first prostate-specific CDCP1-overexpressing transgenic mouse model and assessed the level of CDCP1 in different prostate cancer TMAs, including more than 990 cases spanning benign, primary, and metastatic prostate cancer. We demonstrated that CDCP1 is overexpressed in a subset of advanced and metastatic prostate cancers, where it is frequently associated with loss of *PTEN*. Moreover, we showed in vivo that CDCP1 cooperates with *PTEN* loss to promote the emergence of metastases and CRPC through the upregulation of the MAPK pathway. Previous evidence demonstrates that patients who develop resistance to ADT present tumors with elevated levels of MAPK pathway and that activation of the MAPK pathway cooperates with *PTEN* deficiency to promote mCRPC (8, 54). Mechanistically, we

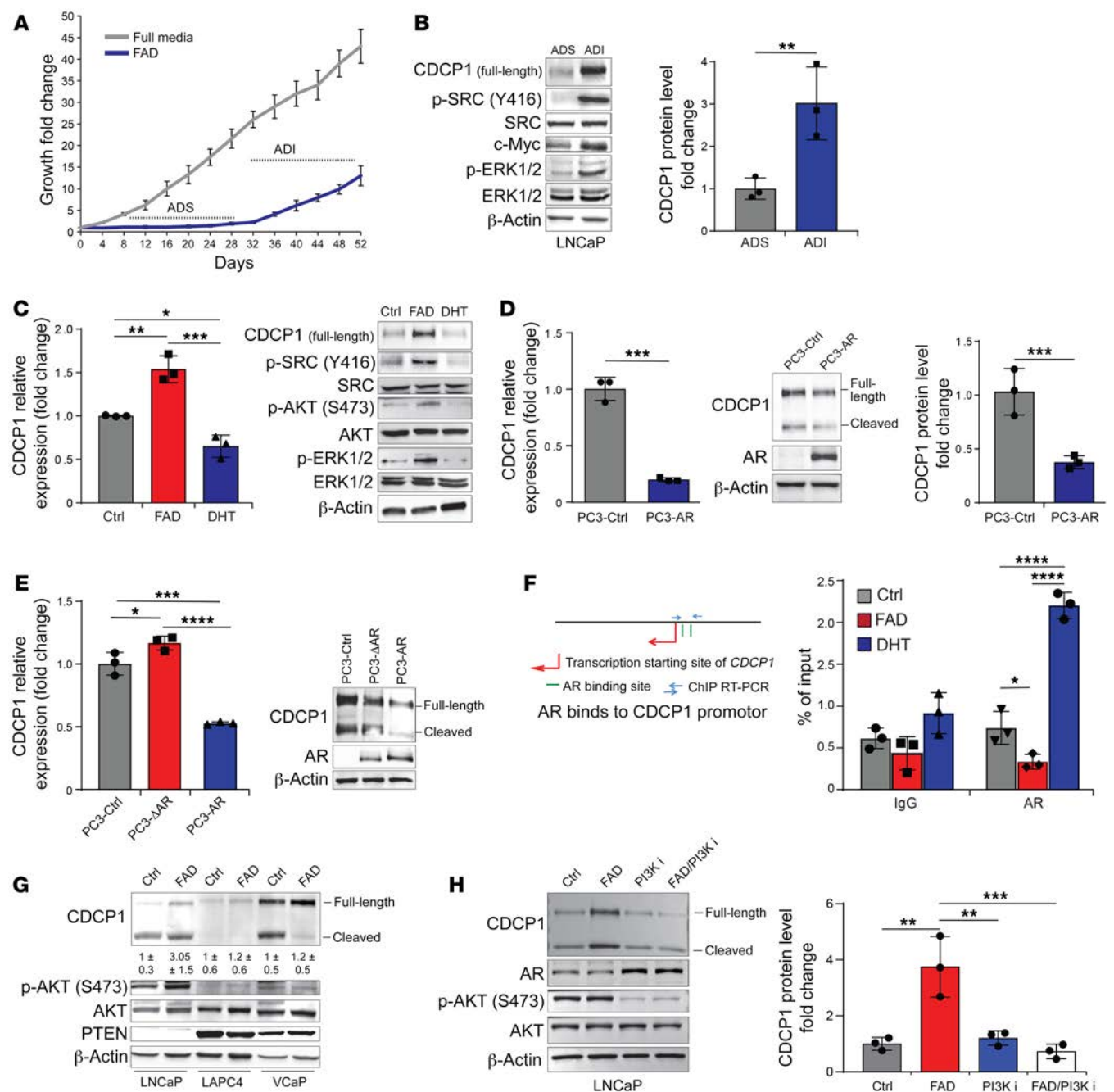


**Figure 5. Androgen deprivation in human tumor samples and cells induces CDCP1 expression.** (A) Quantification of fold change in growth by crystal violet in LNCaP cell line grown in full media and in FAD. Dotted lines indicate ADS and ADI phases ( $n = 3$ ). (B) Western blot analysis of indicated proteins in LNCaP-ADS and LNCaP-ADI. Quantification of fold change in CDCP1 protein levels in LNCaP-ADS and LNCaP-ADI ( $n = 3$ ). (C) qRT-PCR analysis of CDCP1 mRNA levels in LNCaP grown in full media; FAD and stimulated with dihydrotestosterone (DHT, 1  $\mu$ M, 16 hours) after being grown for 2 days in FAD. Western blot analysis of indicated proteins in LNCaP grown under the described conditions ( $n = 3$ ). (D) qRT-PCR of CDCP1 mRNA levels in PC3 expressing empty vector (PC3-Ctrl) and in PC3 overexpressing full-length androgen receptor (PC3-AR). Western blot analysis and protein fold change quantification of indicated proteins in PC3-Ctrl and PC3-AR cell lines ( $n = 3$ ). (E) qRT-PCR and Western blot analysis in PC3-Ctrl, PC3-AR, and PC3 overexpressing DNA-binding mutant of AR (PC3- $\Delta$ AR) of CDCP1 mRNA and indicated proteins ( $n = 3$ ). (F) Scheme represents the AR binding site on CDCP1 promoter. qRT-PCR of ChIP-analysis showing the binding of AR to CDCP1 promoter in LNCaP cell line grown in full media; FAD after DHT stimulation. Normal mouse IgG served as a negative control ( $n = 3$ ). (G) Western blot analysis of indicated protein in LNCaP, LAPC4, and VCaP kept in normal conditions and in FAD ( $n = 3$ ). (H) Western blot analysis of indicated proteins in LNCaP treated with PI3K inhibitor in normal conditions or in FAD. Quantification of fold change in CDCP1 protein levels in LNCaP untreated or treated with PI3K inhibitor in normal conditions and in FAD ( $n = 3$ ). Error bars indicate SD. \* $P < 0.05$ ; \*\* $P < 0.01$ ; \*\*\* $P < 0.001$ ; \*\*\*\* $P < 0.0001$ . The following statistical tests were used: 1-way ANOVA adjusted for multiple comparisons using Tukey's test for C, E, F, and H, and unpaired 2-tailed  $t$  test for B and D.

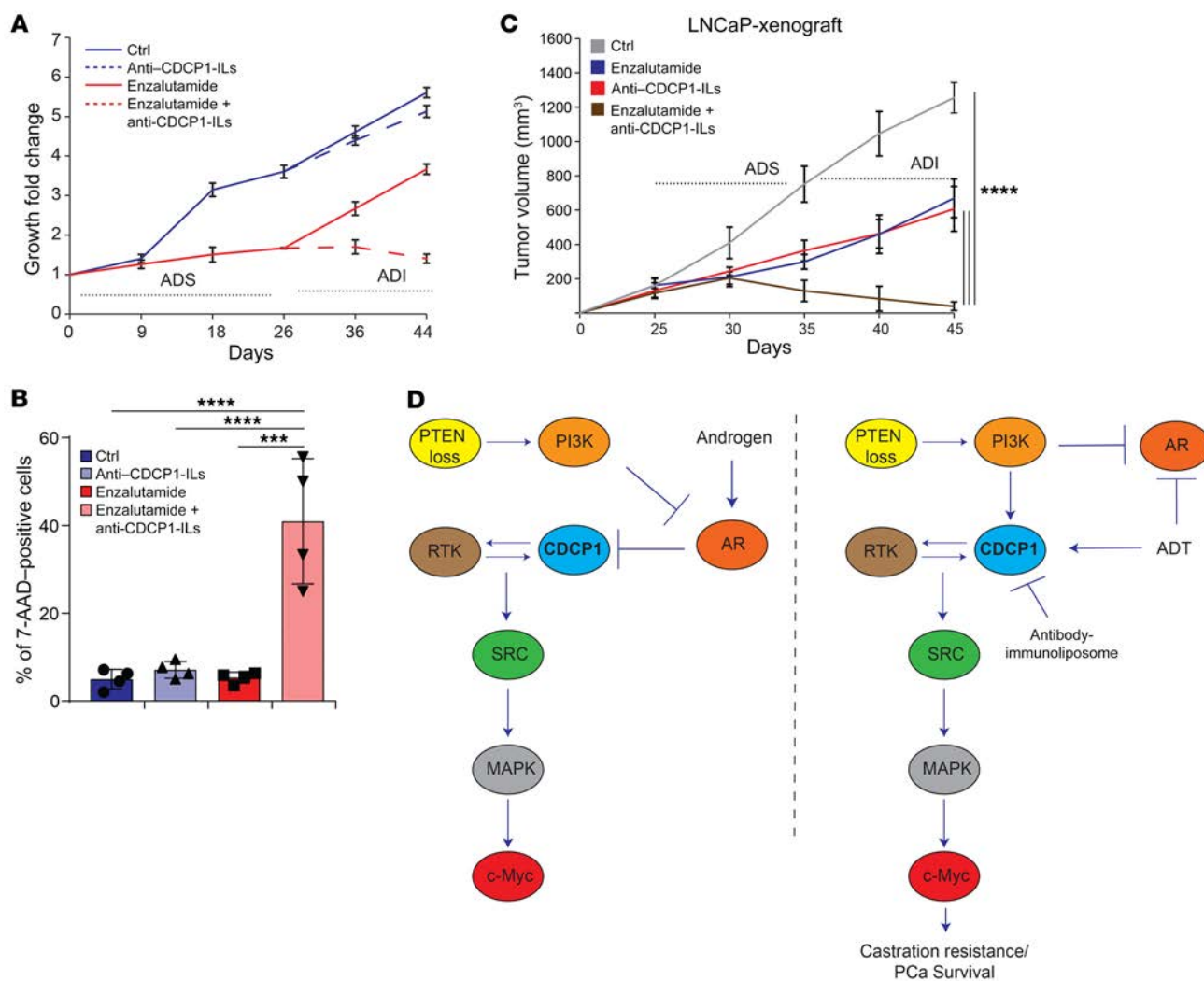


**Figure 6. CDCP1 targeting improves the efficacy of ADTs.** (A) Quantification of fold change in growth by crystal violet in LNCaP cell line untreated and treated with enzalutamide (10  $\mu$ M) in combination with or without the immune-liposome (anti-CDCP1-ILs). Enzalutamide (10  $\mu$ M) treatment lasted for 26 days. After that, cells were treated in combination with anti-CDCP1-ILs. (B) Quantification of cell death with 7-AAD staining in cells untreated and treated with enzalutamide in combination with or without the anti-CDCP1-ILs ( $n = 4$ ). (C) Xenografts tumor growth ( $\text{mm}^3$ ) of LNCaP cell line untreated or treated with enzalutamide in the presence or absence of the anti-CDCP1-ILs. Upon tumor establishment, mice were treated with enzalutamide (10 mg/kg) for 45 days. After the first week of enzalutamide treatments, mice were divided into 2 groups and treated with or without the anti-CDCP1-ILs. Note that the 2 treatments were consecutive ( $n = 4$ ). (D) The model represents the role of CDCP1 in CRPC. PI3K partially blocks AR. ADT blocks AR completely and upregulates CDCP1 levels. Error bars indicate SD for B and SEM for C.  $***P < 0.001$ ;  $****P < 0.0001$ . The following statistical test was used: 1-way ANOVA adjusted for multiple comparisons using Tukey's test.

showed that CDCP1 overexpression increases c-Myc levels in a Src-dependent manner. This, in turn, promotes the activation of COUP-TFII that further inhibits Smad4-dependent transcription. As a result, Cyclin D1 gets upregulated and *CDCP1 Pten<sup>pc-/-</sup>* tumors bypass senescence and progress toward a metastatic phenotype.

Of note, we found that *CDCP1* mRNA and protein levels increase in PTEN-deficient cells treated with enzalutamide, a standard of therapy for CRPC patients. Finally, we provided evidence that the AR can suppress the transcription of CDCP1 in particular in cells carrying the loss of PTEN (Figure 5E). Overexpression of the AR in AR<sup>+</sup> prostate cancer cell lines significantly decreased CDCP1 levels, supporting our observations. The reciprocal feedback regulation of PI3K and androgen receptor signaling in PTEN-deficient prostate cancer can explain the observed

PTEN-CDCP1 dependency (47). Although we did not formally prove it, we believe that AR mutations, AR splicing variants, and the AR rewiring may also account for the upregulation of CDCP1 observed in metastatic prostate cancer patients not treated with ADT due to the lack of AR binding to the CDCP1 promoter. Therapeutically, we demonstrated that CDCP1 inhibition, in combination with ADT, might represent an interesting new therapeutic approach in prostate cancer. Indeed, we showed that inhibition of CDCP1 in combination with enzalutamide has the potential for prostate cancer treatment. Treatment of PTEN-deficient human prostate tumor cells with enzalutamide promoted the upregulation of CDCP1 levels. This treatment rendered PTEN-null cells more sensitive to CDCP1 targeting agents. On the other hand, enzalutamide-untreated cells did not respond to CDCP1-targeting agents.

**Table 5. Mouse primers for real-time PCR**

Primer	Sequence
<i>p16lnk4a</i> forward	5'-CGCAGGTTCTGGTCACTGT-3'
<i>p16lnk4a</i> reverse	5'-TGTTACGAAAGCCAGAGCG-3'
<i>p21</i> forward	5'-GGGCGCAGGATGTTCAAGAA-3'
<i>p21</i> reverse	5'-CACCAACAGGTCGAAATGGG-3'
<i>p27</i> forward	5'-GCAAAACAAAAGGCCAACA-3'
<i>p27</i> reverse	5'-GGGCGTCTGCTCCACAGT-3'
<i>Gapdh</i> forward	5'-AGGTCGGTGTGAACGGATTG-3'
<i>Gapdh</i> reverse	5'-TGTAGACCATGTAGTTGAGGT-3'
<i>Rn18S</i> forward	5'-ACCGCAGCTAGGAATAATG-3'
<i>Rn18S</i> reverse	5'-GCCTCAGTCCGAAAACCA-3'
<i>COUP-TFII</i> forward	5'-TCAACTGCCACTGCTACTGT-3'
<i>COUP-TFII</i> reverse	5'-CATGATGTTGTTAGGCTG-3'
<i>Cyclin D1</i> forward	5'-GGCTACCTGACCAACATC-3'
<i>Cyclin D1</i> reverse	5'-CTCCTCTCGCACTTCTGCTC-3'
<i>c-Myc</i> forward	5'-CTGGACCAGGAGTGGAGT-3'
<i>c-Myc</i> reverse	5'-ACGTAGTAGTCGGTCTCA-3'

Moreover, we demonstrated *in vivo* that enzalutamide, in combination with a new CDCP1 immunoliposome carrying doxorubicin, significantly inhibits tumor progression, inducing a strong apoptotic response. These findings demonstrate that CDCP1-targeting therapies should be combined with ADT to maximize the efficacy of this standard of treatment. Therapeutically, the use of an anti-CDCP1 IL containing doxorubicin has several advantages. First, liposomes loaded with doxorubicin are already in the clinic and are well tolerated by cancer patients. Second, the size of anti-CDCP1 IL allows its extravasation and accumulation preferentially at the tumor site due to the EPR effect (50–52). Third, the conjugation of the liposomes with the human FAB of the CDCP1 antibody increases the specificity and permanence of the IL in tumors overexpressing CDCP1, increasing its anticancer efficacy. On a negative side, since the anti-CDCP1 ILs have been generated with an antibody that recognizes human CDCP1, our experiments in mice cannot exclude the risk of systemic toxicities of this IL, and further experiments should be carried on by using a mouse antibody.

## Methods

**Acquisition of MEFs.** Primary MEFs were prepared as described previously from individual embryos of various genotypes (12). Briefly, MEFs for all genotypes were obtained by crossing male WT and *Pten*<sup>lox/lox</sup> with female *CDCP1*<sup>lox-stop-lox</sup> mice. Pregnant mice were sacrificed by cervical dislocation 13 or 14 days postcoitum. Embryos were harvested and the individual MEFs were cultured in DMEM containing 10% fetal bovine serum and 1% penicillin-streptomycin. Primary *Pten*<sup>lox/lox</sup> MEFs were infected with retroviruses expressing either pMSCV-CRE-PURO-IRES-GFP or pMSCV-PURO-IRES-GFP for 48 hours and selected with puromycin at a concentration of 3 µg/mL and as previously described. All mice were maintained under specific pathogen-free conditions in the animal facilities of the Institute for Research in Biomedicine. Experiments were performed according to state guidelines and approved by the local ethical committee.

**Cell culture and reagents.** Human prostate carcinoma cell lines were purchased from ATCC and maintained according to the supplier's recommendation.

Cells were transduced with PLKO or TRIPZ doxycycline-inducible lentiviral construct, against human CDCP1 gene or empty vector, obtained by Thermo Fisher Scientific (clones V3THS\_329377 and V2THS\_191307). LNCaP-abl and LAPC4 cells were a gift from Jean-Philippe Theurillat (Institute of Oncology Research, Bellinzona, Switzerland). PC3-ARs were generated by infecting them with retroviruses expressing full-length human AR (provided by Jean-Philippe Theurillat). PC3-ΔARs were generated using the expression of human AR with the deletion of amino acids 538 to 614, deletion of AR DNA binding domain (Addgene, catalog 89107). LNCaP-ADI cells were generated from parental LNCaP by growing them in RPMI 1640 containing 10% charcoal-stripped FBS. Androgen stimulation experiments were performed using 1 nM of the 5α-DHT (MilliporeSigma, catalog 521-18-6). The FAD experiment was performed by culturing the cells in RPMI with charcoal-stripped FBS and enzalutamide. Enzalutamide (APEX BIO, catalog A3003) was dissolved in DMSO at a concentration of 10 µM. The following antibodies were used for Western blotting: Tag-Myc (BD Pharmingen, catalog 551101; 1:1000); PTEN (Cell Signaling Technology, catalog 9552S; 1:1000); HSP90 (Cell Signaling Technology, catalog 4877S; 1:1000); c-Myc (Santa Cruz Biotechnology, catalog A713(G-4), 1:500); p21 (Abcam, catalog ab107099, 1:1000); β-actin (MilliporeSigma, catalog A5316; 1:5000); Cyclin D1 (Cell Signaling Technology, catalog 2978S, 1:1000); COUP-TFII (Perseus Proteomics, catalog PP-H7147-00; 1:1000); SMAD4 (Santa Cruz Biotechnology, catalog E0615; 1:500); p-SRC-Tyr416 (Cell Signaling Technology, catalog 6943S; 1:1000); SRC (Cell Signaling Technology, catalog 2123S; 1:1000); AKT (Cell Signaling Technology, catalog 9272S; 1:1000); p-AKT-S473 (Cell Signaling Technology, catalog 9171S; 1:1000); p53 (Abcam, catalog ab131442; 1:1000); CDCP1 (Cell Signaling Technology, catalog 4115; 1:1000); Erk1/2 (Cell Signaling Technology, catalog 4695S; 1:1000); p-Erk1/2-T202/Y204 (Cell Signaling Technology, catalog 4370S; 1:1000); S6 (Cell Signaling Technology, catalog 2317S; 1:1000); p-S6-Ser235/236 (Cell Signaling Technology, catalog 4857; 1:1000); AR (N-20) (Santa Cruz Biotechnology, catalog SC-816; 1:500). For IHC the following antibodies were used: Ki-67 (Thermo Fisher Scientific, clone SP6, catalog RM-9106-R7; rabbit polyclonal; unmasked water bath 98°C, pH 6, 20 minutes; Lab Vision dilution ready to use); CDCP1 (Cell Signaling Technology, catalog 4115, rabbit polyclonal; unmasked water bath 98°C, pH 6, 20 minutes; 1:50); p-HPIγ-Ser83 (Cell Signaling Technology, catalog 2600, unmasked water bath 98°C, pH 6, 20 minutes; 1:50); Cyclin D1 (Cell Signaling Technology, catalog

**Table 6. Human primers for real-time PCR**

Primer	Sequence
<i>p21</i> forward	5'-TGTCGTCGAGAACCCATGC-3'
<i>p21</i> reverse	5'-AAAGTCGAAGTTCATCGCTC-3'
<i>p27</i> forward	5'-TAATTGGGGCTCCGGCTAACT-3'
<i>p27</i> reverse	5'-TGCAGGTCGCTTCTTATTCC-3'
<i>GAPDH</i> forward	5'-AATCCCATCACCATCTTCCA-3'
<i>GAPDH</i> reverse	5'-TGGACTCCAGCAGCTACTCA-3'
<i>c-MYC</i> forward	5'-CGGAACCTTGTGCGTAAGG-3'
<i>c-MYC</i> reverse	5'-CTCAGCCAAGGTTGTGAGGT-3'
<i>CDCP1</i> forward	5'-TGGTTCACCCCAAGAAATGT-3'
<i>CDCP1</i> reverse	5'-GATGATGCACAGACGTTTAT-3'

2978S); AR (N-20) (Santa Cruz Biotechnology, catalog SC-816, rabbit polyclonal; unmasked water bath 98°C, pH 6, 20 minutes; 1:300); wide spectrum cytokeratin (pankeratin) (DAKO, catalog ZO622; rabbit polyclonal; unmasked water bath 98°C, pH 9, 20 minutes; 1:2000). For IF, the following antibodies were used: E-cadherin (BD Biosciences, clone 26, catalog 610181; mouse monoclonal; unmasked water bath 98°C, pH 9, 20 minutes; 1:700); CK5 (Abcam, catalog ab52635; rabbit polyclonal; unmasked water bath 98°C, pH 9, 20 minutes; 1:500); CK8 (Abcam, catalog ab59400; rabbit polyclonal; unmasked water bath 98°C, pH 9, 20 minutes; 1:150); and CDCP1 (Cell Signaling Technology, catalog 4115, 1:100). The E-cadherin antibody (Developmental Studies Hybridoma Bank [DSHB], DCAD2, 1:100) was used for the drosophila experiment in Supplemental Figure 3. *c-Myc* siRNA and negative control siRNA were purchased from MilliporeSigma (catalog 8024873724-000050 and 8024873724-000060). The cells were transfected with Lipofectamine RNAiMAX (Invitrogen, catalog 13778-030) according to the manufacturer's protocol.

**Generation of GAL4-UAS-CDCP1-WT and GAL4-UAS-CDCP1-delta Drosophila melanogaster lines and immunofluorescence.** UAS-*egfr.B* (5368), *src64BP1* (7379), *Src42AK10108* (10969), *GMR-gal4* (1104), and *ptc-gal4* (2017) lines were obtained from the Bloomington Drosophila Stock Centre. Cultures were carried out on a cornmeal/agar diet, (6.65% cornmeal, 7.15% dextrose, 5% yeast, 0.66% agar supplemented with 2.2% nipagin and 3.4 mL propionic acid) and maintained at 25°C and 29°C. To overexpress human CDCP1-WT and CDCP1-delta, UAS transgenic lines were generated from human CDCP1-WT and CDCP1-delta cDNA with the following primer pair: 5'-GATATC-CACCATGGCCGGCCTGAAGTGC GGG-3' and 5'-ACTAGTTCAATGGTGATGGTGATGATG-3'. PCR was performed with Q5 high-fidelity polymerase (New England Biolabs, catalog M0491S). PCR products were cloned using the Zero Blunt TOPO PCR Cloning Kit (Life Technologies, catalog K2800-20) before cloning into the pUAST-attB vector. The constructs were sequence-verified and the transgenic lines established through PhiC31 integrase-mediated transgenesis (BestGene, attP site VK27). Salivary glands were dissected in PBS, fixed in 4% paraformaldehyde (PFA) in PBS, washed in PBT (PBS containing 0.1% Triton X-100), and incubated with primary antibodies in PAXDG (PBS containing 1% BSA, 0.3% Triton X-100, 0.3% deoxycholate, and 5% goat serum) overnight at 4°C. Tissues were washed with PBT, incubated with secondary antibodies in PAXDG for 5 hours at 4°C, and mounted in Vectashield mounting media (Vector Laboratories). Alexa Fluor 568-8-conjugated anti-rabbit and Alexa Fluor 488-conjugated anti-rat antibodies were used as secondary antibodies (Molecular Probes). Images of adult eye and bristle were taken with a Leica M165 FC microscope equipped with SXY-I30 3M Pixel Color Camera. Fluorescent images of salivary glands were taken with Leica M165 FC fluorescent microscope equipped with Leica DFC 3000G digital camera.

**CDCP1 protein expression in human prostate cancer.** The first group of TMAs (Supplemental Figure 1A) was composed of 2 TMAs. The first TMA included benign prostate tissue and prostate cancer at different stages ( $n = 237$ ), as previously reported (32). Spots with metastases were not included in the analysis, to avoid false-negative results due to poor fixation of tissue (mostly material from autopsies). The second TMA ( $n = 192$ ) consisted of locally advanced, inoperable, mostly metastatic prostate cancer including CRPC and hormone naive (untreated) prostate cancer, as previously reported (32). For distant metastasis, CDCP1 staining was performed on 6 regular histological sections of distant and

lymph node prostate cancer metastases. The second group of TMAs (Figure 1, A-D, and Tables 1-4) was composed of 3 different TMAs as previously described (30, 31). Briefly, the first TMA included 201 BHP, RPE, CRPC, and metastasis samples. The second TMA included 323 PCa samples of TUP-P and RPE. The third TMA included 82 CRPC samples. To determine H score, the intensity of membrane CDCP1 staining (on a scale of 0 [no staining], 1+ [weak staining], 2+ [moderate staining], and 3+ [strong staining]) was multiplied by the percentage of positive tumor cells. In the second group of TMAs, PTEN status was determined by FISH or IHC analysis as previously described (30). The use of the clinical samples for TMA construction was approved by the ethics committee of the University of Basel and the University of Zürich. For paired diagnostic (HSPC) and CRPC biopsies (Supplemental Figure 1B), patients were identified from a population of men with mCRPC treated at the Royal Marsden NHS Foundation Trust. All patients provided written informed consent and were enrolled in institutional protocols approved by the Royal Marsden NHS Foundation Trust Hospital (London, United Kingdom) ethics review committee (reference no. 04/Q0801/60). Twenty-five patients with a diagnosis of prostate adenocarcinoma with sufficient formalin-fixed, paraffin-embedded (FFPE), matched diagnostic (archival) hormone-sensitive prostate cancer (HSPC), and CRPC tissue for CDCP1 immunohistochemistry were selected. HSPC tissue demonstrated adenocarcinoma and was obtained from either prostate needle biopsy (21 cases), transurethral resection of the prostate (TURP; 3 cases), or bone biopsy (1 case). CRPC tissue was obtained from the same patients through biopsies of bone (19 cases), lymph node (5 cases), or liver (1 case). All tissue blocks were freshly sectioned and only considered for IHC analyses if adequate material was present ( $\geq 50$  tumor cells).

**Bioinformatic analysis.** Correlation between CDCP1 and PTEN in prostate cancer data sets (5, 54-57) was carried out using Spearman's correlation, which estimates a correlation coefficient value  $R$  and a significant  $P$  value.

We retrieved gene expression and DNA methylation from The Cancer Genome Atlas (TCGA) and performed a correlation analysis between the mRNA expression level and the methylation profile of CDCP1 (Pearson correlation). Methylation level of CDCP1 was determined as the mean of  $\beta$  values within a distance of about 1000 bp from the transcription start site (TSS). Samples were classified into quartiles (Q1-Q4) based on mRNA expression level of CDPI or according to its methylation. Dependency between CDCP1 expression and PTEN deletions/mutations was determined using  $\chi^2$  test. Survival analysis was performed using the Kaplan-Meier estimator and Cox regression model.

**Immunoblotting.** Tissue and cell lysates were prepared with RIPA buffer (Cell Signaling Technology, catalog 9806) with PMSF (phenylmethanesulfonyl fluoride; MilliporeSigma, catalog 329-98-6). Protein concentrations of the lysates were measured by Pierce BCA Protein Assay Kit (Thermo Fisher Scientific, catalog 23225). The lysates were then resolved by SDS-PAGE and immunoblotted with the indicated antibodies. For analysis of fly tissue, wandering third-instar larvae were rinsed in PBS, and salivary glands were dissected out, washed in PBS, and homogenized in SDS sample buffer.

**Real-time PCR.** RNA was extracted using TRIzol Plus RNA Purification Kit (Life Technologies, catalog 12183555). Total RNA (1  $\mu$ g) was used for cDNA synthesis using SuperScript III Platinum One-Step qRT-PCR Kit (Life Technologies, catalog 11732-020). Quantitative real-time PCR (qRT-PCR) was performed as previously described (12). Primers

used are listed in Tables 5 and 6. All qRT-PCR data presented were normalized using GAPDH, HRPT, or 18S rRNA.

**ChIP assay.** Cells were cultured to a confluence of 90%–95% and were cross-linked with 1% formalin for 10 minutes followed by the addition of 2.5 M glycine for 5 minutes at room temperature. The culture medium was aspirated and the cells were washed twice with ice-cold PBS. Nuclear extracts were sonicated using a Misonix 3000 model sonicator to shear cross-linked DNA to an average fragment size of approximately 500 bp. Sonicated chromatin was incubated for 16 hours at 4°C on a rotor with  $\gamma$ -bind Plus sepharose beads (GE Healthcare, catalog 17-0886-01) conjugated with either anti-c-Myc ([9E10]x L0815) anti-SMAD4 ([B-8]; Santa Cruz, catalog E0615) or mouse-IgG antibody (Millipore, catalog 92590). After incubation, beads were washed thoroughly and then centrifuged. The chromatin was eluted from the beads, and cross-links were removed by incubation at 56°C for 12 hours. DNA was then purified using the QIAquick PCR Purification Kit (Qiagen, catalog 28104). The binding of the transcription factor, c-Myc, on Cyclin D1 promoter was determined using SABiosciences' proprietary database (DECODE, DECipherment of DNA Elements). The primer mixes used for ChIP assay in MEFs were as follows: (a) to detect Smad4 binding site (SBE) on Cyclin D1 promoter: SBEChIP forward 5'-CCGCTTAGTCCCCATTCTAAAG-3' and SBEChIP reverse 5'-GGCATCTCCATTCTTAATCCAG-3'; (b) to detect c-Myc binding on Coup-tfII promoter: COUP-TFII ChIP forward 5'-GTGCGGGGACAAGTCGAGCGG-3' and COUP-TFII ChIP reverse 5'-GCGGTGGTGTGGTTCGATGGG-3'; (c) to detect c-Myc binding on Cyclin D1 promoter: EpiTect ChIP qPCR Primer Assay For Mouse Ccnd1, NM\_007631.2 (-)04 Kb (catalog GPM1053924(-)04A). The primer mix used for ChIP assay in LNCaP to detect AR binding site on CDCP1 promoter was: forward 5'-GAATTTGCTCTCGATTCAG-3' and reverse 5'-GCCAGAGTCTGTTGGAC-3'. ChIP qPCR was performed using KAPA SYBR FAST ABI qPCR Master Mix solution (KAPA Biosystem, Roche, catalog 07959389001) on Step One Real-Time PCR systems (Applied Biosystems).

**Proliferation and senescence assays.** Proliferation assay in MEFs was performed by plating  $10^4$  cells per well in a 24-well plate in triplicate while that in human prostate cancer cell lines was performed by plating  $1 \times 10^4$ – $2 \times 10^4$  cells per well in a 24-well plate in triplicate. Cell proliferation was monitored at days 0, 3, 6, and 9 whereby cells were fixed for 15 minutes in a solution of 10% buffered formalin washed with PBS (pH 7.2) and subsequently stained with 0.01% Crystal violet solution. Excessive staining was removed by washing the plates with distilled water and by drying them overnight. Crystal violet-stained cells were dissolved in 10% acetic acid solution for 30 minutes on a shaker and the extracted dye was read with a spectrophotometer at 590 nm. Cellular senescence in vitro was assessed using the Senescence  $\beta$ -Galactosidase Staining Kit (Cell Signaling, catalog 9860) as per the manufacturer's instructions and the quantification was done by counting the total number of cells with Hoechst 3342, trihydrochloride, trihydrate (Invitrogen; catalog 953557).

**Liposomes formulation.** Stealth liposomes (SLs) were prepared using HSPC/CHOL/mPEG<sub>5kDa</sub>-DSPE at a molar ratio of 18:9:1. The lipid film, obtained by evaporating a chloroform solution of the components, was hydrated with a solution of 250 mM ammonium sulfate (pH 5.5) and then extruded at 60°C until reaching the vesicle size of approximately 100 nm. The external buffer was exchanged to PBS pH 7.4 by a PD-10 desalting column. Doxorubicin (DXR) was encapsulat-

ed by remote loading (DXR/HSPC 0.2:1 wt/wt) at 60°C. Free DXR was removed using a PD-10 desalting column and the drug loading was determined spectrophotometrically ( $\lambda = 477$  nm) in methanol. The CUB4 Fab'-coupled PEG-phospholipid derivative was prepared by reacting the Fab' of CUB4, obtained by enzymatic digestion of Fc and Fab2 reduction as described below, with maleimide-PEG-DSPE. The synthesized CUB4 Fab'-PEG-DSPE was then introduced on the liposome surface by the post-insertion technique, described below, to provide stealth immunoliposomes (SILs). Briefly, CUB4 was enzymatically digested with pepsin (1:50 wt/wt enzyme/substrate, 3 hours at 37°C) in 0.1 M sodium acetate at pH 3.8, followed by FPLC analysis on a Superose 12 10/300 GL column using PBS pH 7.4 (flow-rate 0.5 mL/min). The F(ab')<sub>2</sub> fragment was collected and treated for 30 minutes at room temperature with 10 mM cysteamine to yield the Fab' fragment, following purification by FPLC using 50 mM phosphate buffer, 150 mM NaCl, and 10 mM EDTA, pH 5. By exploiting its free sulfhydryl groups, Fab' was immediately coupled (overnight at room temperature, pH 7.0–7.5) to the maleimide groups of mixed micelles composed of maleimide-PEG<sub>5kDa</sub>-DSPE/mPEG<sub>5kDa</sub>-DSPE 4:1 mol/mol at a final molar ratio of 10:1 maleimide/Fab'. In the last step, the Fab'-PEG<sub>5kDa</sub>-DSPE:mPEG<sub>5kDa</sub>-DSPE micelles were inserted on SL surface (post-insertion technique) by incubation of these micelles with SL for 1 hour at 60°C at a molar ratio of 0.05:1 PEG/HSPC to achieve SIL, which were purified on a Sepharose CL-4B column using PBS pH 7.4 and Fab' quantification by BCA assay.

**Statistics.** All data points are presented for quantitative data, with an overlay of the mean with SD and SEM (specified in the figure legends). All statistical analysis were performed using Graph Pad Prism 8 or Microsoft Excel 2016 or R-studio. A 1- or 2-tailed Student *t* test was used for statistical analysis (as specified in the figure legends). Other methods of statistical analysis are indicated in the figure legends.

**Study approval.** All mice were maintained under specific pathogen-free conditions in the animal facilities of the Institute for Research in Biomedicine, in Bellinzona, Switzerland. Experiments were performed according to state guidelines and approved by the local ethics committee. The *Pten*<sup>loxP</sup> conditional knockout mice were previously described (12). CDCP1 conditional overexpression was generated as described in the text. However, to check for correct targeting of the transgene, DNAs from different clones were digested with SpeI and analyzed for correct targeting using an internal 840-bp PstI/XbaI the ColA1 3' probe that hybridized also with the WT allele (33). To obtain the prostate-specific overexpression of CDCP1 and deletion of *Pten*, female CDCP1 and/or *Pten*<sup>loxP/loxP</sup> mice were crossed with male Probasin-Cre4 (Pb-Cre4) transgenic mice (34). To shear cross-linked DNA to an average fragment for genotyping, tail-derived DNA was subjected to PCR analyses. For *Pten*<sup>loxP/loxP</sup> genotyping, primer 1 (5'-AAAAGTTC-CCCTGATGATGATTTGT-3') and primer 2 (5'-TGTTTTTGAC-CAATTAAGTAGGCTGTG-3') were used. For detecting the allele in the prostate, primer 3 (5'-TTCTCTTGAGCACTGTTTCACAGGC-3') and primer 1 were used. For Pb-Cre4, primer 1 (5'-TGATGGACAT-GTTCAGGGATC-3') and primer 2 (5'-GCCACCAGTCTGCATGA-3') were used. For CDCP1 mice, primer 1 (5'-CAAGGGAGAAGAGAGT-GCGG-3') and primer 2 (5'-CCCAACAATGGGGATGTAAG-3') were used, both for genotyping and detecting the allele in the prostate. For the downregulation of CDCP1, cells were infected with PLKO-sh-CDCP1 and doxycycline-inducible pTripz-CDCP1-shRNA. As control for both vectors, we used nontarget shRNA. In the xenograft experi-

ments,  $1 \times 10^6$  Tripz-sh*CDCP1* or Tripz-shRNA controls, PC3 cells, and  $1 \times 10^6$  LNCaP cells were injected s.c. in SCID-NOD mice. After tumor cell injection, tumor formation was monitored every 3 days and upon tumor onset, the mice injected with PC3 cells were fed with doxycycline (0.2 g/L) water supplemented with 5% sucrose until the end of the experiment. Necropsies were performed on the animals, and all tissues were examined regardless of their pathological status. Normal and tumor tissue samples were fixed in 10% neutral-buffered formalin (MilliporeSigma, catalog HT501128) overnight. Then, samples were processed by ethanol dehydration and embedded in paraffin according to standard protocols. Sections (5  $\mu$ m) were prepared for antibody detection and hematoxylin and eosin staining.

## Author contributions

A. Alimonti and A. Alajati developed the concept. A. Alimonti, A. Alajati, and MD designed the experiments, interpreted the data, and wrote the manuscript. A. Alimonti, MD, JC, AR, and IG performed experiments. EP performed the mice experiments. LP and A. Calcinetto read and edited the manuscript. SM, ML, and RD performed immunohistochemistry and immunofluorescence staining. LC performed fly-related experiments and SH supervised and interpreted the data. GC and WY performed correlation analysis. AS, IF, DNR, JW, VG, and TV performed and analyzed the TMA from prostate cancer patients, and LB and JDB supervised the experiments and interpreted the data. GP, MM, and EC did the preparation and characterization of immunoliposomes. MT and MB performed bioinformatics analysis. VT, GC, and A. Carracedo contributed to the data set analysis. LG contributed to the pathological analysis of mouse prostate tissues. JHR, PW, and HM contributed to pathological analysis of the human TMA used in Figure

1. JPT provided the LNCaP-ABL and Lapc4 human prostate cancer cell lines and made suggestions for experimental interpretation.

## Acknowledgments

This study was supported by European Research Council Consolidator grant 683136; Swiss Cancer League grant KFS4267-08-2017; the Dr. Josef Steiner Foundation; Swiss Card-Onco-Grant of the Alfred and Annemarie von Sick grant; the Helmut Horten Foundation, SNSF (310030\_176045), Prostate Cancer United Kingdom (RIA15-ST2-018), and Fondazione Italiana per la ricerca sul Cancro (AIRC) Investigator Grant (22030) to A. Alimonti's lab. GP and EC were supported by AIRC (IG2017, code 20224). The work of A Carracedo is supported by the Basque Department of Education (IKERTALDE IT1106-16), the Department of Industry, Tourism, and Trade of the Government of the Autonomous Community of the Basque Country, and the Severo Ochoa Excellence Accreditation from Ministerio de Ciencia, Innovación y Universidades (MCIU) (SEV-2016-0644). Support was also provided by the MCIU (SAF2016-79381-R, FEDER/EU); the Excellence Networks (SAF2016-81975-REDT); Severo Ochoa Excellence Accreditation (SEV-2016-0644), European Training Networks Project (H2020-MSCA-ITN-308 2016 721532), the Spanish Association Against Cancer (AECC) (IDEAS175CARR; GCTRA18006CARR), La Caixa Foundation (HR17-00094), and the European Research Council (starting grant 336343, proof of concept 754627, consolidator grant 819242).

Address correspondence to: Andrea Alimonti, Institute of Oncology Research, Via V. Vela 6, Bellinzona, Switzerland. Phone: 41.91.8210080; Email: andrea.alimonti@ior.usi.ch.

- Torre LA, Bray F, Siegel RL, Ferlay J, Lortet-Tieulent J, Jemal A. Global cancer statistics, 2012. *CA Cancer J Clin*. 2015;65(2):87-108.
- Watson PA, Arora VK, Sawyers CL. Emerging mechanisms of resistance to androgen receptor inhibitors in prostate cancer. *Nat Rev Cancer*. 2015;15(12):701-711.
- Chandrasekar T, Yang JC, Gao AC, Evans CP. Mechanisms of resistance in castration-resistant prostate cancer (CRPC). *Transl Androl Urol*. 2015;4(3):365-380.
- Huang Y, Jiang X, Liang X, Jiang G. Molecular and cellular mechanisms of castration resistant prostate cancer. *Oncol Lett*. 2018;15(5):6063-6076.
- Taylor BS, et al. Integrative genomic profiling of human prostate cancer. *Cancer Cell*. 2010;18(1):11-22.
- Wadosky KM, Koochekpour S. Molecular mechanisms underlying resistance to androgen deprivation therapy in prostate cancer. *Oncotarget*. 2016;7(39):64447-64470.
- Jamaspishvili T, et al. Clinical implications of PTEN loss in prostate cancer. *Nat Rev Urol*. 2018;15(4):222-234.
- Mulholland DJ, et al. Pten loss and RAS/MAPK activation cooperate to promote EMT and metastasis initiated from prostate cancer stem/progenitor cells. *Cancer Res*. 2012;72(7):1878-1889.
- Cho NY, Choi M, Kim BH, Cho YM, Moon KC, Kang GH. BRAF and KRAS mutations in prostatic adenocarcinoma. *Int J Cancer*. 2006;119(8):1858-1862.
- Köller mann J, et al. Activating BRAF gene mutations are uncommon in hormone refractory prostate cancer in Caucasian patients. *Oncol Lett*. 2010;1(4):729-732.
- Alimonti A, et al. A novel type of cellular senescence that can be enhanced in mouse models and human tumor xenografts to suppress prostate tumorigenesis. *J Clin Invest*. 2010;120(3):681-693.
- Chen Z, et al. Crucial role of p53-dependent cellular senescence in suppression of Pten-deficient tumorigenesis. *Nature*. 2005;436(7051):725-730.
- Ding Z, et al. SMAD4-dependent barrier constrains prostate cancer growth and metastatic progression. *Nature*. 2011;470(7333):269-273.
- Qin J, et al. COUP-TFII inhibits TGF- $\beta$ -induced growth barrier to promote prostate tumorigenesis. *Nature*. 2013;493(7431):236-240.
- Hooper JD, et al. Subtractive immunization using highly metastatic human tumor cells identifies SIMA135/CDPC1, a 135 kDa cell surface phosphorylated glycoprotein antigen. *Oncogene*. 2003;22(12):1783-1794.
- Brown TA, et al. Adhesion or plasmin regulates tyrosine phosphorylation of a novel membrane glycoprotein p80/gp140/CUB domain-containing protein 1 in epithelia. *J Biol Chem*. 2004;279(15):14772-14783.
- Takeda H, Fujimori Y, Kai S, Ogawa H, Nakano T. CD318/CUB-domain-containing protein 1 expression on cord blood hematopoietic progenitors. *Exp Ther Med*. 2010;1(3):497-501.
- Bhatt AS, Erdjument-Bromage H, Tempst P, Craik CS, Moasser MM. Adhesion signaling by a novel mitotic substrate of src kinases. *Oncogene*. 2005;24(34):5333-5343.
- He Y, Harrington BS, Hooper JD. New crossroads for potential therapeutic intervention in cancer-intersections between CDCP1, EGFR family members and downstream signaling pathways. *Oncoscience*. 2016;3(1):5-8.
- Uekita T, Sakai R. Roles of CUB domain-containing protein 1 signaling in cancer invasion and metastasis. *Cancer Sci*. 2011;102(11):1943-1948.
- Wortmann A, He Y, Deryugina EI, Quigley JP, Hooper JD. The cell surface glycoprotein CDCP1 in cancer—insights, opportunities, and challenges. *IUBMB Life*. 2009;61(7):723-730.
- Martin GS. The hunting of the Src. *Nat Rev Mol Cell Biol*. 2001;2(6):467-475.
- Pollan SG, et al. Regulation of inside-out  $\beta$ 1-integrin activation by CDCP1. *Oncogene*. 2018;37(21):2817-2836.
- Spassov DS, et al. Phosphorylation of Trask by Src kinases inhibits integrin clustering and functions in exclusion with focal adhesion signaling. *Mol Cell Biol*. 2011;31(4):766-782.
- Spassov DS, Wong CH, Wong SY, Reiter JF,

- Moasser MM. Trask loss enhances tumorigenic growth by liberating integrin signaling and growth factor receptor cross-talk in unanchored cells. *Cancer Res.* 2013;73(3):1168–1179.
26. Nakashima K, et al. Novel small molecule inhibiting CDCP1-PKC $\delta$  pathway reduces tumor metastasis and proliferation. *Cancer Sci.* 2017;108(5):1049–1057.
27. Kollmorgen G, et al. Antibody mediated CDCP1 degradation as mode of action for cancer targeted therapy. *Mol Oncol.* 2013;7(6):1142–1151.
28. Siva AC, et al. Targeting CUB domain-containing protein 1 with a monoclonal antibody inhibits metastasis in a prostate cancer model. *Cancer Res.* 2008;68(10):3759–3766.
29. Liu F, Yang X, Geng M, Huang M. Targeting ERK, an Achilles' Heel of the MAPK pathway, in cancer therapy. *Acta Pharm Sin B.* 2018;8(4):552–562.
30. Cima I, et al. Cancer genetics-guided discovery of serum biomarker signatures for diagnosis and prognosis of prostate cancer. *Proc Natl Acad Sci USA.* 2011;108(8):3342–3347.
31. Fankhauser CD, et al. Comprehensive immunohistochemical analysis of PD-L1 shows scarce expression in castration-resistant prostate cancer. *Oncotarget.* 2018;9(12):10284–10293.
32. Zellweger T, et al. Estrogen receptor  $\beta$  expression and androgen receptor phosphorylation correlate with a poor clinical outcome in hormone-naïve prostate cancer and are elevated in castration-resistant disease. *Endocr Relat Cancer.* 2013;20(3):403–413.
33. Beard C, Hochedlinger K, Plath K, Wutz A, Jaenisch R. Efficient method to generate single-copy transgenic mice by site-specific integration in embryonic stem cells. *Genesis.* 2006;44(1):23–28.
34. Trotman LC, et al. Pten dose dictates cancer progression in the prostate. *PLoS Biol.* 2003;1(3):E59.
35. Culi J, Martín-Blanco E, Modolell J. The EGF receptor and N signalling pathways act antagonistically in *Drosophila* mesothorax bristle patterning. *Development.* 2001;128(2):299–308.
36. Khare S, et al. A KCNC3 mutation causes a neurodevelopmental, non-progressive SCA13 subtype associated with dominant negative effects and aberrant EGFR trafficking. *PLoS ONE.* 2017;12(5):e0173565.
37. Brumby AM, Richardson HE. Using *Drosophila melanogaster* to map human cancer pathways. *Nat Rev Cancer.* 2005;5(8):626–639.
38. Bülow MH, Bülow TR, Hoch M, Pankratz MJ, Jünger MA. Src tyrosine kinase signaling antagonizes nuclear localization of FOXO and inhibits its transcription factor activity. *Sci Rep.* 2014;4:4048.
39. Dodson GS, Guarnieri DJ, Simon MA. Src64 is required for ovarian ring canal morphogenesis during *Drosophila* oogenesis. *Development.* 1998;125(15):2883–2892.
40. Alimonti A, et al. Subtle variations in Pten dose determine cancer susceptibility. *Nat Genet.* 2010;42(5):454–458.
41. Furstoss O, Dorey K, Simon V, Barilà D, Superti-Furga G, Roche S. c-Abl is an effector of Src for growth factor-induced c-myc expression and DNA synthesis. *EMBO J.* 2002;21(4):514–524.
42. Jain S, et al. Src inhibition blocks c-Myc translation and glucose metabolism to prevent the development of breast cancer. *Cancer Res.* 2015;75(22):4863–4875.
43. Barone MV, Courtneidge SA. Myc but not Fos rescue of PDGF signalling block caused by kinase-inactive Src. *Nature.* 1995;378(6556):509–512.
44. Lunardi A, et al. A co-clinical approach identifies mechanisms and potential therapies for androgen deprivation resistance in prostate cancer. *Nat Genet.* 2013;45(7):747–755.
45. Di Mitri D, et al. Tumour-infiltrating Gr-1+ myeloid cells antagonize senescence in cancer. *Nature.* 2014;515(7525):134–137.
46. Hennequin LF, et al. N-(5-chloro-1,3-benzodioxol-4-yl)-7-[2-(4-methylpiperazin-1-yl)ethoxy]-5-(tetrahydro-2H-pyran-4-yloxy)quinazolin-4-amine, a novel, highly selective, orally available, dual-specific c-Src/Abl kinase inhibitor. *J Med Chem.* 2006;49(22):6465–6488.
47. Carver BS, et al. Reciprocal feedback regulation of PI3K and androgen receptor signaling in PTEN-deficient prostate cancer. *Cancer Cell.* 2011;19(5):575–586.
48. Burton DG, et al. Androgen deprivation-induced senescence promotes outgrowth of androgen-refractory prostate cancer cells. *PLoS ONE.* 2013;8(6):e68003.
49. Campisi J. Aging and cancer: the double-edged sword of replicative senescence. *J Am Geriatr Soc.* 1997;45(4):482–488.
50. Jain RK. Normalization of tumor vasculature: an emerging concept in antiangiogenic therapy. *Science.* 2005;307(5706):58–62.
51. Maeda H, Nakamura H, Fang J. The EPR effect for macromolecular drug delivery to solid tumors: Improvement of tumor uptake, lowering of systemic toxicity, and distinct tumor imaging in vivo. *Adv Drug Deliv Rev.* 2013;65(1):71–79.
52. Maeda H, Tsukigawa K, Fang J. A retrospective 30 years after discovery of the enhanced permeability and retention effect of solid tumors: next-generation chemotherapeutics and photodynamic therapy—problems, solutions, and prospects. *Microcirculation.* 2016;23(3):173–182.
53. Yang L, et al. Dysregulated expression of cell surface glycoprotein CDCP1 in prostate cancer. *Oncotarget.* 2015;6(41):43743–43758.
54. Chandran UR, et al. Gene expression profiles of prostate cancer reveal involvement of multiple molecular pathways in the metastatic process. *BMC Cancer.* 2007;7:64.
55. Varambally S, et al. Integrative genomic and proteomic analysis of prostate cancer reveals signatures of metastatic progression. *Cancer Cell.* 2005;8(5):393–406.
56. Grasso CS, et al. The mutational landscape of lethal castration-resistant prostate cancer. *Nature.* 2012;487(7406):239–243.
57. Lefort K, et al. Dual tumor suppressing and promoting function of Notch1 signaling in human prostate cancer. *Oncotarget.* 2016;7(30):48011–48026.